bioRxiv preprint doi: https://doi.org/10.64898/2026.07.24.740446; this version posted July 24, 2026. The copyright holder for this preprint (which was not certified by peer review) is the author/funder, who has granted bioRxiv a license to display the preprint in perpetuity. It is made available under a CC-BY-NC 4.0 International license.

Integrated genomics and transcriptomics reveal mechanisms of extreme dietary adaptation in vampire bats

Shenglin Liu [1,2,3,4], Mariella Bontempo Freitas [5], Sirlene Souza Rodrigues Sartori [5], Michele Albertini [1,2], Evgeny Leushkin [1], Ine Alvarez van Tussenbroek [6], Ariadna E. Morales [1,2], Martin Pippel [7,8], Tom Brown [7,8], Alex Filipe Ramos de Sousa [9], Rosinéa Aparecida de Paula [5], Ilias Patmanidis [10], Willem Jespers [10], Leon Hilgers [1,2], Xueling Yi [1,2], Bernhard Bein [1,2], Yury Malovichko [1,2], Tilman Schell [1], Carola Greve [1], Sylke Winkler [7,8], Alexander Ben Hamadou [1], Moritz Blumer [11], Gisa Prange [2], Julio César Hechavarria Cueria [2], Manfred Kössl [2], York Winter [12], Sean Dilrosun [13], Stephert Daniël Bechan [14], Mark D. Engstrom [15,16], Deirdre Jafferally [17], Zacharias Norman [18], Francisco Sornoza [19], Liliana M. Dávalos [20,21], Burton K. Lim [15], Sonja C. Vernes [6], Michael Hiller [1,2*]

1 Senckenberg – Leibniz Institution for Biodiversity and Earth System Research, Senckenberganlage 25, 60325 Frankfurt, Germany
2 Institute of Cell Biology and Neuroscience, Faculty of Biosciences, Goethe University Frankfurt, Max-von-Laue-Str. 9, 60438 Frankfurt, Germany
3 Department of Molecular Medicine, Aarhus University Hospital (AUH), Aarhus, Denmark
4 Department of Clinical Medicine, Aarhus University, Aarhus, Denmark
5 Department of Animal Biology, Federal University of Viçosa, Campus UFV, 36570-900, Viçosa, Minas Gerais, Brazil
6 School of Biology, The University of St Andrews, St Andrews, UK
7 Max Planck Institute of Molecular Cell Biology and Genetics, Dresden, Germany
8 DRESDEN concept Genome Center, Dresden, Germany
9 Department of Veterinary Medicine, Federal University of Viçosa, Campus UFV, 36570-900, Viçosa, Minas Gerais, Brazil
10 Department of Medicinal Chemistry, Photopharmacology and Imaging, Groningen Research Institute of Pharmacy, Faculty of Science and Engineering, Antonius Deusinglaan 1, 9713 AV Groningen, The Netherlands
11 Department of Genetics, University of Cambridge, Downing Street, CB2 3EH Cambridge, UK
12 Institut für Biologie, Humboldt Universität, Berlin, Germany
13 Environmental Services and Support N.V., Paramaribo, Suriname
14 Advanced Teachers Training College, Biology Course, Suriname
15 Department of Natural History, Royal Ontario Museum, Toronto, Ontario, Canada
16 Department of Ecology and Evolutionary Biology, University of Toronto, Canada
17 Cobra Collective Guyana, Golden Grove Village, East Coast Demerara, Guyana
18 Bina Hill Institute Youth Learning Centre, Bina Hill, Annai Village, North Rupununi District, Region 9, Guyana
19 National Institute of Biodiversity (INABIO), Ministry of Environment and Energy of Ecuador, Quito, Ecuador
20 Department of Ecology and Evolution, Institute for Advanced Computational Science and Consortium for Inter-Disciplinary Environmental Research, SUNY Stony Brook, Stony Brook, NY, USA
21 Consortium for Inter-Disciplinary Environmental Research, SUNY Stony Brook, Stony Brook, NY, USA

bioRxiv preprint doi: https://doi.org/10.64898/2026.07.24.740446; this version posted July 24, 2026. The copyright holder for this preprint (which was not certified by peer review) is the author/funder, who has granted bioRxiv a license to display the preprint in perpetuity. It is made available under a CC-BY-NC 4.0 International license.

*To whom correspondence should be addressed: michael.hiller@senckenberg.de

Running title: Molecular basis of sanguivory in vampire bats

Keywords: vampire bats, genome assembly, comparative genomics, adaptive evolution, comparative metabolism and physiology

Abstract

Vampire bats are the only tetrapods that feed exclusively on blood. To uncover the molecular basis of this extreme dietary specialization, we generated six new reference genomes, including genomes of all three vampire bat species, and integrated comparative analyses of gene sequence evolution (selection signatures, duplications, and losses) with transcriptomic data from six major organs to identify shifts in gene expression. Our integrative analyses reveal sequence or expression changes in 150 genes that illuminate the genetic mechanisms underlying sanguivory. Through comparative analyses and experiments, we show that the enlarged vampire bat stomach has increased connective tissue content enabling extreme expansion, is pH-neutral, and exhibits reduced mucus production, together providing molecular insights into its shift from a digestive to an absorptive organ for water, electrolytes, and vitamins. We further uncover pathway-level molecular changes underlying altered gastrointestinal motility; trypsin-dependent protein digestion; upregulated amino acid catabolism with key aspects diverging from other mammals; impaired dietary fat digestion counterbalanced by increased fatty acid synthesis; defective sugar metabolism and natural insulin deficiency; enhanced heme iron absorption; and adult splenic erythropoiesis. Together, these findings reveal the molecular adaptations that enable one of the most extreme dietary transitions among vertebrates.

bioRxiv preprint doi: https://doi.org/10.64898/2026.07.24.740446; this version posted July 24, 2026. The copyright holder for this preprint (which was not certified by peer review) is the author/funder, who has granted bioRxiv a license to display the preprint in perpetuity. It is made available under a CC-BY-NC 4.0 International license.

Introduction

Extreme dietary specializations impose strong and persistent selective pressures in nature, forcing organisms to reconcile severe nutritional imbalances with existing physiological and metabolic constraints. Deciphering how genomes adapt to such conditions reveals general principles of the evolutionary processes that remodel metabolism and physiology, with potential biomedical relevance (*1*–*6*). Obligate blood feeding (sanguivory), characterized by extreme nutrient bias, chronic caloric limitation, and metabolic states resembling features of human disorders such as insulin resistance, provides a powerful natural experiment for understanding the evolutionary mechanisms of extreme dietary adaptation.

Among more than 30,000 tetrapod species, obligate sanguivory has evolved only once and is restricted to three species of vampire bats (*7*, *8*): the common vampire bat *Desmodus rotundus*, the white-winged vampire bat *Diaemus youngii*, and the hairy-legged vampire bat *Diphylla ecaudata* (bat family Phyllostomidae, subfamily Desmodontinae). Vampire bats have long fascinated scientists for their extreme dietary specialization, which affects morphology, physiology, metabolism, and behavior.

Morphologically, these strictly nocturnal bats have well-developed terrestrial locomotion skills to approach prey, razor-sharp enamel-less upper incisors, salivary anti-coagulants to maintain blood flow, as well as advanced low-frequency hearing and infrared radiation sensing abilities (*9*–*11*). Their stomach transformed from a digestive to a distensible organ, used primarily for short term storage of large blood meals and rapid fluid absorption (*12*, *13*).

Physiologically, vampire bats have adapted to the high iron content and extreme nutrient bias of blood, which contains mostly protein (93%) and very little lipids (1%) and carbohydrates (1%) (*14*, *15*). To compensate for the low caloric content of their 78% water-containing diet, they consume large volumes in a single meal, often approaching half their body weight (*14*). Their low carbohydrate intake resulted in low basal insulin levels and a reduced glucose-stimulated insulin secretion response, resembling human type 2 diabetes (*16*). Limited glycogen and lipid stores make them very sensitive to starvation, with death occurring after 48–72 hours of fasting (*17*). Abundant dietary amino acids are their primary energy source and are rapidly used to fuel exercise such as running (*18*).

Behaviorally, vampire bats show exceptional social and cognitive adaptations. To mitigate risk of starvation, they regurgitate blood to roost mates that failed to forage, preferentially sharing with individuals recognized by social bonds formed through allogrooming and long-term social memory (*19*–*21*). They also adopt non-kin orphaned offspring and maintain long-lasting social bonds, even after captive bats are released into the wild (*22*, *23*). These advanced social behaviors are consistent with their large relative neocortical volume (*24*).

Several studies have shed light on the molecular basis of vampire bat adaptations to sanguivory, revealing signatures of selection in genes involved in digestion, fat and vitamin metabolism, and immunity, a reduction of bitter taste receptor genes, and the loss of trehalase, the enzyme that digests the insect sugar trehalose (*25*–*29*). Comparative genomic studies also identified gene

bioRxiv preprint doi: https://doi.org/10.64898/2026.07.24.740446; this version posted July 24, 2026. The copyright holder for this preprint (which was not certified by peer review) is the author/funder, who has granted bioRxiv a license to display the preprint in perpetuity. It is made available under a CC-BY-NC 4.0 International license.

losses unique to the common vampire bat that relate to insulin secretion, glycogen storage, gastric function and their exceptional cognitive abilities (*30*).

However, previous studies have several limitations. First, almost all genomic studies focused on *Desmodus rotundus*, the only vampire bat species with a sequenced genome so far, leaving it unclear whether observed patterns are shared with *Diaemus youngii* or *Diphylla ecaudata*. Second, the lack of high-quality genomes of other phyllostomid bats limits taxonomic representation, with many studies often lacking the closest sister species of vampire bats. Third, previous work focused on single aspects of genomic change, such as positive selection or gene loss, leaving other types of molecular changes important for adaptations, such as changes in gene expression, unexplored. Consequently, the molecular basis of sanguivory in vampire bats remains incompletely understood.

Here, we present high-quality genomes of six phyllostomid bats, including new haplotype-resolved assemblies of all three vampire bat species (for readability, we use the unique genus names *Desmodus*, *Diaemus* and *Diphylla* in the following). Our integrative analyses discovered changes in gene sequence and expression, inferred from transcriptomics data of six major organs, revealing molecular underpinnings of their enlarged, non-acidic, absorptive stomach; altered gastrointestinal motility; trypsin-dependent protein digestion; upregulated amino acid catabolism; impaired digestion and increased *de novo* synthesis of fatty acids; defective sugar metabolism and natural insulin deficiency; enhanced heme iron absorption; and adult splenic erythropoiesis, providing a comprehensive view of the molecular adaptations underlying sanguivory in vampire bats.

Results

Reference genomes of all three vampire bats

To sequence the *Diphylla* and *Diaemus* genome, we generated 42X and 39X coverage of PacBio HiFi reads and 61X and 66X Arima Hi-C data. For *Desmodus*, we generated 43 GB of additional HiFi data (increasing the total coverage to 57X) and re-assembled the new and existing read data (*30*). For all three species, we used Hifiasm in Hi-C mode and YaHS to generate haplotype-resolved chromosome-level assemblies (*31*, *32*), and performed dual haplotype curation to resolve remaining scaffolding and haplotype-sorting errors in the joint Hi-C map of both haplotypes. The haplotype assemblies of *Diphylla* and *Diaemus* have contig N50 values between 33 and 44 Mb, and at least 98.2% and 92.7% of these assemblies are contained in chromosome-level scaffolds (Fig. 1A-C, Supplementary Figure 1, Supplementary Table 1), matching the described karyotype of these species (*33*). Using the HiFi reads and Merqury (*34*), we estimate high base accuracies with QV values between 69 and 72, indicating only ~1 error per 10 megabases. We note that these values represent an upper bound as the HiFi reads were used for assembly. In comparison to the previous *Desmodus* assembly, our new assembly improved both contig N50 (9 vs. 6.8 Mb and 11.3 vs. 8 Mb for haplotypes 1 and 2) and base accuracy (QV values 69 vs. 64 for both haplotypes).

bioRxiv preprint doi: https://doi.org/10.64898/2026.07.24.740446; this version posted July 24, 2026. The copyright holder for this preprint (which was not certified by peer review) is the author/funder, who has granted bioRxiv a license to display the preprint in perpetuity. It is made available under a CC-BY-NC 4.0 International license.

Since assembly quality and completeness is important for comparative genomic analysis (*35*–*37*) and taxonomic coverage is key to understand which changes truly occurred in vampire bats, we generated three additional high-quality genomes of bats that cover other phyllostomid subfamilies, *Carollia perspicillata* (Carolliinae), *Glossophaga soricina* (Glossophaginae), *Micronycteris megalotis* (Micronycterinae). For these species, we assembled primary genomes, having contig N50 values between 27 to 78 Mb and chromosome-level scaffolds (Fig. 1A-C, Supplementary Table 1).

To evaluate gene completeness, we used TOGA (Tool to infer Orthologs from Genome Alignments) (*38*) to classify 17,648 ancestral placental mammal coding genes into those that have an intact open reading frame, those with inactivating mutations (such as frameshifts, stop codon, exon deletions), and those with missing coding exons, often caused by assembly gaps. The new genomes contain between 16,486 and 16,570 intact genes (Fig. 1D, Supplementary Table 2), which is comparable or better than previous long and short read genomes (*26*, *28*, *39*–*42*). Applying compleasm (*43*) with the mammalia_ODB12 set of 12,277 near-universally conserved mammalian genes to our new genomes revealed a consistently high gene completeness ranging from 99.45% to 99.57% (Supplementary Table 1).

bioRxiv preprint doi: https://doi.org/10.64898/2026.07.24.740446; this version posted July 24, 2026. The copyright holder for this preprint (which was not certified by peer review) is the author/funder, who has granted bioRxiv a license to display the preprint in perpetuity. It is made available under a CC-BY-NC 4.0 International license.

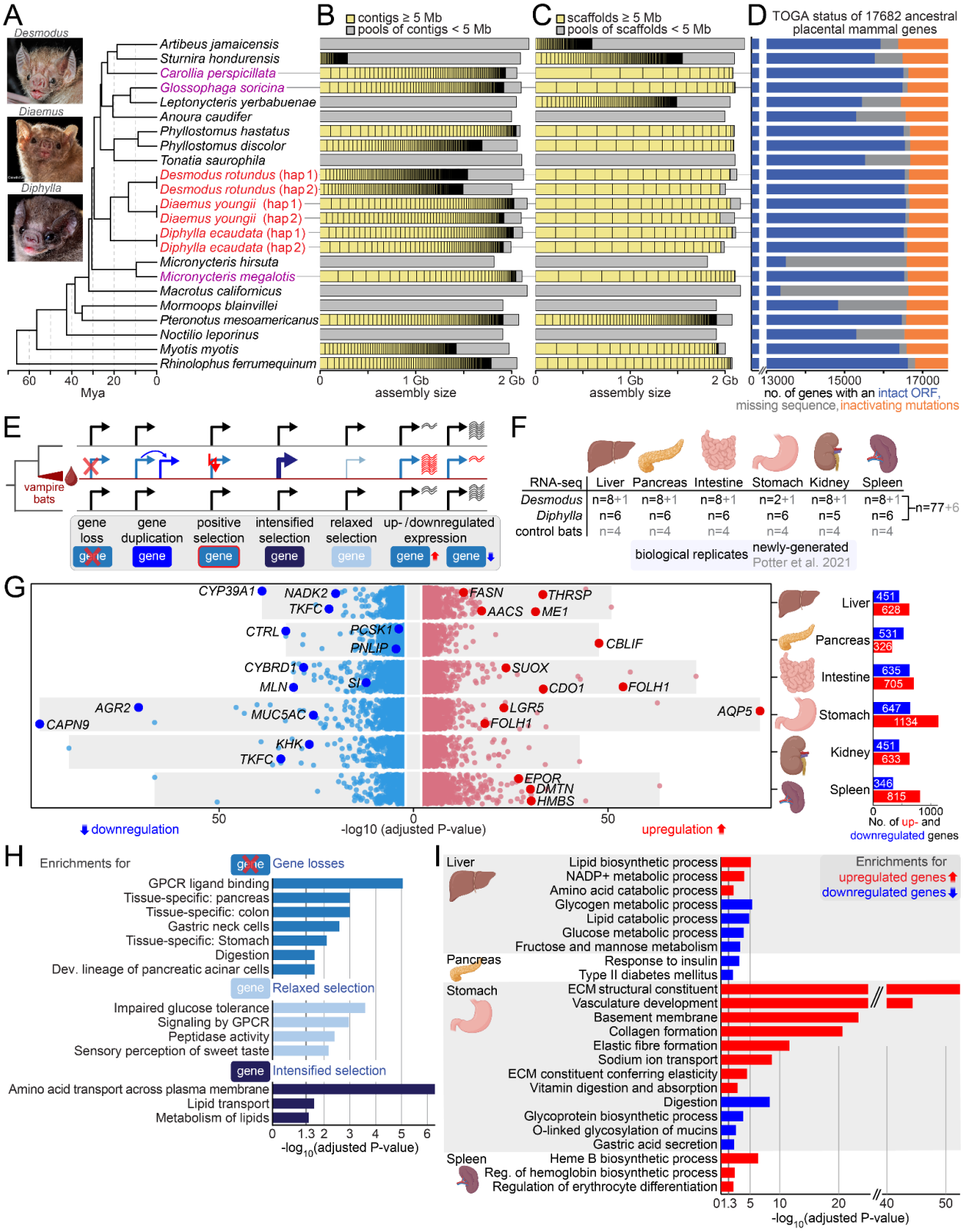


Figure 1: Comparative genomic and transcriptomic analyses illuminate extreme dietary adaptation in vampire bats.

bioRxiv preprint doi: https://doi.org/10.64898/2026.07.24.740446; this version posted July 24, 2026. The copyright holder for this preprint (which was not certified by peer review) is the author/funder, who has granted bioRxiv a license to display the preprint in perpetuity. It is made available under a CC-BY-NC 4.0 International license.

(A) Phylogeny of the bat species analyzed in this study. New genomes are in red and purple fonts. All nodes have 100% bootstrap support. Insets show *Desmodus* (Photo credit Brock Fenton), *Diaemus* (©MerlinTuttle.org), and *Diphylla* (José G. Martínez-Fonseca).
(B,C) Visualization of contig and scaffold sizes.
(D) TOGA classification of ancestral placental mammal genes.
(E) Illustration of comparative genomic and transcriptomic analyses to discover vampire bat changes in gene sequence and expression.
(F) Newly-generated and existing organ transcriptomics data.
(G) Significance (left) and total number (right) of differentially expressed genes identified across six organs, highlighting some of the genes discussed in the text.
(H,I) Significant enrichments of genes with sequence (H) and expression changes (I) relevant to the discussed metabolic and physiological alterations in vampire bats. Supplementary Tables 9 and 10 show all enrichments.

Integrative analyses to discover genes involved in vampire bat adaptations

To elucidate the molecular basis of sanguivory, we compared the genomes of the three vampire bat species with those of 12 other phyllostomids and five non-phyllostomid bats. By including their sister and outgroup species, we were able to identify changes specific to the vampire bat lineage. To obtain a phylogeny of these bats, we used TOGA (*38*) to obtain a set of 15,481 1:1 orthologous genes and used coalescence analysis (*44*, *45*) to infer a highly-supported, time-calibrated species tree (Fig. 1A, Supplementary Table 3).

Adaptations to sanguivory in vampire bats likely involve changes in both the sequence and expression of protein-coding genes. To identify gene sequence changes, we (i) used TOGA (*38*) to detect gene losses and duplications, (ii) applied the branch-site method aBSREL (*46*) to infer episodic positive selection, and (iii) used RELAX (*47*) to detect genes evolving under relaxed or intensified selective pressure to preserve the protein sequence (Fig. 1E, Supplementary Table 4). To uncover gene expression changes, we generated 77 RNA-seq datasets from six organs relevant for metabolism and physiology (stomach, small intestine, liver, pancreas, kidney, spleen) obtained from eight *Desmodus* and six *Diphylla* individuals (Fig. 1F, Supplementary Figure 2, Supplementary Table 5). We combined these datasets with available tissue-matched transcriptomes from one *Desmodus* and four non-vampire phyllostomid species (*3*). Principal component analysis showed that newly-generated and published data clustered by tissue (Supplementary Figure 3), supporting organ-level expression coherence across species. We then used kb-python (*48*) to quantify gene expression and DESeq2 (*49*) to identify orthologous genes significantly up- or downregulated in one or both vampire bats, with many of these genes showing coherent expression shifts across both species (Fig. 1G, Supplementary Tables 6-8). Collectively, these integrative analyses provide a comprehensive view of gene sequence and expression changes in vampire bats.

Functional enrichments highlight many metabolic and physiological processes that are altered in vampire bats (Fig. 1H,I, Supplementary Tables 9-10). Specifically, genes lost or evolving under relaxed selection in vampire bats are enriched for pancreas, colon, and stomach expression and

bioRxiv preprint doi: https://doi.org/10.64898/2026.07.24.740446; this version posted July 24, 2026. The copyright holder for this preprint (which was not certified by peer review) is the author/funder, who has granted bioRxiv a license to display the preprint in perpetuity. It is made available under a CC-BY-NC 4.0 International license.

functions related to digestion, taste perception, and glucose tolerance. Genes evolving under intensified selection are enriched in amino acid and lipid transport and lipid metabolism. Genes upregulated in the liver are enriched in amino acid catabolism and fatty acid synthesis, whereas downregulated genes are enriched in lipid and sugar catabolism. In the pancreas, downregulated genes are enriched in insulin response and type 2 diabetes–associated pathways. In the stomach, upregulated genes are enriched in extracellular matrix organization, vasculature development, and sodium and vitamin absorption (Supplementary Note 1), whereas downregulated genes are enriched in mucus production and gastric acid secretion. Finally, spleen-upregulated genes are enriched for erythropoiesis.

Guided by these functional enrichments and corroborated by new experiments, we reveal in the following sections the mechanisms by which 150 genes with sequence and/or expression changes in vampire bats (Supplementary Table 11) contribute to their remodeled stomach, changes in gastrointestinal motility, adaptations in protein, fat, carbohydrate and iron metabolism, and splenic erythropoiesis. For all presented genes, we also show sequence alignments, amino acid and nucleotide substitution rates, and detailed gene expression profiles in Supplementary Data 1.

Structural and size adaptations in the stomach

Vampire bats exhibit a markedly enlarged stomach (Fig. 2A). Among the most significantly upregulated genes in the vampire bat stomach are three stem cell marker genes, *LGR5*, *MSI1*, and *CD34* (rank 8, 17 and 24) (Fig. 2B). *LGR5* is expressed in mature pyloric glands and a subpopulation of chief cells, where it contributes to renewal of the gastric epithelium (*50*, *51*). *CD34*-expressing cells promote the maintenance of *LGR5*-expressing intestinal epithelial stem cells (*52*). *MSI1*, a gastric stem cell marker, controls the switch of the intestinal stem cells from the quiescent to the active state and is required for regeneration of gastric mucosal epithelium upon injury (*53*, *54*). Upregulation of these genes likely contributes to the distinct cell-type composition of the vampire bat stomach that has acinar rather than deep tubular gastric glands and fewer parietal and chief cells (*55*) (Supplementary Figure 4). Furthermore, since all three genes promote maintenance of stem cell identity, their upregulation likely also contributes to their exceptionally enlarged stomach.

Upregulated genes in the vampire bat stomach are strongly enriched for functions related to "extracellular matrix (ECM) structural constituent", “basement membrane”, “collagen formation”, and “elastic fiber formation” (Fig. 1I). Many of these genes are normally expressed in connective tissue: *ECM1* acts as “biological glue” for various ECM and basement membrane components (*56*), fibronectin (*FN1*) forms fibrillar networks crucial for cell adhesion and ECM organization (*57*), elastic fiber components (*EMILIN1*, *EMILIN2*) contribute to tissue elasticity (*58*), fibulins (*FBLN2*, *EFEMP1*) associate with elastic fibers and stabilize basement membranes (*59*, *60*), *LOXL3* enhances ECM stiffness by crosslinking collagen and elastin (*61*), *TGFB3* regulates ECM and cellular adhesion components and contributes to ECM stiffness (*62*), and numerous collagen genes (Fig. 2B).

bioRxiv preprint doi: https://doi.org/10.64898/2026.07.24.740446; this version posted July 24, 2026. The copyright holder for this preprint (which was not certified by peer review) is the author/funder, who has granted bioRxiv a license to display the preprint in perpetuity. It is made available under a CC-BY-NC 4.0 International license.

To investigate the basis of these gene upregulations, we performed histological comparisons of the stomachs of *Desmodus*, *Diphylla*, the fruit-eating phyllostomid bat *Artibeus lituratus*, and the insect-feeding bat *Myotis nigricans*. Image analysis and quantification revealed that vampire bats have significantly increased connective tissue content, including within the muscular layer, and reduced mucosal thickness (Fig. 2C-D, Supplementary Figure 5, Supplementary Table 12). This marked increase in connective tissue likely confers greater structural integrity and resilience, enabling the extreme stomach expansion that occurs when vampire bats ingest blood volumes approaching 60% of their body weight (*15*) (Fig. 2E). Together, our analysis provides molecular insights into structure and size adaptations of the vampire bat stomach.

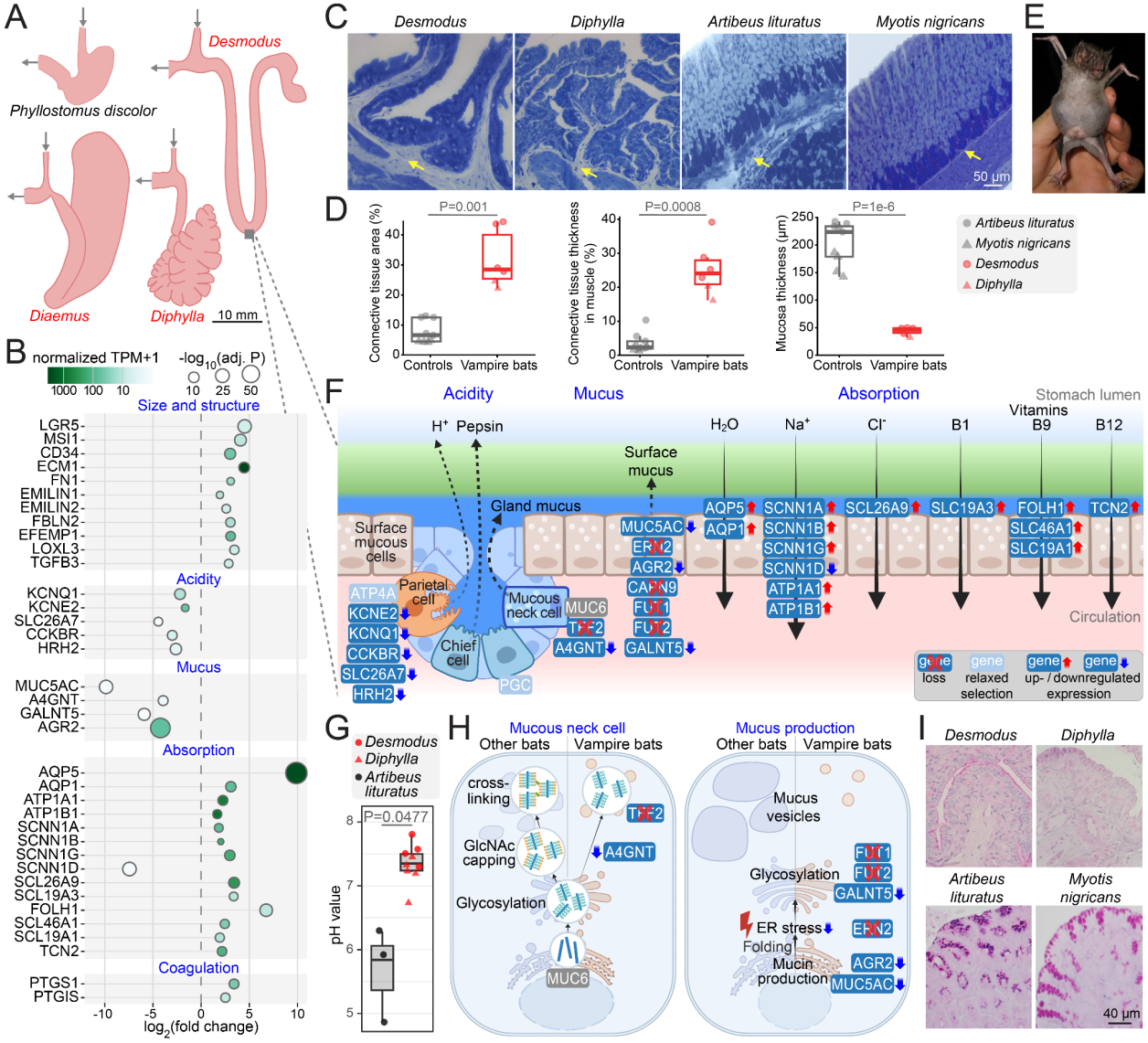


Figure 2: Molecular mechanisms underlying the enlarged, non-acidic, and absorptive vampire bat stomach.

bioRxiv preprint doi: https://doi.org/10.64898/2026.07.24.740446; this version posted July 24, 2026. The copyright holder for this preprint (which was not certified by peer review) is the author/funder, who has granted bioRxiv a license to display the preprint in perpetuity. It is made available under a CC-BY-NC 4.0 International license.

(A) Stomach size and morphology, drawn to scale based on (*63*, *64*), comparing the omnivorous *Phyllostomus discolor* with vampire bats. Inward arrows indicate esophagus, outward arrows duodenum.
(B) Differential gene expression in the stomach, showing fold change (X-axis), expression level (normalized TPM as a color gradient) and significance (circle size). Genes are ordered as discussed in the text.
(C) Histology (Toluidine blue staining) of stomach walls. Yellow arrows highlight connective tissue content. Scale bar is 50 µm for all images.
(D) Comparison of quantified connective tissue content and mucosa thickness, assessing differences with two-tailed Welch's t-tests.
(E) Fed *Desmodus* individual, illustrating the expanded blood-filled stomach (photo credit Jon Flanders).
(F) Illustration of sequence and expression changes of genes involved in reduced gastric acidity, mucus production and absorption.
(G) pH meter measurements show that vampire bats have a significantly higher stomach pH that is neutral. Two-tailed Welch's t-test was used.
(H) Illustration of gene changes relevant for mucus neck cells (left) and general mucus production (right).
(I) Histological analysis with Periodic acid-Schiff/Alcian blue staining shows reduced mucus production in the vampire bat stomach.

Non-acidic stomach

In most mammals, the stomach is an acidic digestive organ. We found that *ATP4A*, the catalytic subunit of the gastric H+,K+-ATPase proton pump responsible for gastric acid secretion (*65*), evolves under relaxed selection in vampire bats (Fig. 2F). Furthermore, genes downregulated in the vampire bat stomach are enriched for "gastric acid secretion" (Fig. 1I), including those encoding the K^+ channel KCNQ1 and its regulatory subunit KCNE2, which replenish luminal K^+ (*66*), the histamine-stimulated chloride/bicarbonate exchanger SLC26A7, which mediates parietal cell chloride uptake (*67*), and the parietal cell receptors for the gastric acid secretagogues gastrin (CCKBR) and histamine (HRH2) (*68*) (Fig. 2B,F). Inhibition or knockout of all these genes impairs gastric acid secretion, and *CCKBR* knockout reduces parietal cell number (*69–73*), corroborating previous anatomical studies reporting fewer parietal cells without canaliculi and fewer gastrin-producing cells (*12*, *74*, *75*).

Together, these genomic and transcriptomic signatures suggest reduced stomach acidity in vampire bats; however, the stomach pH of bats is generally unknown. We therefore measured stomach acidity in *Desmodus* (n=4), *Diphylla* (n=5) and, as a control, in the phyllostomid bat *Artibeus lituratus* (n=3). Indeed, we found that vampire bats have a neutral pH (average 7.36 ± 0.29), while *Artibeus* has a weakly acidic stomach (average 5.67 ± 0.71, two-tailed Welch's t-test P=0.048, Fig. 2G, Supplementary Table 13).

bioRxiv preprint doi: https://doi.org/10.64898/2026.07.24.740446; this version posted July 24, 2026. The copyright holder for this preprint (which was not certified by peer review) is the author/funder, who has granted bioRxiv a license to display the preprint in perpetuity. It is made available under a CC-BY-NC 4.0 International license.

Three factors likely underlie the reduced stomach acidity. First, because blood has a high buffering capacity, achieving acidity in the enlarged vampire bat stomach requires the production of large acid quantities, which is likely energetically prohibitive. Second, the altered gastric mucus profile (below) likely makes the stomach vulnerable to acid-induced damage. Third, and probably most important for vampire bats, their stomach shifted from a digestive to an absorptive organ (below).

Remodeled gastric mucus profile

Gastric mucus protects the stomach epithelium. Our integrative analysis revealed losses and downregulation of several genes related to mucus composition and function (Fig. 2B,F,H, Supplementary Figure 6), supporting the enrichment of stomach-downregulated genes in mucin production and glycosylation (Fig. 1I). *MUC5AC*, the most abundant mucin in a typical mammalian stomach (*76*), is not expressed in the vampire bat stomach. The other major gastric mucin, *MUC6*, is robustly expressed; however, its co-expressed binding lectin *TFF2* (*77*, *78*) is lost in vampire bats. Interactions between TFF2 and MUC6 are required to stabilize the inner mucus layer and *TFF2*-deficient mice exhibit reduced mucus viscoelasticity and mucosal thickness (*79*, *80*). TFF2 binds specifically to an α1,4GlcNAc–capped glycan on MUC6 (*77*). Consistent with *TFF2* loss, the α1,4GlcNAc-capping enzyme *A4GNT* is downregulated in the vampire bat stomach.

Several other genes normally expressed in gastric mucus-producing cells (*81*) show evidence of loss, relaxed selection, or downregulation in the vampire bat stomach (Fig. 2B,F,H, Supplementary Figures 7-11, Supplementary Notes 2-3). These include the protease *CTSE* (*82*), the endocytosis regulator *REP15* (*83*, *84*), the gastric mucosal defense factor *CAPN9* (*85*), the mucus glycosylation enzymes *FUT1*, *FUT2* and *GALNT5* (*86*–*89*), and the disulfide isomerase *AGR2*, which is essential for mucus production (*90*). Furthermore, vampire bats lost *ERN2*, an endoplasmic reticulum (ER) stress sensor that regulates the unfolded protein response factor XBP1 (*91*), likely reflecting reduced ER stress due to diminished production of large glycoproteins such as the 5,654 amino acid MUC5AC.

Changes and losses of these genes predict reduced gastric mucus production. To experimentally investigate this, we performed histological analyses of the fundic stomach region in *Desmodus*, *Diphylla*, *Artibeus lituratus*, and *Myotis nigricans*. Periodic acid-Schiff/Alcian blue staining, which stains mucus-secreting cells, showed the expected abundance of mucus-producing cells in *A. lituratus* and *M. nigricans*, but a markedly reduced staining in *Desmodus* and *Diphylla* (Fig. 2I).

Several factors likely account for the altered gastric mucus profile in vampire bats. First, the protective function of mucus against abrasive food and gastric acid is largely obsolete in species that consume only liquid food and lack an acidic stomach. Second, mucin synthesis is energetically costly (*92*), which may contribute to the absence of *MUC5AC* expression. Third, because vampire bats lack both the mucus-crosslinking factor TFF2 and MUC5AC, which forms a stiff, highly branched, viscoelastic mucus network (*78*, *80*, *93*) (Fig. 2H), their gastric mucus likely has reduced viscoelasticity. This reduction facilitates extreme stomach distensibility (Fig. 2E) and may be required for their unique ability to absorb water in the stomach (below). Hence, remodeling the gastric mucus profile is likely adaptive from an evolutionary perspective.

bioRxiv preprint doi: https://doi.org/10.64898/2026.07.24.740446; this version posted July 24, 2026. The copyright holder for this preprint (which was not certified by peer review) is the author/funder, who has granted bioRxiv a license to display the preprint in perpetuity. It is made available under a CC-BY-NC 4.0 International license.

Functional shift of the stomach from digestion to absorption

Unlike other mammals, the highly-vascularized stomach of vampire bats can efficiently absorb water, which facilitates rapid water extraction and excretion (*94*–*96*); however, the underlying molecular mechanisms remained unclear. Our transcriptome data suggest that vampire bats primarily utilize the aquaporin AQP5, a water channel normally expressed mainly in salivary, lacrimal and sweat glands, and the respiratory tract (*97*, *98*), for water absorption in the stomach (Fig. 2B,F). Whereas *AQP5* expression is very low in the stomach of non-vampire bats (average rank 10362), it is the top upregulated gene in the vampire bat stomach (943-fold increase) and ranks as the 23th most highly expressed gene in this organ. Another water channel, *AQP1*, is 9-fold upregulated in the vampire bat stomach. Since expression of *AQP5* or *AQP1* induces cellular water permeability (*99*, *100*), the gain of expression of these water channels provides a plausible mechanism for water absorption in the vampire bat stomach.

We further discovered additional gene expression changes that support a transformation of the vampire bat stomach from a digestive to an absorptive organ for electrolytes. Blood has an exceptionally high sodium content, ~34-fold higher than a typical human diet (Supplementary Note 4), and common vampire bats excrete most dietary sodium through urine within the first hour after feeding (*101*). This rapid excretion indicates that dietary sodium is already absorbed in the stomach along with water. Indeed, consistent with the enriched term “sodium ion transport” (Fig. 1I), our transcriptome data show that both subunits of the sodium/potassium ATPase (*ATP1A1*, *ATP1B1*) and all three subunits of the epithelial sodium channel αβγ-ENaC (*SCNN1A*, *SCNN1B*, *SCNN1G*), which are normally important for intestinal absorption and renal reabsorption of sodium (*102*), are highly upregulated in the vampire bat stomach (Fig. 2B,F). Interestingly, the δ-ENaC subunit (*SCNN1D*), which can replace the α subunit to form δβγ-ENaC, is downregulated in the stomach. This can be explained by the pH-neutral environment in the vampire bat stomach, because the downregulated δβγ-ENaC is inactive at pH>6.5, whereas the upregulated αβγ-ENaC exhibits maximal activity under pH-neutral conditions (*103*, *104*). High *ATP1A1*/*ATP1B1* expression further aligns with previous observations of a high sodium/potassium ATPase activity in the common vampire bat, and sodium absorption could create an osmotic drive that enhances the water absorption (*94*). High rates of sodium cation uptake raise the question of how vampire bats maintain electroneutrality. We found the chloride transporter gene *SLC26A9* (*105*, *106*) to be 10-fold upregulated and among the most upregulated genes in the vampire bat stomach (Fig. 2B,F); this upregulation likely enhances chloride anion absorption to facilitate electroneutrality.

In addition to electrolytes, we detected expression shifts indicating uptake of the essential vitamins B1, B9, and B12 in the stomach (Fig. 2B,F), consistent with the enrichment of “vitamin digestion and absorption” (Fig. 1I). Intestinal uptake of vitamin B1 (thiamine) is mediated by *SLC19A3* (*107*, *108*). We found this gene to be upregulated in the vampire bat stomach, indicating that thiamine uptake also occurs in this organ. Intestinal uptake of vitamin B9 (folate) requires FOLH1, which hydrolyzes the dietary form of folate (polyglutamate-folate), enabling monoglutamate-folate uptake across the brush border membrane by SLC46A1 and SLC19A1 (*109*, *110*). All three genes are upregulated in the vampire bat stomach. These genes are also highly expressed in the intestine, with *FOLH1* being the third-most strongly upregulated gene (602-fold) in this organ. Finally, *TCN2*, encoding the vitamin B12 transport protein transcobalamin

bioRxiv preprint doi: https://doi.org/10.64898/2026.07.24.740446; this version posted July 24, 2026. The copyright holder for this preprint (which was not certified by peer review) is the author/funder, who has granted bioRxiv a license to display the preprint in perpetuity. It is made available under a CC-BY-NC 4.0 International license.

II (*111*), is upregulated in the stomach. Together, these findings indicate enhanced folate and vitamin B12 absorption in vampire bats, which is likely important for their elevated erythropoiesis (see below).

Finally, *PTGS1* and *PTGIS*, encoding the two enzymes that produce platelet-inhibiting prostacyclins, are upregulated in the vampire bat stomach (Fig. 2B), which likely helps to prevent clotting of the ingested blood and could facilitate regurgitating blood to roost mates. Overall, these expression shifts provide strong evidence that the vampire bat stomach has been evolutionarily repurposed into an absorptive organ.

Altered gastrointestinal motility

We identified losses of several genes regulating gastrointestinal motility in vampire bats (Supplementary Figures 12-13). The gene encoding the peptide hormone motilin (*MLN)* is lost in *Diaemus* and *Diphylla*, and the motilin receptor gene *MLNR* is lost in *Desmodus* and *Diaemus* and exhibits a strong signal of relaxed selection in vampire bats. In most mammals, motilin regulates fasting state gastrointestinal motility by initiating phase III contractions of the migrating motor complex, which clear the intestinal lumen during the interdigestive period (*112*). Consistent with losses of *MLN* and *MLNR*, motilin-producing endocrine cells are absent from the gastrointestinal tract of *Desmodus* (*113*), suggesting that intestinal cleansing is less important for species adapted to an exclusively liquid blood diet with little indigestible material. In addition, the galanin receptor *GALR2*, which stimulates gastrointestinal motility (*114*, *115*), is lost in all vampire bats. Together, these gene losses indicate altered gastrointestinal motility in vampire bats.

To experimentally investigate this, we examined gastrointestinal movement in *Desmodus* (n=3) and *Diphylla* (n=2), alongside three control species. In contrast to *Phyllostomus discolor* (n=2), *Artibeus lituratus* (n=2), and mice (n=3), vampire bats exhibited no detectable gastrointestinal motility (Supplementary Videos 1-5). We deliberately stimulated motility using neostigmine (0.5 mg/mL), a cholinesterase inhibitor that induces gastrointestinal motility in mammals. Whereas neostigmine elicited the expected robust movements in *Artibeus lituratus*, *Phyllostomus discolor*, and mice, vampire bats showed no response (Supplementary Videos 1-5). Together, these experiments reveal that, in adaptation to their exclusively liquid diet, vampire bats have altered gastrointestinal motility.

Reduction of protein digestive enzymes and increased trypsin dependence

Our analyses uncovered losses or relaxed evolutionary constraint on several genes encoding zymogens that digest dietary proteins (Fig. 3A, Supplementary Figures 14-17). *PGC,* encoding the inactive pepsinogen C precursor secreted by gastric chief cells, evolved under relaxation in vampire bats (Fig. 2F). Since pepsinogen C requires an acidic environment (pH<5) for autocatalytic activation (*116*), the neutral stomach pH in vampire bats provides an explanation for relaxation. Among the digestive enzymes secreted by the exocrine pancreas, chymotrypsinogen B2 (*CTRB2)* and the chymotrypsin-like protease (*CTRL)* are lost in all vampire bats. Elastase-1 (*CELA1*) is lost in *Diaemus*, evolves under relaxation in all vampire bats, and is not expressed in the *Desmodus* pancreas (FDR=2.5e-8, Supplementary Table 7). Pancreatic carboxypeptidase A2 (*CPA2*) is lost in *Diphylla* only. Although the reduced repertoire of protein-digestive enzymes in

bioRxiv preprint doi: https://doi.org/10.64898/2026.07.24.740446; this version posted July 24, 2026. The copyright holder for this preprint (which was not certified by peer review) is the author/funder, who has granted bioRxiv a license to display the preprint in perpetuity. It is made available under a CC-BY-NC 4.0 International license.

vampire bats may seem counterintuitive, blood provides a limited diversity of readily digestible proteins, dominated by the soluble globular proteins hemoglobin and albumin. Hence, the larger enzyme repertoire required to digest the protein complexity contained in other diets may be unnecessary for vampire bats.

In contrast to losses of digestive proteases, we found that the pancreatic trypsin-encoding gene *PRSS1* expanded into two copies in *Diphylla* and *Diaemus* and three copies in *Desmodus*. Interestingly, gene tree analysis revealed a complex duplication history with independent trypsin duplications in the *Desmodus*/*Diaemus* and in the *Diphylla* lineage, followed by another duplication in *Desmodus* (Fig. 3B, Supplementary Figure 18). All trypsin copies are expressed in the pancreas of *Diphylla* and *Desmodus* (Fig. 3C,D), likely increasing the trypsin pool. Furthermore, because CTRB2 and CTRL can cleave and degrade trypsinogens (*117*, *118*), their loss could also contribute to an increased trypsin pool. Finally, *SPINK1*, a serine protease inhibitor that protects the pancreas from prematurely activated trypsinogen (*119*), is upregulated in the vampire bat pancreas (FDR 1.3e-5, Supplementary Table 6). Overall, our analysis indicates that while the importance of several digestive proteases decreased, trypsin became increasingly important for vampire bats, likely reflecting the low diversity and high digestibility of blood proteins.

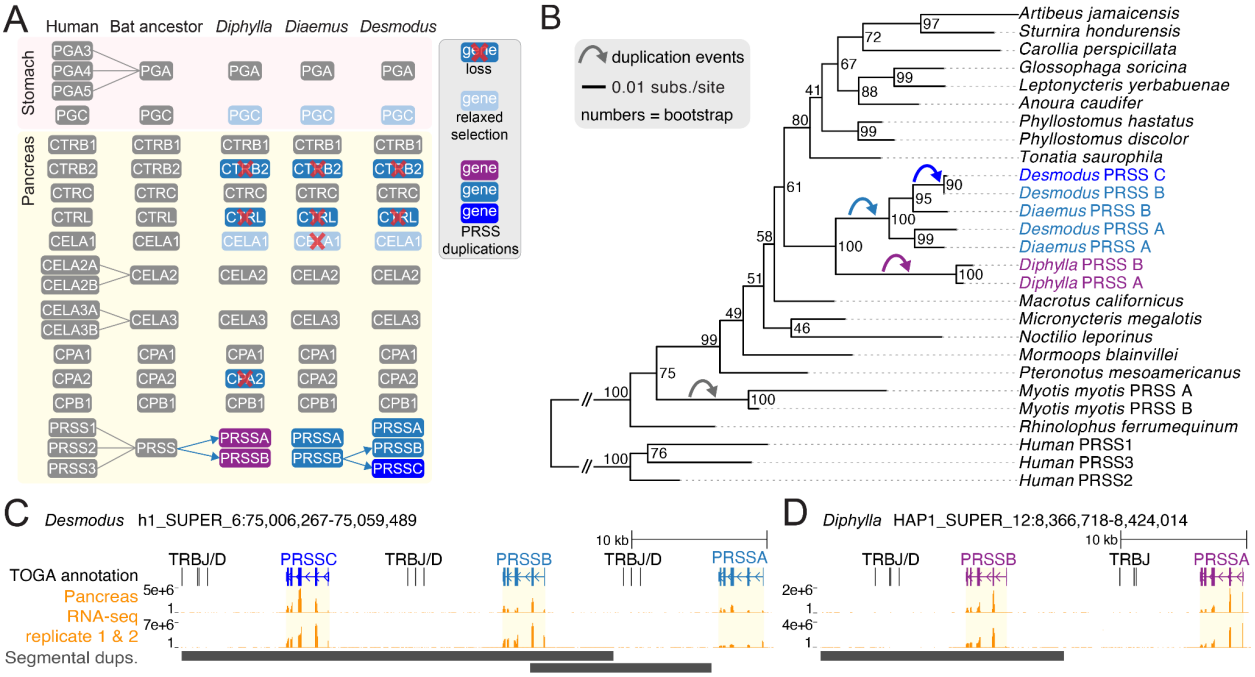


Figure 3: Protein digestion and independent trypsin duplications.

(A) Evolution and changes in protein digestive enzymes in the stomach and pancreas. Trypsin (PRSS) gene colors match panels B-D.

(B) Maximum likelihood tree generated with IQ-TREE v1.6.12 (*120*) showing that the phyllostomid ancestor possessed a single pancreatic trypsin that is co-orthologous to human *PRSS1-3*. This gene independently duplicated in vampire bats. *Myotis myotis* exhibits an independent trypsin duplication, supported by its sister species *Myotis daubentonii* (not shown).

bioRxiv preprint doi: https://doi.org/10.64898/2026.07.24.740446; this version posted July 24, 2026. The copyright holder for this preprint (which was not certified by peer review) is the author/funder, who has granted bioRxiv a license to display the preprint in perpetuity. It is made available under a CC-BY-NC 4.0 International license.

(C,D) Genome browser screenshots showing the expanded trypsin genes in *Desmodus* (C) and *Diphylla* (D) (top) and that they are all expressed in pancreas. Segmental duplications (bottom) were inferred with BISER (*121*).

Increased reliance on intestinal absorption and renal reabsorption of amino acids

After protein digestion, amino acids are absorbed in the small intestine by multiple transporters (*122*). We found that in vampire bats many intestinal amino acid transporters show slightly elevated expression, with *SLC6A20* and *SLC16A10* significantly upregulated, and multiple transporters evolve under intensified selection (Fig. 4A). Notably, *SLC6A19*, encoding the only neutral amino acid transporter at the apical membrane of enterocytes, shows strong intensified selection and is the most highly expressed amino acid transporter in the small intestine of bats. *SLC6A19* is essential for intestinal absorption of branched-chain and aromatic amino acids, which is severely impaired in humans or mice lacking this gene (*122*, *123*). In the large intestine, two additional transporters for neutral amino acids (*SLC1A5*) and glycine, proline, alanine (*SLC36A1*) are also under intensified selection.

To prevent amino acid loss in urine, the kidney reabsorbs amino acids using transporters often shared with the intestine (*124*). The three intestinal transporters under intensified selection (*SLC6A19*, *SLC1A5*, *SLC36A1*) also function in renal reabsorption, with *SLC6A19* and *SLC1A5* being the most highly expressed kidney transporters in bats (Fig. 4B). Furthermore, we observed intensified selection on three additional renal transporters: *SLC6A18* (transporting glycine and alanine), *SLC7A6* (arginine and lysine) and *SLC6A12* (alanine) (*124*, *125*). Together, these intensified selection signatures and expression shifts indicate increased importance of intestinal absorption and renal reabsorption of amino acids in vampire bats.

bioRxiv preprint doi: https://doi.org/10.64898/2026.07.24.740446; this version posted July 24, 2026. The copyright holder for this preprint (which was not certified by peer review) is the author/funder, who has granted bioRxiv a license to display the preprint in perpetuity. It is made available under a CC-BY-NC 4.0 International license.

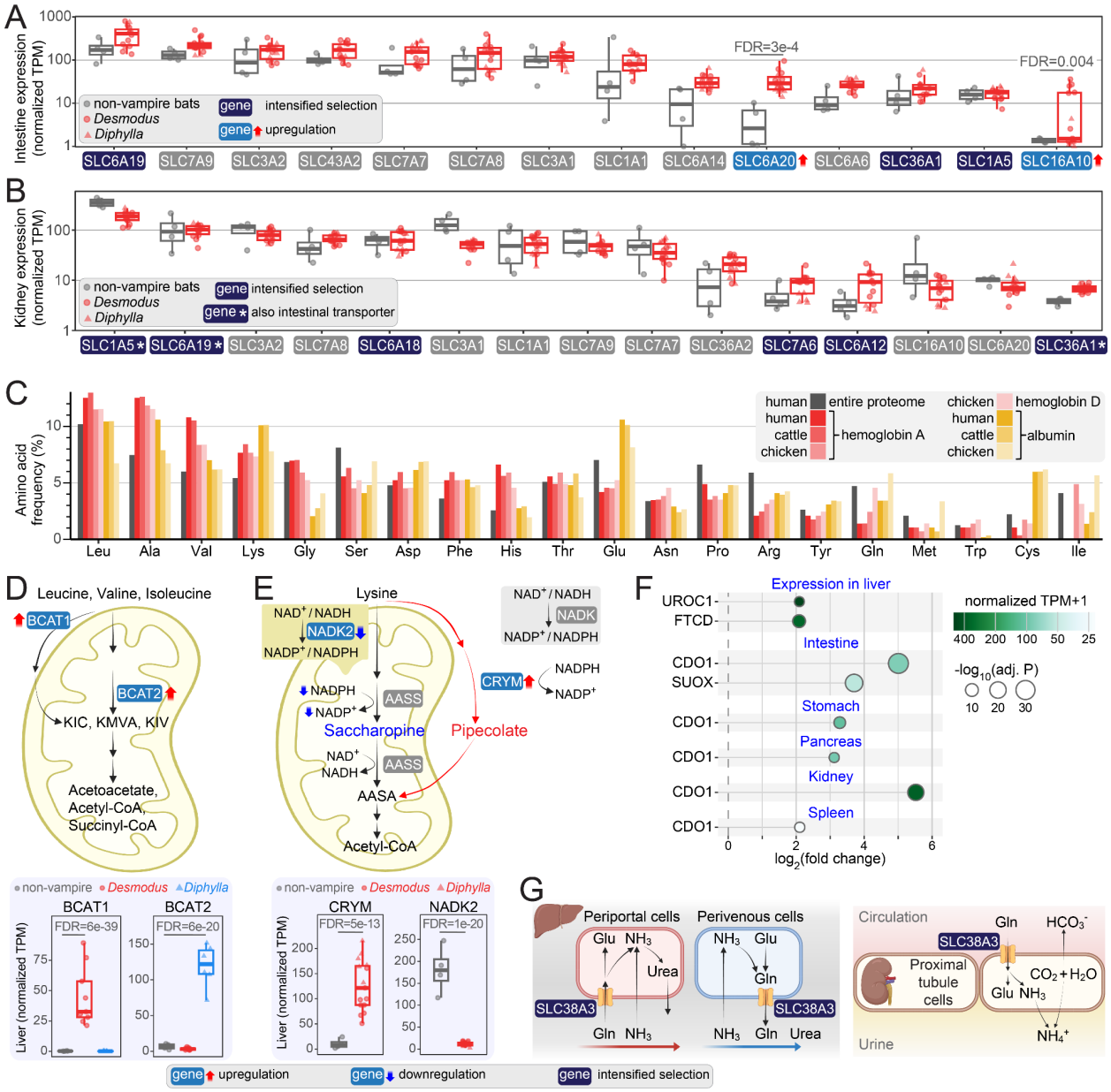


Figure 4: Amino acid transport and catabolism.

(A-B) Expression of intestinal (A) and renal (B) amino acid transporters, ordering genes by vampire bat expression levels, and highlighting genes under intensified selection. Asterisks in (B) highlight intensified transporters mediating both intestinal absorption and renal reabsorption.

(C) Amino acid frequency in all human protein-coding genes in comparison to the most abundant whole blood proteins in mammals and birds. Amino acids are ordered according to cattle hemoglobin A.

(D) Illustration of the initial steps of branched-chain amino acid catabolism, showing the liver upregulation of *BCAT1* in *Desmodus* and *BCAT2* in *Diphylla* at the bottom.

(E) Upregulation of *CRYM* (bottom), the key enzyme in the pipecolate lysine-catabolizing pathway. The saccharopine lysine-catabolizing pathway likely has reduced activity, as it depends

bioRxiv preprint doi: https://doi.org/10.64898/2026.07.24.740446; this version posted July 24, 2026. The copyright holder for this preprint (which was not certified by peer review) is the author/funder, who has granted bioRxiv a license to display the preprint in perpetuity. It is made available under a CC-BY-NC 4.0 International license.

on mitochondrial NADPH and the mitochondrial NADP-generating enzyme *NADK2* is the fourth most significantly downregulated liver gene (12-fold).
(F) Differential expression of genes involved in amino acid catabolism, showing fold change (X-axis), expression level (normalized TPM as a color gradient) and significance (circle size).
(G) Intensified selection on the glutamine transporter *SLC38A3*, which is highly expressed in the liver and kidney of all studied bats. In the liver, SLC38A3 imports glutamine into periportal hepatocytes for hydrolysis to glutamate and ammonia and urea-cycle entry, and exports glutamine from perivenous hepatocytes that condense scavenged ammonia with glutamate via glutamine synthetase. In the kidney, SLC38A3 imports glutamine into proximal tubule cells, where it is metabolized to generate ammonia for urinary ammonium excretion and bicarbonate, which is returned to the blood for pH restoration.

Upregulated amino acid catabolism

Amino acids are the main energy source for vampire bats (*18*). Our analyses provide molecular insights into this energy metabolism shift by revealing upregulation and intensification of key genes in multiple amino acid catabolic pathways, especially those metabolizing amino acids abundant in blood (Leu, Val, Lys; Fig. 4C).

Unlike other amino acids, the initial step of branched-chain amino acid (leucine, valine and isoleucine) catabolism does not occur in liver, because this organ normally lacks the transaminases *BCAT1* and *BCAT2* that catalyze the first reaction (*126*, *127*). In contrast to other mammals, we detected liver expression of *BCAT1* in *Desmodus* and *BCAT2* in *Diphylla* (Fig. 4D), indicating active utilization of branched-chain amino acids as fuel molecules.

Lysine, the fourth most abundant amino acid in blood (*128*), is catabolized via two distinct pathways. The mitochondrial saccharopine pathway predominates in extracerebral tissues, while the pipecolate pathway is restricted to the adult brain (*129*, *130*). However, the saccharopine pathway enzyme AASS is strictly dependent on NADPH (*129*, *130*) and mitochondria of vampire bat liver cells are likely highly deficient in NADP/NADPH, as the mitochondrial NADP-generating enzyme *NADK2* is severely downregulated (Fig. 4E). Because mutations in human *NADK2* impair lysine degradation and cause hyperlysinemia (*131*), the saccharopine pathway likely plays a minor role in vampire bats. Compensating for this, we discovered that *CRYM*, a key enzyme in the pipecolate pathway, is upregulated in both liver and intestine (Fig. 4E). Although CRYM is also NADPH-dependent, it is located in the cytoplasm, where NADPH is not restricted in vampire bats (below). Therefore, the pipecolate pathway may have replaced the saccharopine pathway as the major mechanism for lysine degradation in vampire bats.

While histidine is the second rarest amino acid in human whole body proteins (*132*), it is an abundant amino acid in blood (Fig. 4C). Consistent with vampire bats having a greater dependence of histidine as an energy source, *UROC1* and *FTCD*, two enzymes in the histidine catabolism pathway, are upregulated in the liver (Fig. 4F). Cysteine is a frequent amino acid in albumin (~6% of the mature human or cow albumin residues are Cys), an abundant blood plasma protein (Fig. 4C). The rate-limiting cysteine catabolizing enzyme is *CDO1*, which prevents

bioRxiv preprint doi: https://doi.org/10.64898/2026.07.24.740446; this version posted July 24, 2026. The copyright holder for this preprint (which was not certified by peer review) is the author/funder, who has granted bioRxiv a license to display the preprint in perpetuity. It is made available under a CC-BY-NC 4.0 International license.

oxidative stress and cytotoxicity caused by abnormally elevated cysteine levels (*133*, *134*). While *CDO1* is highly expressed in the liver of all analyzed bat species, we found an upregulation of *CDO1* in vampire bats in all five non-hepatic tissues examined (intestine, stomach, pancreas, kidney, spleen) (Fig. 4F). Cysteine catabolism produces toxic sulfite. Sulfite oxidase (encoded by *SUOX*) detoxifies sulfite to sulfate (*135*) and is upregulated in the vampire bat intestine. Together, this indicates an enhanced importance of cysteine catabolism in non-hepatic tissues. Finally, tryptophan is primarily catabolized via the kynurenine pathway, and TDO2 (tryptophan 2,3-dioxygenase), which encodes the first and rate-limiting enzyme of this pathway, is under intensified selection (Supplementary Table 4).

High reliance on amino acid catabolism imposes two systemic challenges: (i) ammonia toxicity and (ii) metabolic acidosis from catabolized ketonic and sulfur-containing amino acids (*136*, *137*). We found that *SLC38A3*, a glutamine transporter essential for both processes (*138–140*), evolved under intensified selection in vampire bats (Fig. 4G). Since the ancestor of phyllostomid bats lost the related *SLC38A5* transporter gene (Supplementary Figure 19), vampire bats rely particularly on the conserved *SLC38A3* to avoid ammonia toxicity and metabolic acidosis.

Impaired fat digestion

Vampire bats consume an extremely fat-poor diet. We uncovered losses, relaxation and downregulation of key genes required for fat digestion (Fig. 5A-D, Supplementary Figures 20-21). The *LIPF* gene, encoding the gastric lipase that is secreted by the gastric chief cells, is lost in all phyllostomid bats analyzed in this study. The carboxyl ester lipase (*CEL*) is downregulated in the vampire bat pancreas. Most strikingly, pancreatic triglyceride lipase (PNLIP), the primary enzyme for dietary fat digestion, is lost in *Diaemus* and not expressed in the pancreas of *Diphylla* and *Desmodus*. *PNLIP* also exhibits a polymorphic stop codon in *Desmodus*, a potential indication of an early stage of *PNLIP* loss. Overall, the lack of the major enzyme for dietary fat digestion evolved independently in all three vampire bats.

Triglyceride digestion results in fatty acids and monoacylglycerol, which enterocytes absorb and reassemble into triglycerides. *DGAT1*, encoding the enzyme catalyzing the final triglyceride reassembly step (*141*), is under relaxed selection in vampire bats (Fig. 5A). Taken together, these results indicate a substantially reduced capacity for fat digestion in adult vampire bats.

Notably, major enzymes responsible for digesting milk fat in infants (pancreatic lipase related protein 2 (*PNLIPRP2*) and *CEL* (*142*, *143*)) are intact in vampire bats. Genes in the bile acid synthesis pathway are also intact and expressed at normal levels (Supplementary Figure 22), which likely ensures the absorption of fat-soluble vitamins (A, D, E, K), cholesterol, and essential fatty acids, and excretion of the heme degradation product bilirubin (*144*, *145*).

bioRxiv preprint doi: https://doi.org/10.64898/2026.07.24.740446; this version posted July 24, 2026. The copyright holder for this preprint (which was not certified by peer review) is the author/funder, who has granted bioRxiv a license to display the preprint in perpetuity. It is made available under a CC-BY-NC 4.0 International license.

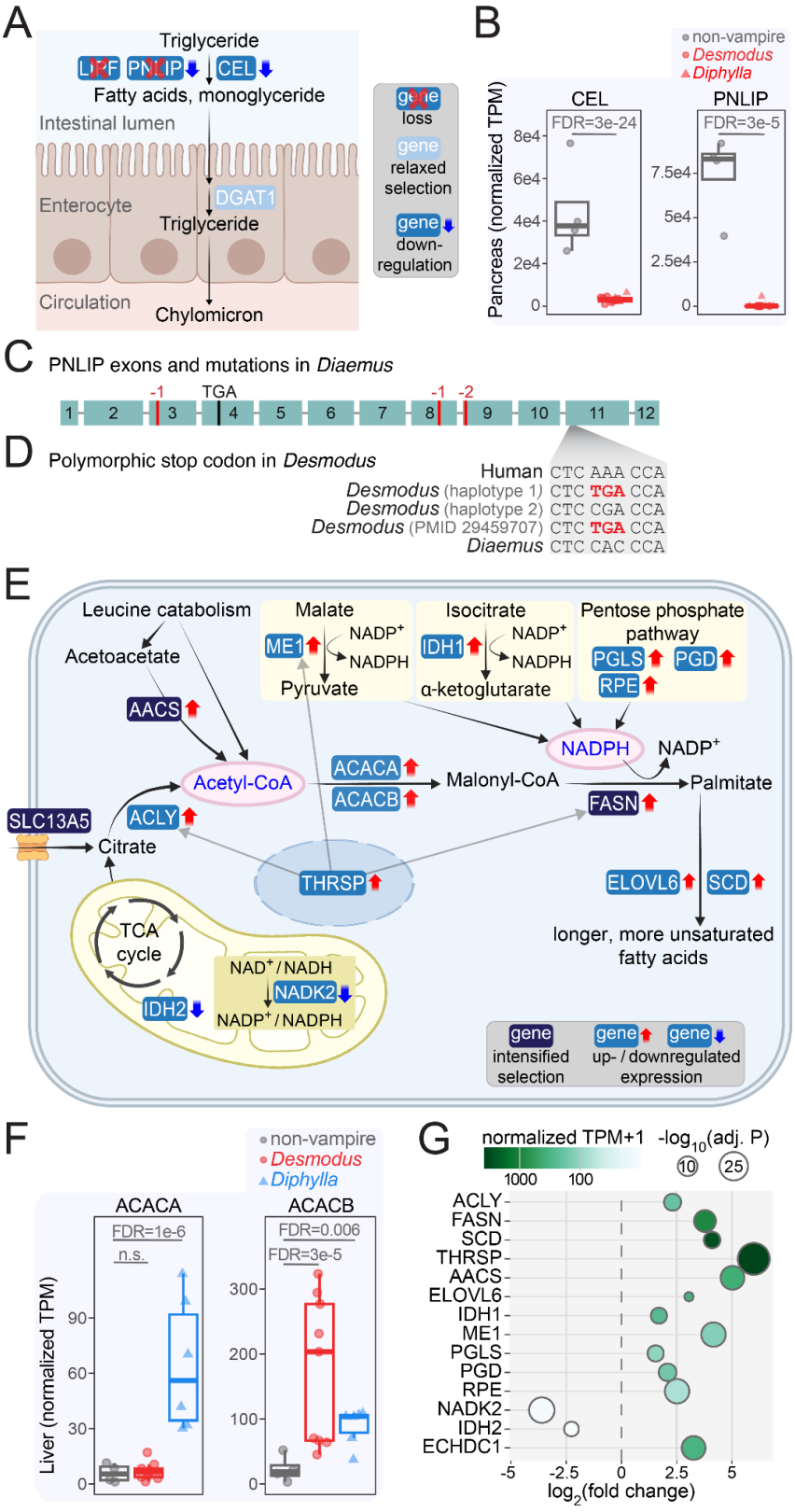


Figure 5: Impaired fat digestion and upregulated fatty acid synthesis

(A) Illustration of intestinal triglyceride digestion and vampire bat changes in key enzymes.

bioRxiv preprint doi: https://doi.org/10.64898/2026.07.24.740446; this version posted July 24, 2026. The copyright holder for this preprint (which was not certified by peer review) is the author/funder, who has granted bioRxiv a license to display the preprint in perpetuity. It is made available under a CC-BY-NC 4.0 International license.

(B) Downregulated pancreas expression of *CEL* and *PNLIP*.
(C) Visualization of the coding exons of *PNLIP* in *Diaemus* showing gene-inactivating mutations inferred by TOGA.
(D) Polymorphic stop codon in *PNLIP* exon 11, found in haplotype 1 of our *Desmodus* assembly and the previous assembly of a different individual (*25*).
(E) Illustration of hepatic fatty acid synthesis, highlighting genes with expression changes and intensified selection.
(F) Liver expression of *ACACB*, upregulated in both vampire bats, and *ACACA*, upregulated in *Diphylla*.
(G) Differential expression of genes involved in fatty acid synthesis in the liver, showing fold change (X-axis), expression level (normalized TPM as the color gradient) and significance (circle size). Genes are ordered as discussed in the text.

Highly active hepatic *de novo* fatty acid synthesis

Since their diet is extremely poor in fat, vampire bats must synthesize fatty acids from non-lipid precursors. Here we show that *de novo* fatty acid synthesis to be drastically upregulated. This process occurs in the cytosol and requires two main substrates, acetyl-CoA and NADPH.

The first substrate (cytosolic acetyl-CoA) is mainly derived from citrate exported from mitochondria. In vampire bats, the enzyme-encoding genes that convert citrate to the fatty acid palmitate (ATP citrate lyase (*ACLY*), acetyl-CoA carboxylase (*ACACB*), fatty acid synthase (*FASN*)) are strongly upregulated in the liver (Fig. 5E-G). *FASN* also evolved under intensified selection and another acetyl-CoA carboxylase, *ACACA,* is upregulated in *Diphylla* (Fig. 5F). *SCD*, which elongates FASN-generated palmitate into longer fatty acids, is also upregulated. Consistent with enhanced fatty acid synthesis, *THRSP*, a nuclear factor that induces *ACLY*, *FASN* and malic enzyme (*ME1*, discussed below) expression (*146*, *147*), is the third-most upregulated gene in the vampire bat liver. Additionally, *SLC13A5*, a high-capacity transporter importing extracellular citrate into the cytoplasm (*148*), evolved under intensified selection.

Acetyl-CoA can also be generated from catabolism of blood-abundant leucine (Fig. 3F), which yields both acetyl-CoA and the ketone body acetoacetate. In the cytosol, acetoacetate can be converted by AACS into acetoacetyl-CoA (consisting of two acetyl-CoA molecules) to fuel *de novo* fatty acid and cholesterol synthesis (*149*, *150*). We found that *AACS* evolved under intensified selection and is one of the most significantly upregulated genes in the vampire bat liver (36-fold; rank 5, Fig. 5E,G), while being barely expressed in other bats. AACS also contributes to the elongation of polyunsaturated fatty acids via elongases (*151*), and we found the elongase gene *ELOVL*6 upregulated in the vampire bat liver. While the *AACS* pathway plays a minor or condition-specific role in human and mouse (*150*), intensified selection and upregulated *AACS* expression indicate that leucine-derived acetoacetyl-CoA is a major substrate for fatty acid and cholesterol synthesis in vampire bats.

The second substrate for fatty acid synthesis (cytosolic NADPH) can be generated from three main sources: (i) the pentose phosphate pathway, which generates two NADPH molecules, (ii)

bioRxiv preprint doi: https://doi.org/10.64898/2026.07.24.740446; this version posted July 24, 2026. The copyright holder for this preprint (which was not certified by peer review) is the author/funder, who has granted bioRxiv a license to display the preprint in perpetuity. It is made available under a CC-BY-NC 4.0 International license.

IDH1, which converts isocitrate to α-ketoglutarate, and (iii) ME1, which converts malate to pyruvate (*152*). The vampire bat liver exhibits a significant upregulation of *PGLS*, *PGD* and *RPE* in the pentose phosphate pathway, *IDH1* as well as *ME1*, indicating that all three sources contribute to NADPH production (Fig. 5E,G). Whereas the substrates for the pentose phosphate pathway and *IDH1* are primarily derived from glucose, which is limited in the vampire bat diet, the ME1 substrate (malate) is readily produced by catabolism of abundant dietary amino acids via the urea cycle. This likely explains why the malate-consuming *ME1* is the most upregulated of these three pathways (17-fold, rank 4). Together, intensified selection signatures and coordinated transcriptional upregulation indicate that fatty acid synthesis is considerably elevated in vampire bats, likely as an adaptation to their fat-poor diet.

The only mechanism of *de novo* NADP(H) generation is the phosphorylation of NAD+, which is executed by *NADK* in the cytosol and by *NADK2* in mitochondria (*153*). While *NADK* is broadly expressed and shows no expression difference in vampire bats, *NADK2*, which is highly expressed in the liver of humans and non-vampire bats, is drastically downregulated in the vampire bat liver (12-fold, rank 4) (Fig. 4E,5E,5G). Furthermore, *IDH2*, encoding the mitochondrial NADP+-dependent enzyme that generates NADPH during isocitrate to α-ketoglutarate conversion, is also downregulated in the vampire bat liver. This suggests a highly unusual situation of low mitochondrial but high cytosolic hepatic NADP(H) levels. Low mitochondrial NADP(H) provides a mechanism to inhibit DECR1, the rate-limiting NADPH-dependent enzyme crucial for β-oxidation of polyunsaturated fatty acids (*154*, *155*), which may indirectly increase the cytosolic NADPH pool and thereby enhance fatty acid synthesis.

The promiscuous FASN enzyme can utilize side products of branched-chain amino acid catabolism, such as methylmalonyl-CoA or ethylmalonyl-CoA, in place of acetyl-CoA, thereby producing branched-chain fatty acids that get incorporated into phospholipids and perturb membrane fluidity. *ECHDC1*, encoding the enzyme preventing branched-chain fatty acid formation (*156*), is highly upregulated in the vampire bat liver (rank: 12, Fig. 5E,G), likely because of increased branched-chain amino acid catabolism.

Decreased reliance on sugar as an energy source

While sugars are a major energy source for many mammals, blood contains extremely low levels of carbohydrates (1%) (*14*, *15*), indicating that vampire bats depend less on sugar as energy source. Our integrative analysis revealed genetic mechanisms underlying vampire bats' decreased capacity to digest, metabolize, and store sugars.

SI, encoding the intestinal brush border sucrase-isomaltase enzyme that cleaves dietary disaccharides into glucose and fructose (*157*), is lost in *Diphylla* and exhibits polymorphic gene-inactivating mutations in *Diaemus* (Fig. 6A, Supplementary Figure 23). The rate-limiting step of aerobic glucose oxidation is catalyzed by the pyruvate dehydrogenase complex (PDC), which converts pyruvate to acetyl-CoA and connects cytosolic glycolysis with the mitochondrial TCA cycle and oxidative phosphorylation (*158–160*). We found *PDHA1* and *PDHB*, which encode the catalytic PDC subunits, to evolve under relaxed selection in vampire bats (Fig. 6B). Notably, numerous mutations affecting the PDC, particularly the *PDHA1* gene, cause lactic acidosis in

bioRxiv preprint doi: https://doi.org/10.64898/2026.07.24.740446; this version posted July 24, 2026. The copyright holder for this preprint (which was not certified by peer review) is the author/funder, who has granted bioRxiv a license to display the preprint in perpetuity. It is made available under a CC-BY-NC 4.0 International license.

humans, which is treated with a ketogenic diet to avoid the glycolytic overproduction of the PDC substrate pyruvate (*158*, *159*, *161*); this therapeutic strategy resembling the natural low-sugar vampire bat diet. Genes involved in fructose catabolism (*KHK* and *TKFC*) are downregulated in the vampire bat liver and kidney (Fig. 6C,D), reflecting the extremely low fructose content of blood, with concentrations even lower than glucose (*162*).

Glucose is primarily stored as glycogen. Protein phosphatase 1 promotes glycogen synthesis and inhibits glycogen breakdown by dephosphorylating glycogen synthase and glycogen phosphorylase, respectively (*163*, *164*). The regulatory subunit of protein phosphatase 1 encoded by *PPP1R3E*, previously found to be lost in *Desmodus* (*30*), is independently lost in all vampire bats (Supplementary Figure 24), consistent with reduced glycogen synthesis. Supporting this, we observed hepatic downregulation of *GYS2*, encoding the liver glycogen synthase, *PYGL*, encoding the liver form of glycogen phosphorylase, and *PGM1* (phosphoglucomutase 1), which interconverts glucose-1-phosphate and glucose-6-phosphate for glycogen synthesis and glycogen breakdown (Fig. 6B,D). Together, these changes provide a molecular explanation for the markedly low glycogen stores in *Desmodus*, which are ~85% lower than in fruit-eating bats and ~60% lower than in other mammals fed on high-protein diets (*17*, *165*).

bioRxiv preprint doi: https://doi.org/10.64898/2026.07.24.740446; this version posted July 24, 2026. The copyright holder for this preprint (which was not certified by peer review) is the author/funder, who has granted bioRxiv a license to display the preprint in perpetuity. It is made available under a CC-BY-NC 4.0 International license.

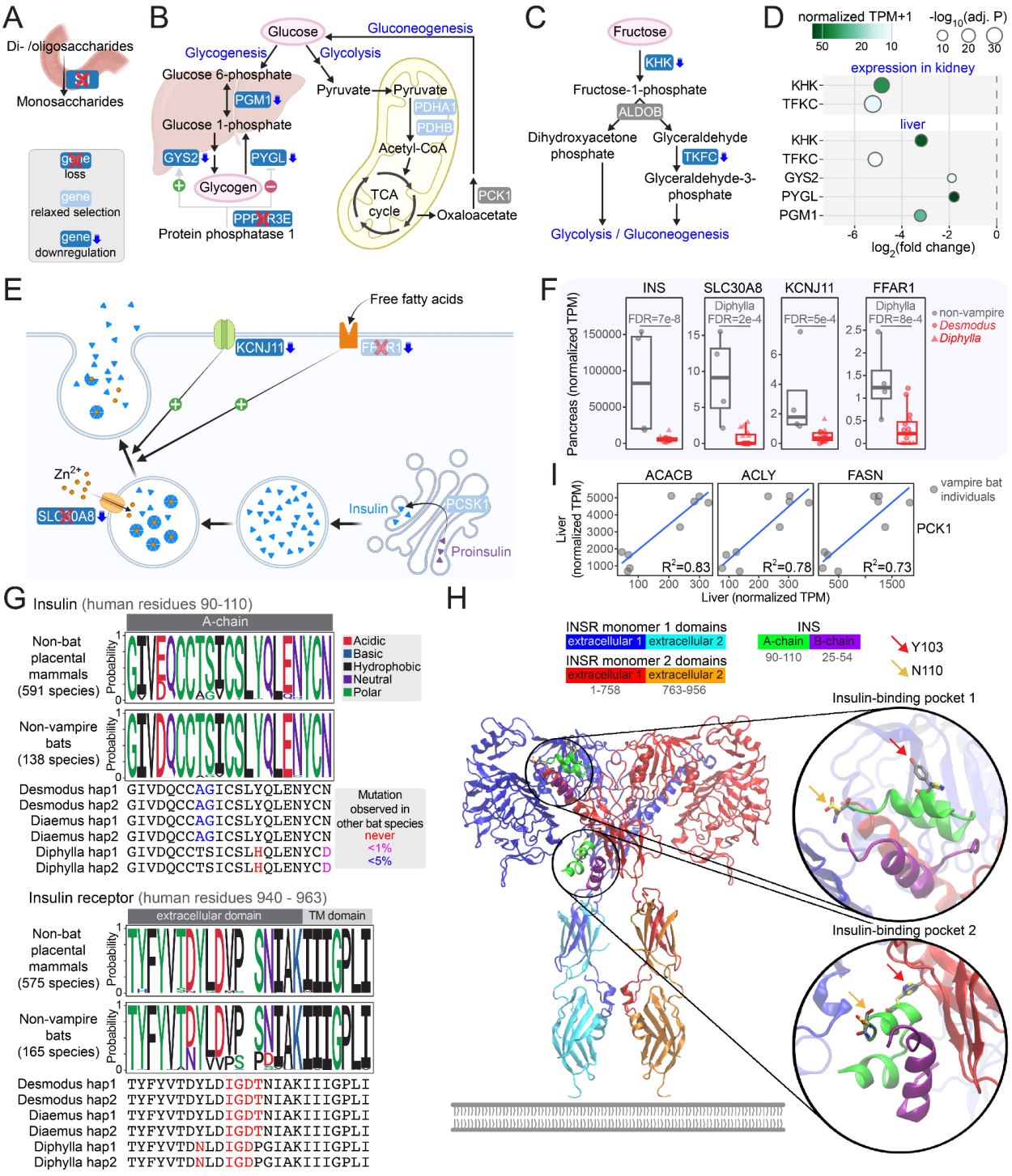


Figure 6: Impaired sugar and insulin metabolism

(A-C) Losses, relaxation and downregulation of genes for intestinal sucrose digestion (A), glucose oxidation and glycogenesis (B), and fructose catabolism (C).

(D) Differential expression of genes involved in sugar metabolism, showing fold change (X-axis), expression level (normalized TPM as the color gradient) and significance (circle size).

(E) Sequence and expression changes in genes important for insulin storage and secretion. Schematics as in (A).

bioRxiv preprint doi: https://doi.org/10.64898/2026.07.24.740446; this version posted July 24, 2026. The copyright holder for this preprint (which was not certified by peer review) is the author/funder, who has granted bioRxiv a license to display the preprint in perpetuity. It is made available under a CC-BY-NC 4.0 International license.

(F) Expression level of insulin and genes involved in insulin secretion.
(G) Mutations in insulin and insulin receptor. Sequence logos represent the relative frequency of residues. The *Diphylla* Y103H and N110D INS mutations occur in no and only one other bat species. Highlighted mutations in vampire bat *INSR* are also never observed in other bats.
(H) Cryo-EM structure of the homodimeric insulin receptor extracellular domain bound to insulin (PDB 6PXV). Close-up views highlight insulin-binding pockets, showing the residues differing between human (Y103 and N110) and *Diphylla* (H103 and D110) INSR with carbon atoms colored grey and yellow, respectively. The transmembrane and intracellular domains are unresolved in the cryo-EM structure; a simplified membrane is therefore shown at the base of the extracellular domain.

Decreased importance of insulin

Vampire bats have smaller pancreatic islets with a reduced beta cell mass, lower insulin levels than other mammals, and exhibit a reduced glucose-stimulated insulin secretion response (*16*, *166*). Here, we uncover molecular underpinnings of their insulin secretion deficiency, revealing that several genes critical for insulin production and secretion are lost, relaxed or downregulated (Fig. 6E-F, Supplementary Figures 25-26). *PCSK1*, encoding the prohormone convertase that processes proinsulin into mature insulin (*167*, *168*), is under strong relaxed selection in vampire bats. *KCNJ11*, encoding a glucose sensitive potassium channel that triggers membrane depolarization and insulin release (*169*, *170*), is downregulated in the vampire bat pancreas. *SLC30A8*, encoding the major beta-cell zinc transporter required for the formation of zinc-insulin crystals (the main insulin storage form) (*171*, *172*), was previously found to be lost in *Desmodus (30)*. Our analysis revealed an independent loss in *Diaemus* and a downregulation in the *Diphylla* pancreas. Similarly, *FFAR1*, encoding a G-protein-coupled receptor that senses circulating free fatty acids and amplifies glucose-stimulated insulin secretion (*173*, *174*), is lost in *Desmodus* and *Diaemus*, unexpressed in *Diphylla*, and exhibits strongly relaxed selection in vampire bats.

Importantly, we found a pronounced decrease in insulin gene expression in the vampire bat pancreas (Fig. 6F). In addition, the alpha chain of vampire bat insulin exhibits amino acid mutations at otherwise highly conserved positions (Fig. 6G). Notably, *Diphylla* exhibits a mutation (Y103H) that occurs in no other bat species. Mutations affecting INS residues 97, 98, and 103 have been reported in human patients with permanent neonatal diabetes (*175*, *176*). The crystal structure of the insulin receptor shows that Y103 is located at the interaction surface with the receptor (insulin-binding pocket 2, Fig. 6H), suggesting that it could influence insulin conformation and receptor interaction. Interestingly, *INSR*, encoding the insulin receptor, showed a signature of positive selection, driven by several consecutive vampire bat–specific amino acid changes, including an insertion. The affected residues lie directly upstream of the transmembrane domain in the extracellular region of INSR, a region critical for insulin-induced structural rearrangements, receptor internalization, and ligand degradation (*177*, *178*). Notably, distinct INSR mutations have also been identified in Mexican tetra cavefish populations, another system exhibiting naturally evolved insulin resistance (*179*). Together, reduced insulin expression and sequence changes in both insulin and its receptor point to attenuated insulin signaling in vampire bats.

bioRxiv preprint doi: https://doi.org/10.64898/2026.07.24.740446; this version posted July 24, 2026. The copyright holder for this preprint (which was not certified by peer review) is the author/funder, who has granted bioRxiv a license to display the preprint in perpetuity. It is made available under a CC-BY-NC 4.0 International license.

Finally, insulin normally suppresses gluconeogenesis while promoting lipogenesis in the liver, leading to an inverse regulation of the two processes. Consistent with insulin deficiency in vampire bats, we observed a positive correlation between the liver expression of *PCK1*, the first-step enzyme of gluconeogenesis, and key lipogenesis genes *ACACB*, *ACLY* and *FASN* (Fig. 6I), indicating a synchronized regulation of gluconeogenesis and lipogenesis. This resembles the situation in type 2 diabetic patients, where insulin resistance impairs the suppression of gluconeogenesis, leading to both gluconeogenesis and lipogenesis occurring at the same time (*180*). For vampire bats, this regulatory paradigm shift is likely favorable, because unlike most mammals that use gluconeogenesis for energy supply during fasting, they use gluconeogenesis to convert amino acids to glucose after feeding.

Upregulated heme iron absorption

Compared to other diets, blood contains considerably higher iron (about 800-fold higher than a typical human diet (*181*)), primarily as heme-bound iron. Although iron absorption normally occurs in the small intestine, our results indicate that the vampire bat stomach has also acquired this capacity. Specifically, their stomach shows an upregulation of the heme transporter genes *SLCO2B1* and *SLC46A1* (*182*, *183*), and heme oxygenase 1 (*HMOX1*), the rate-limiting enzyme that degrades heme to ferrous (Fe^{2+}) iron and biliverdin (*184*) (Fig. 7A,B). Notably, *SLCO2B1* and *HMOX1* are also upregulated in the intestine. We also observed increased stomach expression of ferroportin (*SLC40A1*), the only mammalian iron exporter transporting iron from cells into the bloodstream (*185*), and the liver downregulation of hepcidin (*HAMP*), a hormone that lowers circulating iron levels by promoting ferroportin degradation (*186*). Both changes likely contribute to elevated blood iron levels observed in vampire bats (*30*). Finally, increased stomach expression of two ferroxidase enzymes hephaestin (*HEPH*) and ceruloplasmin (*CP*), which convert ferrous (Fe^{2+}) to ferric (Fe^{3+}) iron, enables transferrin-mediated iron transport in the bloodstream (*187*). In contrast to the upregulation of heme iron–absorbing genes, *CYBRD1*, the plasma membrane ferrireductase required for absorbing free dietary iron (*188*), is ~53-fold downregulated in the intestine (Fig. 7A,B). Whereas most mammals rely on free iron uptake as the main iron source and thus require *CYBRD1*, the abundance of heme iron likely reduces its importance in vampire bats. Together, these findings indicate that both the stomach and intestine of vampire bats adapted to efficiently absorb and metabolize dietary heme-bound iron.

Two intracellular ferrireductases involved in iron recycling exhibit notable changes in vampire bats: *CYB561A3* evolved under positive selection on the ancestral vampire bat branch and *STEAP3* is upregulated in the intestine and spleen (Fig. 7A,C). Both enzymes generate bioavailable ferrous iron in macrophages that engulf defective erythrocytes and recycle iron to sustain erythropoiesis (*189*). In addition, *STEAP3* is found in endosomes of erythroid cells, where it is required for efficient erythropoiesis (*190*, *191*).

While a previous study described an expansion of iron-storing ferritin genes in *Desmodus* (*25*), our reanalysis revealed a single ferritin heavy chain ortholog across bats as well as an ancient, non-vampire bat-specific duplication of the ferritin light chain gene (Supplementary Figures 27-29, Supplementary Table 14). We attribute the previously-reported ferritin expansion to processed

bioRxiv preprint doi: https://doi.org/10.64898/2026.07.24.740446; this version posted July 24, 2026. The copyright holder for this preprint (which was not certified by peer review) is the author/funder, who has granted bioRxiv a license to display the preprint in perpetuity. It is made available under a CC-BY-NC 4.0 International license.

pseudogene copies. Importantly, ferritin processed pseudogenes occur in all analyzed phyllostomid and outgroup bats, hence are unlikely to be related to the iron rich vampire bat diet.

Overall, our findings indicate that vampire bats have evolved mechanisms that promote, rather than limit, the absorption of dietary heme-bound iron.

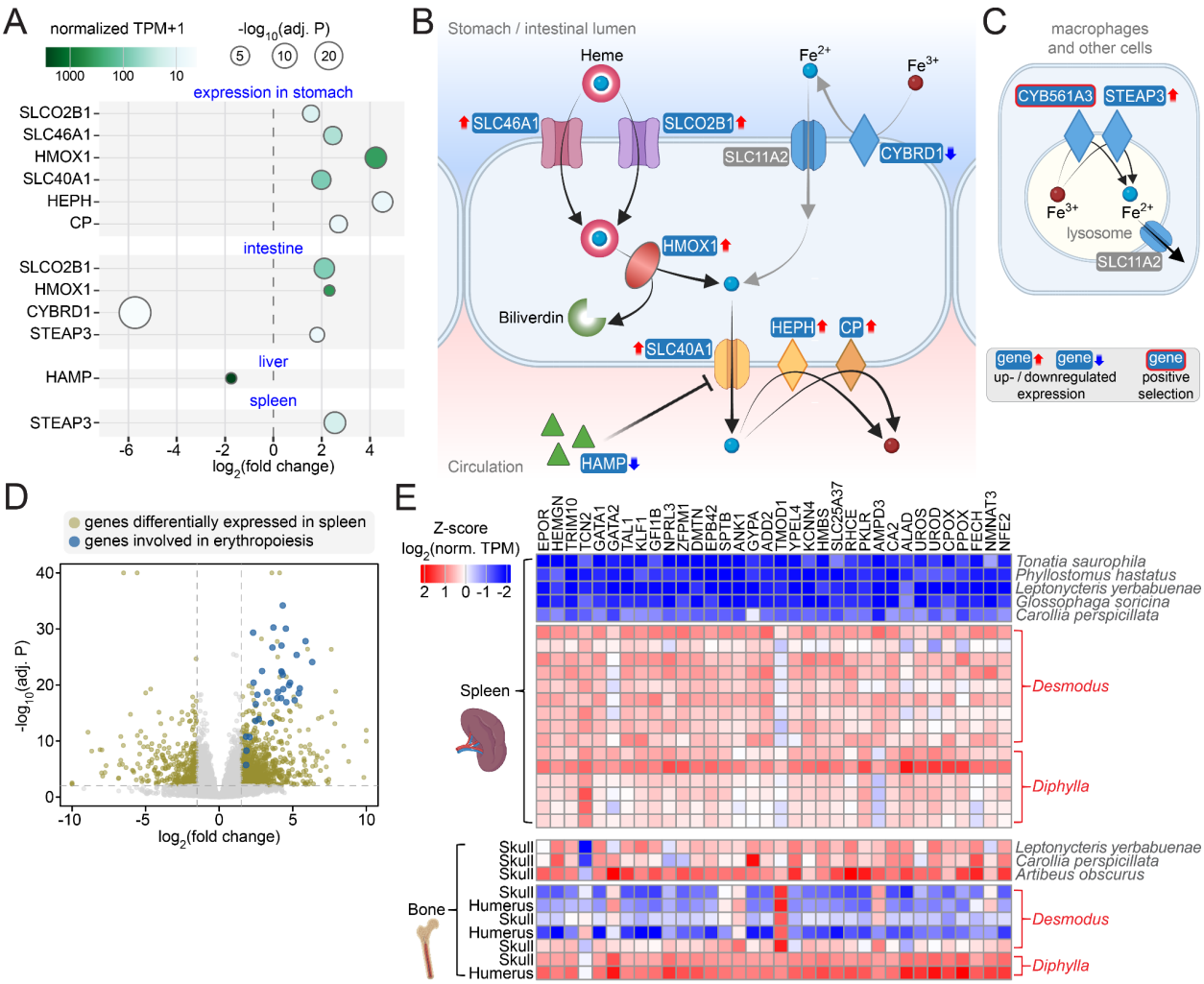


Figure 7: Upregulated heme iron absorption and splenic erythropoiesis.
(A) Differential expression of genes involved in iron absorption, showing fold change (X-axis), expression level (normalized TPM as the color gradient) and significance (circle size).
(B-C) Illustration of sequence and expression changes of genes involved in heme and free iron absorption (B) and iron recycling (C).
(D) Volcano plot showing genes up- and downregulated genes in the vampire bat spleen, highlighting in blue genes directly involved in erythropoiesis.
(E) Expression levels of key erythropoietic genes in adult spleen and bone of vampire (red font) and control bats (black font), visualized as per-gene Z-scores of $\log_2$(normalized TPM + 1).

bioRxiv preprint doi: https://doi.org/10.64898/2026.07.24.740446; this version posted July 24, 2026. The copyright holder for this preprint (which was not certified by peer review) is the author/funder, who has granted bioRxiv a license to display the preprint in perpetuity. It is made available under a CC-BY-NC 4.0 International license.

Vampire bat spleen is an erythropoietic organ

Red blood cell production (erythropoiesis) requires large amounts of iron, vitamin B9, and vitamin B12 (*192*); all appear to be absorbed at elevated levels in vampire bats. In most placental mammals, erythropoiesis occurs primarily in the bone marrow, with the spleen performing erythropoiesis only during fetal development or under stress and pathological conditions in adults (*193*, *194*).

Strikingly, we found strong evidence that the spleen is a major erythropoietic organ in adult vampire bats. Specifically, genes upregulated in the spleen are highly enriched for heme and hemoglobin biosynthesis, and erythrocyte differentiation (Fig. 1I). Of the 50 most significantly upregulated genes, 26 are directly involved in erythropoiesis (Fig. 7D,E). These include genes required for erythroid differentiation (erythropoietin receptor (*EPOR*), hemogen (*HEMGN*), *TRIM10*, *TCN2*, *GATA1*, *GATA2*, *TAL1*, *KLF1*, *GFI1B*, *NPRL3*, *ZFPM1*), erythrocyte membrane stability (*DMTN*, *EPB42*, *SPTB*, *ANK1*, *GYPA*, *ADD2*, *TMOD1*, *YPEL4*) and cell volume regulation (*KCNN4*), iron uptake and hemoglobin synthesis (*STEAP3*, *HMBS*, Mitoferrin-1 (*SLC25A37*)), blood group antigen expression (*RHCE*), erythrocyte metabolism (*PKLR*, *AMPD3*, *CA2*) (*195*–*198*). Nearly all heme biosynthesis genes (*ALAD*, *HMBS*, *UROS*, *UROD*, *CPOX*, *PPOX*, *FECH)* are significantly upregulated. Furthermore, *NMNAT3*, encoding the main NAD+ producing enzyme required for erythrocyte glycolysis and energy metabolism (*199*, *200*), is upregulated in the spleen. Transcriptional regulators of megakaryocyte and platelet development (*GFI1B*, *NFE2*) are also upregulated.

To test whether bone marrow remains an erythropoietic site in vampire bats, we generated ten additional RNA-seq datasets from skull and humerus bones, which are typical sites of adult erythropoiesis, in *Desmodus*, *Diphylla*, and three non-vampire bat species (Supplementary Table 5). As expected, non-vampire bats showed high expression of the erythropoietic gene program (Fig. 7E). For vampire bats, erythropoietic gene expression in bone marrow was generally low in *Desmodus* but high in Diphylla, indicating that the spleen became the primary erythropoietic organ in *Desmodus* and that both spleen and bone marrow likely contribute to erythropoiesis in *Diphylla*. Although the reasons for splenic erythropoiesis in vampire bats remain to be investigated, the spleen may provide a favorable site by spatially coupling macrophage-mediated erythrocyte clearance, iron recycling, and erythrocyte production within a single organ.

bioRxiv preprint doi: https://doi.org/10.64898/2026.07.24.740446; this version posted July 24, 2026. The copyright holder for this preprint (which was not certified by peer review) is the author/funder, who has granted bioRxiv a license to display the preprint in perpetuity. It is made available under a CC-BY-NC 4.0 International license.

Discussion

Our high-quality reference genomes of all three vampire bat species enabled integrative comparative genomic and transcriptomic analyses that uncovered molecular adaptations underlying obligate sanguivory in vampire bats, the only tetrapods to have evolved this extreme diet. We identified molecular mechanisms underlying a radical transformation of the vampire bat stomach from an acidic, digestive organ into an enlarged, non-acidic chamber that exhibits an altered mucus profile and is specialized for water, electrolyte, vitamin and heme absorption. Upregulation of connective tissue–related genes matched our histological evidence of increased connective tissue content, likely providing structural support for extreme stomach expansion during a single feeding bout.

The extreme dietary specialization of vampire bats is mirrored by extensive molecular remodeling in key metabolic pathways. Consistent with their fat-poor diet, digestive lipases are lost or evolve under relaxed selection, whereas lipogenic enzymes and genes generating the lipogenic substrates (acetyl-CoA and NADPH) are under intensified selection and transcriptionally upregulated. Low dietary sugar content is reflected by loss, relaxation, or downregulation of genes involved in carbohydrate metabolism and insulin signaling, revealing molecular insights into the evolutionary origins of natural insulin deficiency in vampire bats. Notably, the naturally low-fat, low-sugar vampire bat diet parallels the therapeutic diets prescribed to manage human metabolic disorders caused by deficiencies in *DGAT1*, *PDHA1*, or *INSR* (*161*, *201*, *202*), genes that are also altered in these bats. Adaptation to a protein-rich diet is supported by independent duplications of trypsin genes, as well as by intensified selection and upregulation of genes involved in intestinal absorption, renal reabsorption, and catabolism of amino acids. Our results also indicate that key aspects of amino acid catabolism in vampire bats diverge from those of other mammals, including (i) hepatic catabolism of branched-chain amino acids, (ii) a shift in lysine catabolism, with the normally brain-restricted pipecolate pathway expanded to liver and intestine, and (iii) use of leucine-derived acetoacetyl-CoA as a major substrate for fatty acid synthesis. Although many molecular changes are shared between *Desmodus* and *Diphylla*, they also sometimes deploy distinct but functionally equivalent genes, such as *BCAT1*/*BCAT2* and *ACACA*/*ACACB*, revealing different genetic routes to the same metabolic solution.

Most genes lost in vampire bats are associated with gastric mucosal function, gastrointestinal motility, and nutrient digestion. Many of these losses likely reflect relaxed selection on functions that became obsolete with their exclusive blood diet. In line with the “use it or lose it” principle (*203*), most of these genes were lost independently across vampire bats, and our haplotype-resolved assemblies revealed polymorphic inactivating mutations in several genes (*CTSE*, *MLNR*, *SI*, *PNLIP*), indicative of ongoing gene erosion. However, gene loss can also confer adaptive benefits (*4*, *203–205*). For instance, the loss of the 24S-hydroxycholesterol-degrading enzyme *CYP39A1* may have contributed to their exceptional social behavior and cognitive abilities (*30*). Consistent with this, we found *CYP39A1* to be among the few genes already inactivated in the common ancestor of vampire bats (Supplementary Figure 30).

Comparative genomic analyses uncover gene sequence changes such as gene losses, duplications, and signatures of selection, but they often highlight individual loci and therefore

bioRxiv preprint doi: https://doi.org/10.64898/2026.07.24.740446; this version posted July 24, 2026. The copyright holder for this preprint (which was not certified by peer review) is the author/funder, who has granted bioRxiv a license to display the preprint in perpetuity. It is made available under a CC-BY-NC 4.0 International license.

provide a fragmented view of adaptation. Our study shows that incorporating comparative transcriptomic data across multiple organs adds a complementary layer by revealing coordinated sequence and expression changes across pathways and molecular processes. This integrative approach was essential for obtaining a comprehensive view of the molecular adaptations underlying sanguivory in vampire bats. More generally, our work demonstrates how genome-wide, integrative analyses can yield deep insights into the molecular mechanisms underlying adaptive traits.

bioRxiv preprint doi: https://doi.org/10.64898/2026.07.24.740446; this version posted July 24, 2026. The copyright holder for this preprint (which was not certified by peer review) is the author/funder, who has granted bioRxiv a license to display the preprint in perpetuity. It is made available under a CC-BY-NC 4.0 International license.

Materials and Methods

Sample collection, ethical statements and permits

Tissue samples for genome sequencing of the three vampire bat species were obtained from the Royal Ontario Museum mammal collection, where samples were kept frozen since their collection. Samples of a *Desmodus rotundus* male individual (F63247) were collected at Sabajo, Para, Suriname on 2017-09-26. Samples of a *Diaemus youngii* male individual (F50745) were collected at the Ceiba Biological Center in Guyana on 2001-10-16. Samples of a *Diphylla ecaudata* male individual (F37596) were collected at the Parque Nacional Yasuni (66 km S of Pompeya Sur) in Napo, Ecuador on 1995-10-15. All three vampire bat samples are from male individuals caught in the wild.

Samples of *Carollia perspicillata* for genome sequencing were obtained on 2018-02-21 from a captive breeding colony in Frankfurt, Germany, in accordance with the guidelines of the Darmstadt Regional Council. The colony was established in 1980 from founding animals that were caught at Hacienda La Pacifica, Guanacaste in Costa Rica. Samples of a *Glossophaga soricina* juvenile were obtained on 2018-02-20 from a captive breeding colony in Berlin, Germany, that was established in 1987 from founding animals that were caught in central Mexico. The orphaned juvenile had been permanently abandoned by the mother and therefore had to be euthanized, in compliance with the institutional animal welfare regulations. We observed half-coverage of PacBio reads only for scaffold 9, which aligns to the human X chromosome, indicating that the juvenile was a male. A liver sample of a *Micronycteris megalotis* male adult individual was collected from the wild on 2019-03-14 in Santa Maria, Boyaca, Colombia.

All samples were flash frozen in liquid nitrogen after being collected and stored at -80℃ until further processing. The ethical statements of collecting and processing tissue samples for each species followed the procedures required by the following permits:

- *Diphylla ecaudata* (ROMM105272) – Permit number 048IC from the Instituto Ecuatoriano Forestal y de Áreas Naturales y Vida Silvestre
- *Diaemus youngii* (ROMM113765) – Permit number 20011025 from the Guyana Environmental Protection Agency, Natural Resources Management Division
- *Desmodus rotundus* (ROMM126221) – Permit number 12049 from the Suriname Forest Service, Nature Conservation Division
- *Micronycteris megalotis* (Mm_FF)– Permit number DECRETO 1076 DE 2015 (Mayo 26) issued by the The Ministry of Environment and Sustainable Development of Colombia (Spanish: Ministerio de Ambiente y Desarrollo Sostenible de Colombia)

To perform transcriptomics, we obtained wild *Desmodus* and *Diphylla* individuals from a farm in Divinesia, Minas Gerais, Brazil, and a wild *Artibeus obscurus* individual from Vicosa, Minas Gerais, Brazil under the sampling and capturing permit SISBIO 91340-3. The access of these genetic resources from Brazil is registered at SISGEN under the number A3D3AA5. A *Leptonycteris yerbabuenae* individual was obtained from a captive breeding colony in Tübingen, Germany that was established in 1988 from founding animals that were caught in Mexico.

bioRxiv preprint doi: https://doi.org/10.64898/2026.07.24.740446; this version posted July 24, 2026. The copyright holder for this preprint (which was not certified by peer review) is the author/funder, who has granted bioRxiv a license to display the preprint in perpetuity. It is made available under a CC-BY-NC 4.0 International license.

To perform histology, stomach pH measurements, and gastrointestinal motility assessments, we obtained wild *Desmodus* and *Diphylla* individuals from a farm in Divinesia, Minas Gerais, Brazil, wild *Artibeus lituratus* and *Myotis nigricans* individuals from Vicosa, Minas Gerais, Brazil (permit number CEUA 33/2025). Captive *Phyllostomus discolor* individuals were obtained from a captive breeding colony at St. Andrews, UK.

Transcriptome sequencing

All tissue samples for transcriptome sequencing were immediately stored in RNAlater to ensure RNA preservation. The only exceptions are the *Leptonycteris yerbabuenae* skull and spleen samples, which were flash-frozen. Total RNA was extracted using the RNeasy Plus Mini Kit (Qiagen) according to the manufacturer's instructions. RNA concentration was measured using fluorometric quantification, and RNA integrity was assessed prior to library preparation using an Agilent TapeStation instrument. Polyadenylated RNA was enriched from total RNA by oligo-dT priming and reverse transcribed into first- and second-strand cDNA followed by indexing adaptor ligation. Strand-specific RNA sequencing libraries were prepared with the Illumina Stranded mRNA Library Prep protocol (Illumina), according to the manufacturer's instructions. Library quality and fragment size distribution were evaluated, libraries were quantified, and equimolar amounts of each library were pooled for sequencing. Libraries were sequenced on an Illumina platform using paired-end sequencing (2x150 bp), generating approximately 20 million read pairs per sample.

Genome sequencing

For *Diaemus* and *Diphylla*, we generated PacBio HiFi and Dovetail Omni-C data according to the following protocols. To extract high molecular weight genomic DNA, we followed the protocol of (*206*). DNA concentration and DNA fragment length were assessed using the Qubit dsDNA BR Assay kit on the Qubit Fluorometer (Thermo Fisher Scientific) and the Genomic DNA Screen Tape on the Agilent 2200 TapeStation system (Agilent Technologies), respectively. For each species, one SMRTbell library was prepared according to the instructions of the SMRTbell Express Prep Kit v2.0 with a final size selection using AMPure PB beads. Quality control of the final libraries was performed on the Agilent 2200 TapeStation system (Agilent Technologies). Total input DNA was approximately 1.5 µg per library. The library of each species was loaded three times on the Sequel System IIe in CCS mode, using 30 hours of movie time with two hours of pre-extension and sequencing chemistry v2.0. The on-plate concentration for each Sequel IIe run was 80 pM using diffusion loading. For *Desmodus*, we used existing HiFi and Omni-C data (*30*), and to further improve the assembly, we generated additional HiFi data from one SMRT cell, constructing the SMRTbell library according to the instructions of the SMRTbell Express Prep Kit v3.0.

To generate long-range data for *Diaemus* and *Diphylla* for scaffolding, we used the Dovetail Omni-C kit (Dovetail Genomics, Scotts Valley, CA, USA) following the manufacturer's protocol (manual version 1.2 for mammalian samples). We used approximately 30 mg (*Diphylla*) and 60 mg (*Diaemus*) of liver tissue from the same individual used for PacBio sequencing. Fragment size distribution and concentration of the Dovetail Omni-C libraries were assessed using the TapeStation 2200 (Agilent Technologies) and the Qubit Fluorometer and Qubit dsDNA HS reagents Assay kit (Thermo Fisher Scientific, Waltham, MA), respectively. The libraries were

bioRxiv preprint doi: https://doi.org/10.64898/2026.07.24.740446; this version posted July 24, 2026. The copyright holder for this preprint (which was not certified by peer review) is the author/funder, who has granted bioRxiv a license to display the preprint in perpetuity. It is made available under a CC-BY-NC 4.0 International license.

sequenced on the NovaSeq 6000 platform at Novogene (UK) using 150 bp paired-end sequencing to about 60X coverage totaling 120 Gb.

For *Micronycteris megalotis*, HMW gDNA was extracted and PacBio HiFi data was generated as follows. HMW gDNA was extracted from liver tissue according to the Circulomics Nanobind Tissue Big DNA Kit (PacBio / Circulomics, Handbook v1.0 (11/2019)). Briefly, snap-frozen liver tissue was finely minced with a scalpel and homogenised on ice in chaotropic buffer using the Tissue Ruptor (Qiagen). Tissue lysis was performed by adding Proteinase K and cell debris was removed by centrifugation. The released gDNA was bound to a Nanobind disk after the addition of salt buffer and isopropanol. After several washes, the gDNA was eluted from the Nanobind disk. Genomic DNA concentration was determined using the Qubit dsDNA BR (Broad Range) assay kit (ThermoFisher, USA). The purity of the sample was measured using the NanoDrop by evaluating the curve shape and the 260/280 nm and 260/230 nm values. Pulse-field gel electrophoresis (PFGE) using the Pippin Pulse™ instrument (SAGE Science) revealed HMW DNA molecules <200 kb in length. The HMW gDNA was post-purified with Ampure beads and entered into library preparation using the PacBio HiFi library preparation protocol “Preparing HiFi Libraries from Low DNA Input Using SMRTbell Express Template Prep Kit 2.0”. Briefly, gDNA was sheared to 20 kb using the MegaRuptor device (Diagenode) and 3.9 µg of sheared gDNA was used for library preparation. Fragments shorter than 3 kb were removed using Ampure beads size selection. The size-selected library was prepared for loading according to the instructions generated by the SMRT Link software and the ‘HiFi Reads’ application. The HiFi library was sequenced on 8M SMRT™ Cells for 30 hours with the Sequel® II Binding 2.0 and the Sequel® II Sequencing 2.0 chemistry on the Sequel® II. Circular Consensus sequences were called using PacBio ccs (v6.0.0).

For *Carollia perspicillata* and *Glossophaga soricina*, we generated PacBio CLR and 10x Genomics data as follows. High molecular weight (HMW) genomic DNA (gDNA) was extracted according to the Bionano Prep Animal Tissue DNA Isolation Soft Tissue Protocol (document number 30077, document revision C). Briefly, 20-40 mg of snap-frozen spleen (*Carollia perspicillata*) and liver (*Glossophaga soricina*) tissues were thawed and chopped into small pieces. Tissues were homogenised on ice in a homogenisation buffer using a tissue grinder to isolate nuclei. These were washed in ice-cold ethanol, enriched by centrifugation and embedded in 2% agarose plugs. The plugs were further treated with Proteinase K and RNase A, and then washed with 1X Wash Buffer from the kit and home-made 1X TE buffer (pH 8.0). Ultra-long gDNA was recovered from the plugs and finally purified by drop dialysis against the TE buffer (pH 8.0). gDNA concentration was determined using the Qubit dsDNA BR (Broad Range) assay kit (ThermoFisher, USA). Sample purity was measured with the NanoDrop by evaluating the shape of the curve and the 260/280 nm and 260/230 nm values. The integrity of the HMW gDNA was determined by pulse-field gel electrophoresis using the Pippin Pulse™ device (SAGE Science). The majority of the long and ultra-long gDNA was between 50 and 500 kb in length. All pipetting steps of the ultra-long gDNA were performed very carefully with wide-bore pipette tips.

To sequence PacBio CLR for both species, long insert libraries were prepared as recommended according to the ‘Guidelines for preparing size-selected >30 kb SMRTbell templates making use

bioRxiv preprint doi: https://doi.org/10.64898/2026.07.24.740446; this version posted July 24, 2026. The copyright holder for this preprint (which was not certified by peer review) is the author/funder, who has granted bioRxiv a license to display the preprint in perpetuity. It is made available under a CC-BY-NC 4.0 International license.

of the SMRTbell express Template kit 1.0. Briefly, ultra-long gDNA was sheared to 60 kb fragments with the MegaRuptor1 device (Diagenode) and 4-5 µg of sheared gDNA was used for library preparation. The PacBio SMRTbell library was size-selected for fragments larger than 30 kb (*Carollia perspicillata*) and larger than 25 kb (*Glossophaga soricina*) with the BluePippin™ device according to the manufacturer's instructions. All size-selected libraries were sequenced for 10 hours on the Pacbio Sequel® on 1M SMRT™ cells v2 using the Sequel® Binding 2.1 and the Sequel® Sequencing 2.1 v2 chemistry at the DcGC, Germany.

Ultra-long gDNA from *Carollia perspicillata* and *Glossophaga soricina* was used for 10x genomic linked read sequencing according to the manufacturer's instructions (10x Genomics Chromium Reagent Kit v2, revision B). Briefly, 1 ng of ultra-long gDNA was loaded into 10x Genomics GEM droplets (Gel Bead-In-EMulsions) using the Chromium device. Genomic DNA molecules were amplified in these individual GEMS in an isothermal incubation using primers containing a specific 16 bp 10x barcode and the Illumina R1 sequence. After breaking the emulsions, pooled amplified barcoded fragments were purified, enriched and used for Illumina sequencing library preparation, as described in the protocol. Sequencing was performed either on a Nextseq 500 High Output flow cell using the 2x150 cycles paired-end regime plus 8 cycles of i7 index at the DcGC, Germany and on a NovaSeq 6000 S1 flow cell using the same sequencing regime at the MPI of Molecular Genetics, Germany.

Chromatin conformation capture (Hi-C) was performed using the Arima Hi-C kit for *Carollia perspicillata* and *Glossophaga soricina* and Arima Hi-C High Coverage kit for *Micronycteris megalotis* according to the Arima documents (User Guide for Animal Tissues, part number A160132 V00 and part number A160162 v00). Briefly, 75 mg of flash-frozen liver tissue from *Carollia perspicillata*, 40 mg flash-frozen brain tissue from *Glossophaga soricina*, and 15 mg of flash-frozen muscle tissue from *Micronycteris megalotis* were chemically crosslinked. The crosslinked genomic DNA was digested with a cocktail of two (*Carollia perspicillata* and *Glossophaga soricina*) and four (*Micronycteris megalotis*) restriction enzymes. The 5'-overhangs were filled in and labelled with biotin. Spatially proximal digested DNA ends were ligated, and the ligated biotin-containing fragments were enriched and used for Illumina library preparation according to the Arima user guide for library preparation using the Kapa Hyper Prep kit (Arima document part number A160139 v00). The barcoded Hi-C libraries were run on S2 and S4 flow cells of an Illumina NovaSeq 6000 at 2x150 cycles at the DcGC, Germany.

Genome assembly

For the three vampire bats, we produced haplotype-specific assemblies from HiFi reads using Hifiasm (for *Desmodus* v.0.16.1, *Diaemus* v.0.16.1, *Diphylla* v.0.19.3), integrating Hi-C reads for phasing (*31*). Both haplotypes were subject to filtering procedure using Foreign Contamination Screen (FCS) (*207*). Contamination filtered assemblies were then polished to remove unambiguous heterozygous sites. Specifically, we mapped HiFi reads back to each assembly with minimap2 v.2.26 (*208*), removed duplicates using picard MarkDuplicates tool v.3.1.0 (http://broadinstitute.github.io/picard), and called variants using DeepVariant v1.5.0 (*209*). We then filtered for sites with genotype 1/1 and a 'PASS' filter value, meaning that all or nearly all reads support an alternative sequence at this position and passed DeepVariants internal filters.

bioRxiv preprint doi: https://doi.org/10.64898/2026.07.24.740446; this version posted July 24, 2026. The copyright holder for this preprint (which was not certified by peer review) is the author/funder, who has granted bioRxiv a license to display the preprint in perpetuity. It is made available under a CC-BY-NC 4.0 International license.

Finally, we corrected corresponding nucleotide sites in the assembly with bcftools consensus v.1.13 (*210*).

To scaffold the polished haplotype assemblies of vampire bats, we first mapped the Omni-C reads to each of the two assemblies independently using chromap v.0.2.5 (*211*) and then used YaHS v1.1a (*32*). Finally, we performed manual curation of the two scaffolded haplotypes jointly analyzing them in PretextView v.0.2.5 (https://github.com/wtsi-hpag/PretextView). To this end, we remapped the Hi-C reads to both haplotype assemblies concatenated together using again chromap but allowing for multi-mapping reads (-q 0) to avoid discarding information in regions identical between two haplotypes. We also identified telomeric sequences with tidk v.0.2.31 (https://github.com/tolkit/telomeric-identifier) and where necessary corrected wrong contigs orientations to have telomeres in the ends of resulting scaffolds. To finalize changes made via manual dual haplotype curation, as recently proposed by the Vertebrate Genome Project and Darwin Tree of Life Project, we used the rapid curation framework (https://gitlab.com/wtsi-grit/rapid-curation/-/tree/main) from the Genome Reference Informatics Team (*212*).

For *Micronycteris megalotis*, we generated a primary assembly. Contigs were assembled using PacBio HiFi reads and Hifiasm (v0.15.4-r347) (*31*) with argument -l2. Retained haplotigs were removed from the contig assemblies using Purge_Dups (v1.2.6, parameter -e) (*213*). For scaffolding, Hi-C reads were first mapped to the contig assembly using bwa (v0.7.17, parameter -B8) (*214*) and the Arima mapping pipeline (https://github.com/VGP/vgp-assembly/blob/master/pipeline/salsa/arima_mapping_pipeline.sh). The resulting bam file was used as input for SALSA2 (v2.3, parameters -e GATC,GANTC,CTNAG,TTAA -s 2000000000) (*215*). To manually curate the scaffolded assembly, Hi-C reads were mapped using bwa (v0.7.17, parameter -SP5M), followed by filtering, sorting and deduplication with pairtools (v0.3.0). The resulting pairsam file was then split to bam and converted to .cool and .mcool files using pairx (v0.3.7) and cooler (v0.8.11). Finally, the resulting map was visualised using HiGlass (v1.11.7) and missing or false joins were corrected manually. To close gaps in the scaffolded assembly, we mapped raw subreads to the genome using pbmm2 (v1.7.0, parameters --preset SUBREAD -N 1). Consensus sequences 2 kb upstream and downstream of each gap were then called using PacBio's gcpp (v2.0.2) and for gap regions which were filled entirely with capital letter substitutions and no gaps (i.e. a high confidence gap fill), the sequences were inserted into the genome around the gap sequences. To correct base errors, the PacBio HiFi reads were mapped using pbmm2 (v1.7.0, parameters: --preset CCS -N 1) and variants were called using DeepVariant (v1.2.0, parameter --model_type=PACBIO) (*209*). The resulting vcf was then filtered with bcftools (v1.16) view with parameter 'FILTER="PASS" && GT="1/1"' and finally a consensus sequence called with bcftools consensus.

Mitochondrial assemblies were created using MitoHiFi (v2.0) (*216*), but MitoHiFi failed to assemble a mitochondrial genome from the *Diaemus* and from the *Micronycteris* HiFi data. To estimate the assembly base accuracy for the HiFi-based assemblies, we used Merqury (*34*) with the HiFi reads. It should be noted that the QV estimates represent an upper bound as they are based on the HiFi reads used for assembly.

bioRxiv preprint doi: https://doi.org/10.64898/2026.07.24.740446; this version posted July 24, 2026. The copyright holder for this preprint (which was not certified by peer review) is the author/funder, who has granted bioRxiv a license to display the preprint in perpetuity. It is made available under a CC-BY-NC 4.0 International license.

For *Carollia perspicillata* and *Glossophaga soricina*, we generated primary genome assemblies using the DAmar v1 pipeline (https://github.com/MartinPippel/DAmar/blob/master-v1), which orchestrates all assembly steps, including contig building, error correction, and scaffolding. Specifically, the initial contig assembly was performed with the MARVEL assembler (*217*) and the PacBio CLR reads. MARVEL employs a two-phase read-correction procedure that maintains the integrity of long PacBio CLR reads during assembly. Haplotypic duplications were identified and removed with Purge_Dups v1.0.1 (*213*). To increase base level accuracy, we conducted two rounds of error correction using the PacBio data and gcpp (previously known as Arrow; git commit 974589f; https://github.com/PacificBiosciences/gcpp). Subsequently, two additional rounds of error correction were performed using 10x Genomics linked-read data. To this end, 10x linked reads were mapped to the genome using LongRanger v2.2.2 (https://github.com/10XGenomics/longranger) and variants were called using freebayes v1.3.2 (https://github.com/freebayes/freebayes/) with argument "-g 600" to ignore regions with coverage over 600X. The variants were filtered using bcftools view (v1.12) with argument: '-i 'QUAL>1 && (GT="AA" || GT="Aa")' and consensus called using bcftools consensus with argument: '-Hla'.

Scaffolding of the *Carollia* and *Glossophaga* assemblies was carried out in two stages. First, Bionano optical map data were used with Bionano Solve (version Solve3.3_10252018; https://bionano.com/software-downloads/). Second, the resulting scaffolds underwent further scaffolding using Hi-C data and SALSA2 (git commit 974589f) (*215*). The assembly was phased using LongRanger v2.2.2 and the 10x linked-read data. To correct scaffolding errors (missing or false joins), we manually curated the assembly by using HiGlass and a HiC map generated with https://github.com/VGP/vgp-assembly/blob/master/pipeline/salsa/arima_mapping_pipeline.sh.

To assess gene completeness, we used compleasm v0.2.7 (https://github.com/huangnengCSU/compleasm) (*43*) with the BUSCO mammalia_ODB12 set of 12,277 near-universally conserved mammalian genes and the TOGA classification of ancestral genes (below).

Repeat masking

To align newly-sequenced genomes, we generated for each genome a *de novo* repeat library assembly using RepeatModeler 2.0.5 (*218*). We then used the resulting library and RepeatMasker v.4.0.9 (parameters: -engine crossmatch -s) to soft-mask the genome.

Pairwise genome alignments

To infer orthologous genes with TOGA (below), pairwise alignments between a reference and a query genome are needed. We used the human (hg38) assembly as a reference and generated pairwise genome alignments to the newly-sequenced genomes and other species. Briefly, we used LASTZ 1.04.15 (*219*) with parameters (K = 2400, L = 3000, Y = 9400, H = 2000, default scoring matrix) that are sensitive enough to detect alignments between orthologous exons across placental mammals (*220*). The resulting local LASTZ alignments were then chained using axtChain(*221*) (default parameters, except setting linearGap=loose), followed by using RepeatFiller (*222*) (default parameters) to add missed repeat-overlapping local alignments to the

bioRxiv preprint doi: https://doi.org/10.64898/2026.07.24.740446; this version posted July 24, 2026. The copyright holder for this preprint (which was not certified by peer review) is the author/funder, who has granted bioRxiv a license to display the preprint in perpetuity. It is made available under a CC-BY-NC 4.0 International license.

alignment chains and chainCleaner (*223*) (default parameters, except setting minBrokenChainScore = 75,000 and -doPairs) to improve alignment specificity.

Orthology inference and codon alignments

To identify orthologous genes, we used TOGA v1.1.4 (*38*) (https://github.com/hillerlab/TOGA) with the human hg38 genome and GENCODE V38 annotation (*224*) as the reference and the generated pairwise alignment chains to annotate coding genes and infer orthologs across all considered bat genomes.

Multiple codon alignments were used for phylogenomics and screens for selection signatures. To this end, we extracted 1:1 orthologs from TOGA, taking the longest transcript of each gene. Leveraging that TOGA is aware of exon-level orthology (*38*), we used an exon-by-exon strategy that aligns each orthologous exon individually with MACSE v2 (*225*) and default parameters, followed by concatenating exon alignments into complete codon alignments.

Phylogenetic and divergence time estimation

To generate a phylogeny that includes both newly sequenced and existing genomes, we used codon alignments of 1:1 orthologous genes. We applied a coalescent-based approach to infer gene trees from each alignment, which were then used to reconstruct a species tree. We included only orthologs classified by TOGA as I (intact), PI (partially intact), or UL (uncertain loss). We excluded codon alignments that were missing sequences for any vampire bat or for more than three non-vampire bat species, and we removed codons that were present in fewer than 50% of species. With these filters, we obtained codon alignments for a total of 15,481 orthologous genes.

For each gene alignment, we inferred maximum-likelihood trees with RAxML v.8.1.16 (*226*) under a GTR+GAMMA model, using three independent replicates and the rapid hill climbing algorithm. Then, we used ASTRAL v.5.5.9 (*44*, *45*) to estimate a species tree, using default settings and 100 bootstrap replicates to calculate node support.

To estimate a time-calibrated tree, we used a penalized likelihood method implemented in treePL (*227*, *228*) and five fossil calibration points (Supplementary Table 3). We first carried out an analysis to determine the optimal optimization parameters for treePL, and subsequently ran a second analysis incorporating these optimized settings. Fossil calibrations were applied to constrain minimum divergence times at relevant nodes.

Gene losses

We used TOGA's gene classification to identify inactivated (lost) genes based on the presence of gene-inactivating mutations (frameshifts, premature stop codons, splice site disruptions, and deletions of entire coding exons). We extracted all genes containing at least one inactivating mutation within the middle 80% of the coding region (TOGA status L=loss or UL=uncertain loss) and retained those showing evidence of gene loss in at least one vampire bat species but in no more than five non-vampire bat species. We allowed apparent gene losses in non-vampire bats to avoid false negatives caused by low genome assembly quality. To ensure accuracy, we

bioRxiv preprint doi: https://doi.org/10.64898/2026.07.24.740446; this version posted July 24, 2026. The copyright holder for this preprint (which was not certified by peer review) is the author/funder, who has granted bioRxiv a license to display the preprint in perpetuity. It is made available under a CC-BY-NC 4.0 International license.

manually verified each candidate by examining inactivating mutations, codon alignment plots, genomic context, and alignment chains (Supplementary Data 1).

Positive selection using aBSREL

We used the aBSREL method in the HyPhy v2.5.51 package (*46*) to identify genes under positive selection in the vampire bats. This method implements a sensitive branch-site model to detect phylogenetic branches under positive selection. We used the same codon alignments of 15,481 orthologous genes described in the phylogenomics section above, and ran aBSREL with default parameters, except setting the environmental parameter ENV='TOLERATE_NUMERICAL_ERRORS=1'. In addition, we applied the MEME method in HyPhy with default parameters to detect codons under episodic positive selection.

We extracted all genes with a significant positive selection signal (corrected P-value < 0.05) on any of the five branches in the vampire bat lineage. We manually curated the list of candidate genes to ensure accuracy (Supplementary Data 1). Specifically, we excluded genes that contain inactivating mutations in vampire bats. We also excluded genes where the selection signal appeared to come from problematic alignment regions (e.g. caused by fast-evolving protein regions or potentially mis-annotated exons), as such alignment regions can create spurious signals in aBSREL analyses.

Relaxed and intensified selection using RELAX

We used the RELAX method (*47*) in the HyPhy v2.5.51 package to identify genes evolving under relaxed or intensified selection in the vampire bat lineage. Like aBSREL, RELAX analyzes codon alignments of orthologous genes, but it compares two user-defined sets of branches (a test and a reference branch set) to determine whether selection to preserve the encoded protein sequence is relaxed or intensified in the test branches relative to the reference branches. In our analyses, the five branches in the vampire bat lineage were defined as the test set, and all other branches in the phylogeny were defined as the reference set. We generated codon alignments as described in the phylogenomics section above, with one key difference of including remnant sequences of genes classified as lost in the codon alignments. Applying the same filters yielded 16,094 codon alignments, a higher number than in the phylogenomics and aBSREL analysis.

For each gene, RELAX was run with parameters “CPU=1 --starting-points 100 --grid-size 2000 --models Minimal”. We obtained the k value to infer the direction of selection, with k < 1 indicating relaxation and k > 1 indicating intensification, and the P-values, which we corrected for multiple testing over the genes using the Benjamini-Hochberg method. Genes with corrected P-values < 0.05 for relaxation or intensification were retained. Because RELAX results can exhibit stochastic variation, we repeated the analysis ten times and merged the resulting gene lists to generate our final set. We then manually curated this gene list by examining the codon alignment visualizations (Supplementary Data 1). As for aBSREL, we removed genes with problematic alignment regions. We also removed genes lost in nearly all species. Finally, we excluded genes that are “hyperconserved” across all species and contain only very few mutations overall, because their alignments provide limited information for reliable inference of relaxation or intensification.

bioRxiv preprint doi: https://doi.org/10.64898/2026.07.24.740446; this version posted July 24, 2026. The copyright holder for this preprint (which was not certified by peer review) is the author/funder, who has granted bioRxiv a license to display the preprint in perpetuity. It is made available under a CC-BY-NC 4.0 International license.

Differential expression analysis

RNA-seq reads were quality-checked using FastQC v0.11.9 (https://www.bioinformatics.babraham.ac.uk/projects/fastqc/) and MultiQC v1.12 (*229*). Read pairs were filtered using Trimmomatic v0.39 (*230*) setting the following parameters: "ILLUMINACLIP:TruSeq3-PE.fa:2:30:10 LEADING:3 TRAILING:3 SLIDINGWINDOW:4:15 MINLEN:36".

To quantify gene-level expression, we used kb-python (v0.29.5) (*48*), a wrapper that leverages the pseudoalignment algorithm implemented in kallisto (*231*) to map sequencing reads directly to transcript sequences rather than performing genome-based alignment. We used TOGA coding sequence annotations as input transcripts. To reduce spurious read assignments, we included the genome sequence with hard-masked coding regions as decoy. Kb-python outputs two expression measures for each gene: read count and transcripts per million (TPM). Read counts were used for differential gene expression analysis in DESeq2 (below). To visualize gene expression across tissues, we normalized TPM values with the median-of-ratios method in DESeq2.

To identify genes differentially expressed in different organs between vampire and non-vampire bats, we used DESeq2 v1.46.0 (*232*). We excluded genes with 1:many or many:many orthology relationships according to TOGA, and excluded genes with a median TPM < 0.5 in both vampire and non-vampire bats. Genes with a log2 fold change > 1.5 and adjusted P-value < 0.01 were considered differentially expressed genes.

Functional enrichment analysis

Gene lists obtained from our comparative genomic and differential expression analyses were subjected to functional enrichment analysis using Metascape (database update: 2025-07-01) (*233*). The following ontological categories were included in the analysis: GO Biological Process, GO Molecular Function, GO Cellular Component, KEGG Pathways, WikiPathways, Canonical Pathways, Reactome, Cell Type Signatures, DisGeNET and PaGenBase. We only considered enrichments with an adjusted P-value < 0.05. The complete enrichment results are provided in Supplementary Tables 9 and 10.

Insulin and insulin receptor analysis

To analyze the prevalence of mutations in *INS* and *INSR* in an extended set of mammals, we used TOGA2 (https://github.com/hillerlab/TOGA2) to identify 1:1 orthologs of both genes in available mammalian genomes, which includes bat species that represent all 21 currently recognized bat families (*42*). A multiple alignment was generated with Prank (*234*).

To examine the location of INS mutations in an INS-INSR structural model, we used the crystal structure of the extracellular domain of the insulin receptor bound to insulin (PDB 6PXV), refined using the Protein Preparation Wizard in the Maestro suite (*235*, *236*). Missing side chains and loops were built using the Prime module.

bioRxiv preprint doi: https://doi.org/10.64898/2026.07.24.740446; this version posted July 24, 2026. The copyright holder for this preprint (which was not certified by peer review) is the author/funder, who has granted bioRxiv a license to display the preprint in perpetuity. It is made available under a CC-BY-NC 4.0 International license.

Visualization

Schematics in the main figures were created using BioRender.com. Sequence logos for INS and INSR were generated with the R package ggseqlogo (https://cran.r-project.org/web/packages/ggseqlogo/index.html).

Histological analysis of stomach

We used histological methods to investigate three aspects of vampire bat stomach: connective tissue content, mucosa thickness and mucus secretion profile. For this purpose, we captured four *Desmodus,* two *Diphylla*, five *Artibeus lituratus* and four *Myotis nigricans* individuals. Animals were euthanized by decapitation, and the digestive tract was dissected. Fragments of the fundic stomach were washed in saline, then fixed in buffered formalin for 24 h, and stored in 70% ethanol until processing. Fragments were dehydrated in alcoholic solutions of increasing concentration (80/90/100%; 30 min each), immersed in glycol methacrylate resin overnight followed by 2 h in fresh resin. Fragments were subsequently embedded using plastic molds and resin with added polymerizer (hardener). The resulting blocks were sectioned using a rotary microtome and glass blades. The sections obtained were 3 µm thick, with ten semi-serial sections per histological slide (30 µm between sections). Two slides were prepared for each fragment; one was stained with Toluidine blue, and the other with Periodic acid-Schiff conjugated with Alcian blue (PAS-AB). The slides were dried and mounted with coverslips using Entellan resin. Photomicrographs were acquired using a microscope with a camera and image capture system.

Images from Toluidine blue-stained slides were used to quantify the connective tissue content and mucosa thickness, as illustrated in Supplementary Figure 5. Images were annotated for connective tissue, mucosa and muscle using QuPath v0.6.0 (*237*). Connective tissue content was measured both as (i) the percentage of the stomach wall area, and (ii) connective tissue thickness as a percentage of the muscular region (Supplementary Figure 5). Differences between vampire bats and control species were tested using two-tailed Welch's t-tests. Images from PAS-AB-stained slides were used to assess the mucus secretion profile, with vacuoles showing magenta and blue colors indicating neutral and acidic mucus, respectively.

Stomach pH

We measured the stomach pH in *Desmodus* (n=4), *Diphylla* (n=5), and *Artibeus lituratus* (n=3). Animals were euthanized by decapitation. For each animal, stomach contents were removed with a small spatula and transferred to an Eppendorf tube, which was then filled with water to the 2 mL mark. The material was further diluted to 20 mL in a test tube for pH measurement using a pH meter. The pH meter recordings are provided in Supplementary Table 13 and shown in the main text figure.

Gastrointestinal motility

We examined and video-recorded gastrointestinal motility in *Desmodus* (n = 3), *Diphylla* (n = 2), *Artibeus lituratus* (n = 2), *Phyllostomus discolor* (n = 3), and *Mus musculus* (n = 3). Animals were euthanized by decapitation or overdose of isoflurane, and then dissected to expose the abdominal cavity. Gastrointestinal motility was recorded before and after administration of neostigmine (0.5

bioRxiv preprint doi: https://doi.org/10.64898/2026.07.24.740446; this version posted July 24, 2026. The copyright holder for this preprint (which was not certified by peer review) is the author/funder, who has granted bioRxiv a license to display the preprint in perpetuity. It is made available under a CC-BY-NC 4.0 International license.

mg/mL), a cholinergic stimulant of gastrointestinal motility in mammals. Videos of the recordings are provided in Supplementary Videos 1–5.

Ferritin processed pseudogene copies

Motivated by a previous study that identified an expansion of ferritin genes in the common vampire bat genome (*25*), we reanalyzed ferritin genes in our extended set of genomes. As shown in Supplementary Figures 27-29, we analyzed *FTL* and *FTH1* orthologs detected by TOGA and inspected the alignment chains in the *FTL* and *FTH1* locus, which revealed a single *FTH1* ortholog, an ancient *FTL* duplication, and for all analyzed bats a large number of processed pseudogene copies. To determine whether there is a vampire bat specific expansion of ferritin processed pseudogene copies, we compared the three vampire bats with four other species that have long read-based genomes, representing non-vampire phyllostomid bats (*Micronycteris megalotis*, *Carollia perspicillata*, *Glossophaga soricina*) and the outgroup *Mormoopidae* family (*Pteronotus mesoamericanus*). Since RepeatModeler may detect processed pseudogenes as an unknown repeat family if they have several hundred copies in an assembly, we removed any soft-masking corresponding to repeat families with sequence similarity to *FTL* or *FTH1* before computed alignment chains. To systematically compare the number of processed pseudogene copies, we leveraged a new functionality of TOGA2 (https://github.com/hillerlab/TOGA2) to detect processed pseudogenes and determine whether they have an intact open reading frame. To detect all processed pseudogenes, we lowered the minimum chain score from 15,000 to 5,000 for these TOGA2 runs. The number of detected processed pseudogenes and how many have intact reading frames are listed in Supplementary Table 14.

bioRxiv preprint doi: https://doi.org/10.64898/2026.07.24.740446; this version posted July 24, 2026. The copyright holder for this preprint (which was not certified by peer review) is the author/funder, who has granted bioRxiv a license to display the preprint in perpetuity. It is made available under a CC-BY-NC 4.0 International license.

Competing interests

The authors have no competing interests.

Acknowledgment

We thank Leandro Costa do Nascimento and Maria Carolina Svidnicki for RNA-sequencing, Matheus Canal, Monika Fischer, Sasha Newar, Emilia NovilloSuarez and Tom Jenks for helping with experiments, and the Genome Technology Center (RGTC) at Radboudumc for the use of the Sequencing Core Facility (Nijmegen, The Netherlands), which provided the PacBio SMRT sequencing service on the Sequel IIe platform, the Environment Services and Support (ESS) in Suriname. We thank Brock Fenton, Merlin Tuttle, José G. Martínez-Fonseca and Jon Flanders for permission to use bat photographs. For support in the Colombia 2019 expedition, we thank Andrés Cuervo, Mailyn Gonzalez, Andrés Julián Lozano Florez, Darwin M. Morales Martinez, Paola Pulido Santacruz, Danny Rojas, and Laurel Yohe. We acknowledge support by the Sector Plan Pharmaceutical Sciences, implemented in the overarching Sector Plan Beta II and put into action by the Ministry of Education, Culture, and Science (OCW) of The Netherlands.

This work was supported by the German Research Foundation (grants HI1423/5-1 and HI1423/6-1 to MH, and HI2214/1-1 to LH), the LOEWE-Centre for Translational Biodiversity Genomics (TBG) funded by the Hessen State Ministry of Higher Education, Research and the Arts (HMWK) (LOEWE/1/10/519/03/03.001(0014)/52), the Max Planck Society, and the European Research Council (ERC-2023-SyG, 101118919). LMD was supported by National Science Foundation Grants NSF RoL: FELS: EAGER 1838273 and NSF-IOS 2032063 and 2031906, and a Colciencias Seed Grant. BKL received funding from Environmental Services & Support (ESS) for fieldwork in Suriname, the Royal Ontario Museum Department of Natural History for fieldwork in Guyana, and the Ecuambiente Consulting Group for fieldwork in Ecuador. SCV was supported by a UKRI Future Leaders Fellowship, (MR/T021985/1). Genome sequencing of non-vampire bats was performed by the LongRead Project of the Max-Planck Institute of Molecular Cell Biology and Genetics (MPI-CBG) as part of the DcGC Dresden-concept Genome Center and was supported by the Next Generation Sequencing Competence Network (DFG project 423957469).

Data availability

Genomic and transcriptomic data and the genome assemblies of *Desmodus rotundus* (PRJNA789159), *Diaemus youngii* (PRJNA1256700), *Diphylla ecaudata* (PRJNA1256387), *Micronycteris megalotis* (PRJNA1263771), *Carollia perspicillata* (PRJNA1265070), and *Glossophaga soricina* (PRJNA1265439), and transcriptomic data for *Artibeus obscurus* (PRJNA1399465) and *Leptonycteris yerbabuenae* (biosample SAMEA120952157, BioProject ID pending) are available on NCBI under the listed BioProject IDs.

Code availability

No new code was generated for this study.

bioRxiv preprint doi: https://doi.org/10.64898/2026.07.24.740446; this version posted July 24, 2026. The copyright holder for this preprint (which was not certified by peer review) is the author/funder, who has granted bioRxiv a license to display the preprint in perpetuity. It is made available under a CC-BY-NC 4.0 International license.

References

1. F. Luca, G. H. Perry, A. Di Rienzo, Evolutionary adaptations to dietary changes. *Annu. Rev. Nutr.* **30**, 291–314 (2010).
2. J. R. S. Meadows, K. Lindblad-Toh, Dissecting evolution and disease using comparative vertebrate genomics. *Nat. Rev. Genet.* **18**, 624–636 (2017).
3. J. H. T. Potter, K. T. J. Davies, L. R. Yohe, M. K. R. Sanchez, E. M. Rengifo, M. Struebig, K. Warren, G. Tsagkogeorga, B. K. Lim, M. Dos Reis, L. M. Dávalos, S. J. Rossiter, Dietary diversification and specialization in Neotropical bats facilitated by early molecular evolution. *Mol. Biol. Evol.* **38**, 3864–3883 (2021).
4. E. Osipova, R. Barsacchi, T. Brown, K. Sadanandan, A. H. Gaede, A. Monte, J. Jarrells, C. Moebius, M. Pippel, D. L. Altshuler, S. Winkler, M. Bickle, M. W. Baldwin, M. Hiller, Loss of a gluconeogenic muscle enzyme contributed to adaptive metabolic traits in hummingbirds. *Science* **379**, 185–190 (2023).
5. J. Camacho, A. Bernal-Rivera, V. Peña, P. Morales-Sosa, S. M. C. Robb, J. Russell, K. Yi, Y. Wang, D. Tsuchiya, O. E. Murillo-García, N. Rohner, Sugar assimilation underlying dietary evolution of Neotropical bats. *Nat. Ecol. Evol.* **8**, 1735–1750 (2024).
6. M. D. Pollard, W. K. Meyer, E. E. Puckett, Convergent relaxation of molecular constraint in herbivores reveals the changing role of liver and kidney functions across mammalian diets. *Genome Res.* **34**, 2176–2189 (2024).
7. R. J. Baker, *Evolutionary History of Bats* (Cambridge University Press, Cambridge, 2012).
8. G. S. Wilkinson, Vampire bats. *Curr. Biol.* **29**, R1216–R1217 (2019).
9. D. K. Riskin, J. W. Hermanson, Biomechanics: independent evolution of running in vampire bats. *Nature* **434**, 292 (2005).
10. D. H. W. Low, K. Sunagar, E. A. B. Undheim, S. A. Ali, A. C. Alagon, T. Ruder, T. N. W. Jackson, S. Pineda Gonzalez, G. F. King, A. Jones, A. Antunes, B. G. Fry, Dracula's children: molecular evolution of vampire bat venom. *J. Proteomics* **89**, 95–111 (2013).
11. E. O. Gracheva, J. F. Cordero-Morales, J. A. González-Carcacía, N. T. Ingolia, C. Manno, C. I. Aranguren, J. S. Weissman, D. Julius, Ganglion-specific splicing of TRPV1 underlies infrared sensation in vampire bats. *Nature* **476**, 88–91 (2011).
12. C. S. Rouk, B. P. Glass, Comparative Gastric Histology of Five North and Central American Bats. *J. Mammal.* **51**, 455–472 (1970).
13. T. H. Huxley, On The Structure Of The Stomach In Desmodus Rufus. *Proceedings of the Zoological Society of London* **33**, 386–390 (1865).
14. W. A. Wimsatt, A. Guerriere, Observations on the Feeding Capacities and Excretory Functions Of Captive Vampire Bats1. *J. Mammal.* **43**, 17–27 (1962).
15. C. P. Breidenstein, Digestion and Assimilation of Bovine Blood by a Vampire Bat (Desmodus rotundus). *J. Mammal.* **63**, 482–484 (1982).
16. M. B. Freitas, J. F. Queiroz, C. I. Dias Gomes, C. B. Collares-Buzato, H. C. Barbosa, A. C. Boschero, C. A. Gonçalves, E. C. Pinheiro, Reduced insulin secretion and glucose intolerance are involved in the fasting susceptibility of common vampire bats. *Gen. Comp. Endocrinol.* **183**, 1–6 (2013).
17. M. B. Freitas, A. F. Welker, S. F. Millan, E. C. Pinheiro, Metabolic responses induced by fasting in the common vampire bat Desmodus rotundus. *J. Comp. Physiol. B* **173**, 703–707 (2003).
18. G. S. Rossi, K. C. Welch Jr, Vampire bats rapidly fuel running with essential or non-essential amino acids from a blood meal. *Biol. Lett.* **20**, 20240453 (2024).
19. G. S. Wilkinson, Reciprocal food sharing in the vampire bat. *Nature* **308**, 181–184 (1984).
20. G. S. Wilkinson, Social grooming in the common vampire bat, Desmodus rotundus. *Anim. Behav.* **34**, 1880–1889 (1986).
21. G. G. Carter, G. S. Wilkinson, Food sharing in vampire bats: reciprocal help predicts donations more than relatedness or harassment. *Proc. Biol. Sci.* **280**, 20122573 (2013).
22. I. Razik, B. K. G. Brown, R. A. Page, G. G. Carter, Non-kin adoption in the common vampire bat. *R. Soc. Open Sci.* **8**, 201927 (2021).
23. S. P. Ripperger, G. G. Carter, N. Duda, A. Koelpin, B. Cassens, R. Kapitza, D. Josic, J. Berrío-

bioRxiv preprint doi: https://doi.org/10.64898/2026.07.24.740446; this version posted July 24, 2026. The copyright holder for this preprint (which was not certified by peer review) is the author/funder, who has granted bioRxiv a license to display the preprint in perpetuity. It is made available under a CC-BY-NC 4.0 International license.

Martínez, R. A. Page, F. Mayer, Vampire bats that cooperate in the lab maintain their social networks in the wild. *Curr. Biol.* **29**, 4139–4144.e4 (2019).

24. G. Baron, H. Stephan, H. D. Frahm, “Brain Characteristics in Functional Systems, Ecoethological Adaptation, Adaptive Radiation, and Evolution” in *Comparative Neurobiology in Chiroptera* (Springer, 1996).
25. M. L. Zepeda Mendoza, Z. Xiong, M. Escalera-Zamudio, A. K. Runge, J. Thézé, D. Streicker, H. K. Frank, E. Loza-Rubio, S. Liu, O. A. Ryder, J. A. Samaniego Castruita, A. Katzourakis, G. Pacheco, B. Taboada, U. Löber, O. G. Pybus, Y. Li, E. Rojas-Anaya, K. Bohmann, A. Carmona Baez, C. F. Arias, S. Liu, A. D. Greenwood, M. F. Bertelsen, N. E. White, M. Bunce, G. Zhang, T. Sicheritz-Pontén, M. P. T. Gilbert, Hologenomic adaptations underlying the evolution of sanguivory in the common vampire bat. *Nat. Ecol. Evol.* **2**, 659–668 (2018).
26. Y. T. Gutiérrez-Guerrero, E. Ibarra-Laclette, C. Martínez Del Río, J. Barrera-Redondo, E. A. Rebollar, J. Ortega, L. León-Paniagua, A. Urrutia, E. Aguirre-Planter, L. E. Eguiarte, Genomic consequences of dietary diversification and parallel evolution due to nectarivory in leaf-nosed bats. *Gigascience* **9** (2020).
27. W. Hong, H. Zhao, Vampire bats exhibit evolutionary reduction of bitter taste receptor genes common to other bats. *Proc. Biol. Sci.* **281**, 20141079 (2014).
28. K. Wang, S. Tian, J. Galindo-González, L. M. Dávalos, Y. Zhang, H. Zhao, Molecular adaptation and convergent evolution of frugivory in Old World and neotropical fruit bats. *Mol. Ecol.* **29**, 4366–4381 (2020).
29. H. Jiao, L. Zhang, H.-W. Xie, N. B. Simmons, H. Liu, H. Zhao, Trehalase gene as a molecular signature of dietary diversification in mammals. *Mol. Biol. Evol.* **36**, 2171–2183 (2019).
30. M. Blumer, T. Brown, M. B. Freitas, A. L. Destro, J. A. Oliveira, A. E. Morales, T. Schell, C. Greve, M. Pippel, D. Jebb, N. Hecker, A.-W. Ahmed, B. M. Kirilenko, M. Foote, A. Janke, B. K. Lim, M. Hiller, Gene losses in the common vampire bat illuminate molecular adaptations to blood feeding. *Sci Adv* **8**, eabm6494 (2022).
31. H. Cheng, G. T. Concepcion, X. Feng, H. Zhang, H. Li, Haplotype-resolved de novo assembly using phased assembly graphs with hifiasm. *Nat. Methods* **18**, 170–175 (2021).
32. C. Zhou, S. A. McCarthy, R. Durbin, YaHS: yet another Hi-C scaffolding tool. *Bioinformatics* **39** (2023).
33. C. G. Sotero-Caio, J. C. Pieczarka, C. Y. Nagamachi, A. J. B. Gomes, T. C. Lira, P. C. M. O’Brien, M. A. Ferguson-Smith, M. J. Souza, N. Santos, Chromosomal homologies among vampire bats revealed by chromosome painting (phyllostomidae, chiroptera). *Cytogenet. Genome Res.* **132**, 156–164 (2011).
34. A. Rhie, B. P. Walenz, S. Koren, A. M. Phillippy, Merqury: reference-free quality, completeness, and phasing assessment for genome assemblies. *Genome Biol.* **21**, 245 (2020).
35. B. J. Ko, C. Lee, J. Kim, A. Rhie, D. A. Yoo, K. Howe, J. Wood, S. Cho, S. Brown, G. Formenti, E. D. Jarvis, H. Kim, Widespread false gene gains caused by duplication errors in genome assemblies. *Genome Biol.* **23**, 205 (2022).
36. D. Yoo, A. Rhie, P. Hebbar, F. Antonacci, G. A. Logsdon, S. J. Solar, D. Antipov, B. D. Pickett, Y. Safonova, F. Montinaro, Y. Luo, J. Malukiewicz, J. M. Storer, J. Lin, A. N. Sequeira, R. J. Mangan, G. Hickey, G. Monfort Anez, P. Balachandran, A. Bankevich, C. R. Beck, A. Biddanda, M. Borchers, G. G. Bouffard, E. Brannan, S. Y. Brooks, L. Carbone, L. Carrel, A. P. Chan, J. Crawford, M. Diekhans, E. Engelbrecht, C. Feschotte, G. Formenti, G. H. Garcia, L. de Gennaro, D. Gilbert, R. E. Green, A. Guarracino, I. Gupta, D. Haddad, J. Han, R. S. Harris, G. A. Hartley, W. T. Harvey, M. Hiller, K. Hoekzema, M. L. Houck, H. Jeong, K. Kamali, M. Kellis, B. Kille, C. Lee, Y. Lee, W. Lees, A. P. Lewis, Q. Li, M. Loftus, Y. H. E. Loh, H. Loucks, J. Ma, Y. Mao, J. F. I. Martinez, P. Masterson, R. C. McCoy, B. McGrath, S. McKinney, B. S. Meyer, K. H. Miga, S. K. Mohanty, K. M. Munson, K. Pal, M. Pennell, P. A. Pevzner, D. Porubsky, T. Potapova, F. R. Ringeling, J. L. Rocha, O. A. Ryder, S. Sacco, S. Saha, T. Sasaki, M. C. Schatz, N. J. Schork, C. Shanks, L. Smeds, D. R. Son, C. Steiner, A. P. Sweeten, M. G. Tassia, F. Thibaud-Nissen, E. Torres-González, M. Trivedi, W. Wei, J. Wertz, M. Yang, P. Zhang, S. Zhang, Y. Zhang, Z. Zhang, S. A. Zhao, Y. Zhu, E. D. Jarvis, J. L. Gerton, I. Rivas-González, B. Paten, Z. A. Szpiech, C. D. Huber, T. L. Lenz, M. K. Konkel, S. V. Yi, S. Canzar,

bioRxiv preprint doi: https://doi.org/10.64898/2026.07.24.740446; this version posted July 24, 2026. The copyright holder for this preprint (which was not certified by peer review) is the author/funder, who has granted bioRxiv a license to display the preprint in perpetuity. It is made available under a CC-BY-NC 4.0 International license.

C. T. Watson, P. H. Sudmant, E. Molloy, E. Garrison, C. B. Lowe, M. Ventura, R. J. O'Neill, S. Koren, K. D. Makova, A. M. Phillippy, E. E. Eichler, Complete sequencing of ape genomes. *Nature* **641**, 401–418 (2025).

37. A. E. Morales, Y. Dong, T. Brown, K. Baid, D.-G. Kontopoulos, V. Gonzalez, Z. Huang, A.-W. Ahmed, A. Bhuinya, L. Hilgers, S. Winkler, G. Hughes, X. Li, P. Lu, Y. Yang, B. M. Kirilenko, P. Devanna, T. M. Lama, Y. Nissan, M. Pippel, L. M. Dávalos, S. C. Vernes, S. J. Puechmaille, S. J. Rossiter, Y. Yovel, J. B. Prescott, A. Kurth, D. A. Ray, B. K. Lim, E. Myers, E. C. Teeling, A. Banerjee, A. T. Irving, M. Hiller, Bat genomes illuminate adaptations to viral tolerance and disease resistance. *Nature* **638**, 449–458 (2025).
38. B. M. Kirilenko, C. Munegowda, E. Osipova, D. Jebb, V. Sharma, M. Blumer, A. E. Morales, A.-W. Ahmed, D.-G. Kontopoulos, L. Hilgers, K. Lindblad-Toh, E. K. Karlsson, Zoonomia Consortium‡, M. Hiller, Integrating gene annotation with orthology inference at scale. *Science* **380**, eabn3107 (2023).
39. D. Jebb, Z. Huang, M. Pippel, G. M. Hughes, K. Lavrichenko, P. Devanna, S. Winkler, L. S. Jermiin, E. C. Skirmuntt, A. Katzourakis, L. Burkitt-Gray, D. A. Ray, K. A. M. Sullivan, J. G. Roscito, B. M. Kirilenko, L. M. Dávalos, A. P. Corthals, M. L. Power, G. Jones, R. D. Ransome, D. K. N. Dechmann, A. G. Locatelli, S. J. Puechmaille, O. Fedrigo, E. D. Jarvis, M. Hiller, S. C. Vernes, E. W. Myers, E. C. Teeling, Six reference-quality genomes reveal evolution of bat adaptations. *Nature* **583**, 578–584 (2020).
40. A. Scheben, O. Mendivil Ramos, M. Kramer, S. Goodwin, S. Oppenheim, D. J. Becker, M. C. Schatz, N. B. Simmons, A. Siepel, W. R. McCombie, Long-Read Sequencing Reveals Rapid Evolution of Immunity- and Cancer-Related Genes in Bats. *Genome Biol. Evol.* **15** (2023).
41. Zoonomia Consortium, A comparative genomics multitool for scientific discovery and conservation. *Nature* **587**, 240–245 (2020).
42. A. Morales, Bat1K 21 family group, D. Ray, S. C. Vernes, L. Davalos, M. Hiller, E. C. Teeling, Reference genomes reveal family level evolutionary history and biogeography of bats. *submitted* (2025).
43. N. Huang, H. Li, compleasm: a faster and more accurate reimplementation of BUSCO. *Bioinformatics* **39** (2023).
44. S. Mirarab, T. Warnow, "ASTRAL-II: Coalescent-based species tree estimation with many hundreds of taxa and thousands of genes" in *Bioinformatics* (2015)vol. 31, pp. i44–i52.
45. S. Mirarab, R. Reaz, M. S. Bayzid, T. Zimmermann, M. S. Swenson, T. Warnow, ASTRAL: Genome-scale coalescent-based species tree estimation. *Bioinformatics* **30**, 541–548 (2014).
46. M. D. Smith, J. O. Wertheim, S. Weaver, B. Murrell, K. Scheffler, S. L. Kosakovsky Pond, Less is more: an adaptive branch-site random effects model for efficient detection of episodic diversifying selection. *Mol. Biol. Evol.* **32**, 1342–1353 (2015).
47. J. O. Wertheim, B. Murrell, M. D. Smith, S. L. Kosakovsky Pond, K. Scheffler, RELAX: detecting relaxed selection in a phylogenetic framework. *Mol. Biol. Evol.* **32**, 820–832 (2015).
48. D. K. Sullivan, K. H. J. Min, K. E. Hjörleifsson, L. Luebbert, G. Holley, L. Moses, J. Gustafsson, N. L. Bray, H. Pimentel, A. S. Booeshaghi, P. Melsted, L. Pachter, kallisto, bustools and kb-python for quantifying bulk, single-cell and single-nucleus RNA-seq. *Nat. Protoc.* **20**, 587–607 (2025).
49. M. I. Love, W. Huber, S. Anders, Moderated estimation of fold change and dispersion for RNA-seq data with DESeq2, *bioRxiv* (2014). https://doi.org/10.1101/002832.
50. N. Barker, M. Huch, P. Kujala, M. van de Wetering, H. J. Snippert, J. H. van Es, T. Sato, D. E. Stange, H. Begthel, M. van den Born, E. Danenberg, S. van den Brink, J. Korving, A. Abo, P. J. Peters, N. Wright, R. Poulsom, H. Clevers, Lgr5(+ve) stem cells drive self-renewal in the stomach and build long-lived gastric units in vitro. *Cell Stem Cell* **6**, 25–36 (2010).
51. M. Leushacke, S. H. Tan, A. Wong, Y. Swathi, A. Hajamohideen, L. T. Tan, J. Goh, E. Wong, S. L. I. J. Denil, K. Murakami, N. Barker, Lgr5-expressing chief cells drive epithelial regeneration and cancer in the oxyntic stomach. *Nat. Cell Biol.* **19**, 774–786 (2017).
52. I. Stzepourginski, G. Nigro, J.-M. Jacob, S. Dulauroy, P. J. Sansonetti, G. Eberl, L. Peduto, CD34+ mesenchymal cells are a major component of the intestinal stem cells niche at homeostasis and after injury. *Proc. Natl. Acad. Sci. U. S. A.* **114**, E506–E513 (2017).
53. T. Takahashi, H. Suzuki, T. Imai, S. Shibata, Y. Tabuchi, K. Tsuchimoto, H. Okano, T. Hibi, Musashi-

bioRxiv preprint doi: https://doi.org/10.64898/2026.07.24.740446; this version posted July 24, 2026. The copyright holder for this preprint (which was not certified by peer review) is the author/funder, who has granted bioRxiv a license to display the preprint in perpetuity. It is made available under a CC-BY-NC 4.0 International license.

1 post-transcriptionally enhances phosphotyrosine-binding domain-containing m-Numb protein expression in regenerating gastric mucosa. *PLoS One* **8**, e53540 (2013).

54. M. Yousefi, N. Li, A. Nakauka-Ddamba, S. Wang, K. Davidow, J. Schoenberger, Z. Yu, S. T. Jensen, M. G. Kharas, C. J. Lengner, Msi RNA-binding proteins control reserve intestinal stem cell quiescence. *J. Cell Biol.* **215**, 401–413 (2016).
55. R. J. Baker, J. K. Jones, D. C. Carter, *Biology of Bats of the New World Family Phyllostomatidae* (Texas Tech Press, Lubbock, 1976-1979).
56. S. Sercu, M. Zhang, N. Oyama, U. Hansen, A. E. L. Ghalbzouri, G. Jun, K. Geentjens, L. Zhang, J. H. Merregaert, Interaction of extracellular matrix protein 1 with extracellular matrix components: ECM1 is a basement membrane protein of the skin. *J. Invest. Dermatol.* **128**, 1397–1408 (2008).
57. A. J. Zollinger, M. L. Smith, Fibronectin, the extracellular glue. *Matrix Biol.* **60-61**, 27–37 (2017).
58. A. Schiavinato, F. Marcous, A. V. Zuk, D. R. Keene, S. F. Tufa, L. M. Mosquera, P. Zigrino, C. Mauch, B. Eckes, K. Francois, J. De Backer, N. Hunzelmann, P. Moinzadeh, T. Krieg, B. Callewaert, G. Sengle, New insights into the structural role of EMILINs within the human skin microenvironment. *Sci. Rep.* **14**, 30345 (2024).
59. W. S. Argraves, L. M. Greene, M. A. Cooley, W. M. Gallagher, Fibulins: physiological and disease perspectives. *EMBO Rep.* **4**, 1127–1131 (2003).
60. S. de Vega, T. Iwamoto, Y. Yamada, Fibulins: multiple roles in matrix structures and tissue functions. *Cell. Mol. Life Sci.* **66**, 1890–1902 (2009).
61. T. de S. Laurentino, R. da S. Soares, S. K. N. Marie, S. M. Oba-Shinjo, LOXL3 function beyond amino oxidase and role in pathologies, including cancer. *Int. J. Mol. Sci.* **20**, 3587 (2019).
62. V. K. Raghunathan, J. T. Morgan, Y.-R. Chang, D. Weber, B. Phinney, C. J. Murphy, P. Russell, Transforming growth factor beta 3 modifies mechanics and composition of extracellular matrix deposited by human trabecular meshwork cells. *ACS Biomater. Sci. Eng.* **1**, 110–118 (2015).
63. C. S. Rouk, Gastric morphology and adaptive radiation in the phyllostomatidae, *Texas Tech University* (1973). https://ttu-ir.tdl.org/items/3137b49b-5a66-41f7-9747-db41a548374f.
64. R. J. Baker, D. C. Carter, J. K. Jones, *Biology of Bats of the New World Family Phyllostomatidae /* (Texas Tech Press, Lubbock :, 1976).
65. Z. Spicer, M. L. Miller, A. Andringa, T. M. Riddle, J. J. Duffy, T. Doetschman, G. E. Shull, Stomachs of mice lacking the gastric H,K-ATPase alpha -subunit have achlorhydria, abnormal parietal cells, and ciliated metaplasia. *J. Biol. Chem.* **275**, 21555–21565 (2000).
66. D. Heitzmann, R. Warth, No potassium, no acid: K+ channels and gastric acid secretion. *Physiology (Bethesda)* **22**, 335–341 (2007).
67. O. Kosiek, S. M. Busque, M. Föller, N. Shcheynikov, P. Kirchhoff, M. Bleich, S. Muallem, J. P. Geibel, SLC26A7 can function as a chloride-loading mechanism in parietal cells. *Pflugers Arch.* **454**, 989–998 (2007).
68. H. Kulaksiz, R. Arnold, B. Göke, E. Maronde, M. Meyer, F. Fahrenholz, W. G. Forssmann, R. Eissele, Expression and cell-specific localization of the cholecystokinin B/gastrin receptor in the human stomach. *Cell Tissue Res.* **299**, 289–298 (2000).
69. F. Grahammer, A. W. Herling, H. J. Lang, A. Schmitt-Gräff, O. H. Wittekindt, R. Nitschke, M. Bleich, J. Barhanin, R. Warth, The cardiac K+ channel KCNQ1 is essential for gastric acid secretion. *Gastroenterology* **120**, 1363–1371 (2001).
70. T. K. Roepke, A. Anantharam, P. Kirchhoff, S. M. Busque, J. B. Young, J. P. Geibel, D. J. Lerner, G. W. Abbott, The KCNE2 potassium channel ancillary subunit is essential for gastric acid secretion. *J. Biol. Chem.* **281**, 23740–23747 (2006).
71. J. Xu, P. Song, S. Nakamura, M. Miller, S. Barone, S. L. Alper, B. Riederer, J. Bonhagen, L. J. Arend, H. Amlal, U. Seidler, M. Soleimani, Deletion of the chloride transporter slc26a7 causes distal renal tubular acidosis and impairs gastric acid secretion. *J. Biol. Chem.* **284**, 29470–29479 (2009).
72. N. Langhans, G. Rindi, M. Chiu, J. F. Rehfeld, B. Ardman, M. Beinborn, A. S. Kopin, Abnormal gastric histology and decreased acid production in cholecystokinin-B/gastrin receptor-deficient mice. *Gastroenterology* **112**, 280–286 (1997).
73. T. Kobayashi, S. Tonai, Y. Ishihara, R. Koga, S. Okabe, T. Watanabe, Abnormal functional and morphological regulation of the gastric mucosa in histamine H2 receptor-deficient mice. *J. Clin.*

bioRxiv preprint doi: https://doi.org/10.64898/2026.07.24.740446; this version posted July 24, 2026. The copyright holder for this preprint (which was not certified by peer review) is the author/funder, who has granted bioRxiv a license to display the preprint in perpetuity. It is made available under a CC-BY-NC 4.0 International license.

Invest. **105**, 1741–1749 (2000).
74. C. S. Rouk, Gastric morphology and adaptive radiation in the phyllostomatidae. (1973).
75. C. Machado-Santos, A. A. do Nascimento, A. L. Peracchi, J. S. Mikalauskas, P. A. Rocha, A. Sales, Distributions of the endocrine cells in the gastrointestinal tract of nectarivorous and sanguivorous bats: a comparative immunocytochemical study. *Tissue Cell* **41**, 222–229 (2009).
76. A. M. Rodríguez-Piñeiro, J. H. Bergström, A. Ermund, J. K. Gustafsson, A. Schütte, M. E. V. Johansson, G. C. Hansson, Studies of mucus in mouse stomach, small intestine, and colon. II. Gastrointestinal mucus proteome reveals Muc2 and Muc5ac accompanied by a set of core proteins. *Am. J. Physiol. Gastrointest. Liver Physiol.* **305**, G348–56 (2013).
77. F. Heuer, R. Stürmer, J. Heuer, T. Kalinski, A. Lemke, F. Meyer, W. Hoffmann, Different forms of TFF2, A lectin of the human gastric mucus barrier: In vitro binding studies. *Int. J. Mol. Sci.* **20**, 5871 (2019).
78. M. A. Järvå, J. P. Lingford, A. John, N. M. Soler, N. E. Scott, E. D. Goddard-Borger, Trefoil factors share a lectin activity that defines their role in mucus. *Nat. Commun.* **11**, 1–9 (2020).
79. J. J. Farrell, D. Taupin, T. J. Koh, D. Chen, C.-M. Zhao, D. K. Podolsky, T. C. Wang, TFF2/SP-deficient mice show decreased gastric proliferation, increased acid secretion, and increased susceptibility to NSAID injury. *J. Clin. Invest.* **109**, 193–204 (2002).
80. W. Hoffmann, Trefoil Factor Family (TFF) Peptides and Their Diverse Molecular Functions in Mucus Barrier Protection and More: Changing the Paradigm. *Int. J. Mol. Sci.* **21** (2020).
81. S. Öling, E. Struck, M. Noreen-Thorsen, M. Zwahlen, K. von Feilitzen, J. Odeberg, F. Pontén, C. Lindskog, M. Uhlén, P. Dusart, L. M. Butler, A human stomach cell type transcriptome atlas. *BMC Biol.* **22**, 36 (2024).
82. H. Fukamachi, M. Ichinose, S. Ishihama, S. Tsukada, S. Yasugi, K. Shiokawa, C. Furihata, S. Yonezawa, K. Miki, Fetal rat glandular stomach epithelial cells differentiate into surface mucous cells which express cathepsin E in the absence of mesenchymal cells in primary culture. *Differentiation* **56**, 83–89 (1994).
83. D. J. Strick, L. A. Elferink, Rab15 effector protein: a novel protein for receptor recycling from the endocytic recycling compartment. *Mol. Biol. Cell* **16**, 5699–5709 (2005).
84. Y. Wang, W. Song, J. Wang, T. Wang, X. Xiong, Z. Qi, W. Fu, X. Yang, Y.-G. Chen, Single-cell transcriptome analysis reveals differential nutrient absorption functions in human intestine. *J. Exp. Med.* **217** (2020).
85. S. Hata, M. Abe, H. Suzuki, F. Kitamura, N. Toyama-Sorimachi, K. Abe, K. Sakimura, H. Sorimachi, Calpain 8/nCL-2 and calpain 9/nCL-4 constitute an active protease complex, G-calpain, involved in gastric mucosal defense. *PLoS Genet.* **6**, e1001040 (2010).
86. A. López-Ferrer, C. de Bolós, C. Barranco, M. Garrido, J. Isern, I. Carlstedt, C. A. Reis, J. Torrado, F. X. Real, Role of fucosyltransferases in the association between apomucin and Lewis antigen expression in normal and malignant gastric epithelium. *Gut* **47**, 349–356 (2000).
87. A. López-Ferrer, C. de Bolós, The expression of human FUT1 in HT-29/M3 colon cancer cells instructs the glycosylation of MUC1 and MUC5AC apomucins. *Glycoconj. J.* **19**, 13–21 (2002).
88. A. Magalhães, Y. Rossez, C. Robbe-Masselot, E. Maes, J. Gomes, A. Shevtsova, J. Bugaytsova, T. Borén, C. A. Reis, Muc5ac gastric mucin glycosylation is shaped by FUT2 activity and functionally impacts Helicobacter pylori binding. *Sci. Rep.* **6**, 25575 (2016).
89. E. P. Bennett, U. Mandel, H. Clausen, T. A. Gerken, T. A. Fritz, L. A. Tabak, Control of mucin-type O-glycosylation: a classification of the polypeptide GalNAc-transferase gene family. *Glycobiology* **22**, 736–756 (2012).
90. S.-W. Park, G. Zhen, C. Verhaeghe, Y. Nakagami, L. T. Nguyenvu, A. J. Barczak, N. Killeen, D. J. Erle, The protein disulfide isomerase AGR2 is essential for production of intestinal mucus. *Proceedings of the National Academy of Sciences* **106**, 6950–6955 (2009).
91. M. J. Grey, H. De Luca, D. V. Ward, I. A. Kreulen, K. Bugda Gwilt, S. E. Foley, J. R. Thiagarajah, B. A. McCormick, J. R. Turner, W. I. Lencer, The epithelial-specific ER stress sensor ERN2/IRE1β enables host-microbiota crosstalk to affect colon goblet cell development. *J. Clin. Invest.* **132** (2022).
92. A. McShane, J. Bath, A. M. Jaramillo, C. Ridley, A. A. Walsh, C. M. Evans, D. J. Thornton, K. Ribbeck, Mucus. *Curr. Biol.* **31**, R938–R945 (2021).

bioRxiv preprint doi: https://doi.org/10.64898/2026.07.24.740446; this version posted July 24, 2026. The copyright holder for this preprint (which was not certified by peer review) is the author/funder, who has granted bioRxiv a license to display the preprint in perpetuity. It is made available under a CC-BY-NC 4.0 International license.

93. J. Carpenter, Y. Wang, R. Gupta, Y. Li, P. Haridass, D. B. Subramani, B. Reidel, L. Morton, C. Ridley, W. K. O'Neal, M.-P. Buisine, C. Ehre, D. J. Thornton, M. Kesimer, Assembly and organization of the N-terminal region of mucin MUC5AC: Indications for structural and functional distinction from MUC5B. *Proc. Natl. Acad. Sci. U. S. A.* **118**, e2104490118 (2021).
94. H. J. Harlow, E. J. Braun, Gastric Na+K+ATPase activity and intestinal urea hydrolysis of the common vampire bat, Desmodus rotundus. *Comp. Biochem. Physiol. A Physiol.* **118**, 665–669 (1997).
95. E. R. Price, A. Brun, M. Gontero-Fourcade, G. Fernández-Marinone, A. P. Cruz-Neto, W. H. Karasov, E. Caviedes-Vidal, Intestinal Water Absorption Varies with Expected Dietary Water Load among Bats but Does Not Drive Paracellular Nutrient Absorption. *Physiol. Biochem. Zool.* **88**, 680–684 (2015).
96. W. N. McFarland, W. A. Wimsatt, Renal function and its relation to the ecology of the vampire bat, Desmodus rotundus. *Comp. Biochem. Physiol.* **28**, 985–1006 (1969).
97. T. Matsuzaki, Y. Tajika, A. Ablimit, T. Aoki, H. Hagiwara, K. Takata, Aquaporins in the digestive system. *Med. Electron Microsc.* **37**, 71–80 (2004).
98. S. Törnroth-Horsefield, C. Chivasso, H. Strandberg, C. D'Agostino, C. V. T. O'Neale, K. L. Schey, C. Delporte, Insight into the Mammalian Aquaporin Interactome. *Int. J. Mol. Sci.* **23** (2022).
99. M. D. Lee, K. Y. Bhakta, S. Raina, R. Yonescu, C. A. Griffin, N. G. Copeland, D. J. Gilbert, N. A. Jenkins, G. M. Preston, P. Agre, The human Aquaporin-5 gene. Molecular characterization and chromosomal localization. *J. Biol. Chem.* **271**, 8599–8604 (1996).
100. G. M. Preston, T. P. Carroll, W. B. Guggino, P. Agre, Appearance of water channels in Xenopus oocytes expressing red cell CHIP28 protein. *Science* **256**, 385–387 (1992).
101. C. Busch, Consumption of blood, renal function and utilization of free water by the vampire bat, Desmodus rotundus. *Comp. Biochem. Physiol. A Comp. Physiol.* **90**, 141–146 (1988).
102. T. R. Kleyman, D. C. Eaton, Regulating ENaC's gate. *Am. J. Physiol. Cell Physiol.* **318**, C150–C162 (2020).
103. H. Yamamura, S. Ugawa, T. Ueda, M. Nagao, S. Shimada, Protons activate the delta-subunit of the epithelial Na+ channel in humans. *J. Biol. Chem.* **279**, 12529–12534 (2004).
104. A. A. Konstas, D. Mavrelos, C. Korbmacher, Conservation of pH sensitivity in the epithelial sodium channel (ENaC) with Liddle's syndrome mutation. *Pflugers Arch.* **441**, 341–350 (2000).
105. J. Xu, P. Song, M. L. Miller, F. Borgese, S. Barone, B. Riederer, Z. Wang, S. L. Alper, J. G. Forte, G. E. Shull, J. Ehrenfeld, U. Seidler, M. Soleimani, Deletion of the chloride transporter Slc26a9 causes loss of tubulovesicles in parietal cells and impairs acid secretion in the stomach. *Proc. Natl. Acad. Sci. U. S. A.* **105**, 17955–17960 (2008).
106. J. D. Walter, M. Sawicka, R. Dutzler, Cryo-EM structures and functional characterization of murine Slc26a9 reveal mechanism of uncoupled chloride transport. *Elife* **8**, e46986 (2019).
107. A. Rajgopal, A. Edmondnson, I. D. Goldman, R. Zhao, SLC19A3 encodes a second thiamine transporter ThTr2. *Biochim. Biophys. Acta* **1537**, 175–178 (2001).
108. A. Wen, Y. Zhu, S. W. Yee, B. I. Park, K. M. Giacomini, A. S. Greenberg, J. W. Newman, The impacts of Slc19a3 deletion and intestinal SLC19A3 insertion on thiamine distribution and brain metabolism in the mouse. *Metabolites* **13**, 885 (2023).
109. R. Zhao, I. D. Goldman, Folate and thiamine transporters mediated by facilitative carriers (SLC19A1-3 and SLC46A1) and folate receptors. *Mol. Aspects Med.* **34**, 373–385 (2013).
110. T. O. Findley, J. C. Tenpenny, M. R. O'Byrne, A. C. Morrison, J. E. Hixson, H. Northrup, K. S. Au, Mutations in folate transporter genes and risk for human myelomeningocele. *Am. J. Med. Genet. A* **173**, 2973–2984 (2017).
111. Y. Kihara, J. Chun, Neuroprotective crosstalk from vitamin B12 and sphingolipid signaling pathways in therapy for multiple sclerosis. *Int. Immunol.*, doi: 10.1093/intimm/dxaf058 (2025).
112. T. Kitazawa, H. Kaiya, Regulation of gastrointestinal motility by motilin and ghrelin in vertebrates. *Front. Endocrinol. (Lausanne)* **10**, 278 (2019).
113. J. Yamada, V. J. Campos, N. Kitamura, A. C. Pacheco, T. Yamashita, U. Caramaschi, Immunocytochemical study of gastro-entero-pancreatic (GEP) endocrine cells in the vampire bat (Desmodos rotundus). *Gegenbaurs Morphol. Jahrb.* **130**, 845–856 (1984).
114. S. Wang, L. Ghibaudi, T. Hashemi, C. He, C. Strader, M. Bayne, H. Davis, J. J. Hwa, The

bioRxiv preprint doi: https://doi.org/10.64898/2026.07.24.740446; this version posted July 24, 2026. The copyright holder for this preprint (which was not certified by peer review) is the author/funder, who has granted bioRxiv a license to display the preprint in perpetuity. It is made available under a CC-BY-NC 4.0 International license.

GalR2 galanin receptor mediates galanin-induced jejunal contraction, but not feeding behavior, in the rat: differentiation of central and peripheral effects of receptor subtype activation. *FEBS Lett.* **434**, 277–282 (1998).

115. C.-Y. Lin, M. Zhang, T. Huang, L.-L. Yang, H.-B. Fu, L. Zhao, L. L. D. Zhong, H.-X. Mu, X.-K. Shi, C. F. P. Leung, B.-M. Fan, M. Jiang, A.-P. Lu, L.-X. Zhu, Z.-X. Bian, Spexin enhances bowel movement through activating L-type voltage-dependent calcium channel via Galanin receptor 2 in mice. *Sci. Rep.* **5**, 12095 (2015).
116. S. Shen, J. Jiang, Y. Yuan, Pepsinogen C expression, regulation and its relationship with cancer. *Cancer Cell Int.* **17**, 57 (2017).
117. D. Mosztbacher, Z. Jancsó, M. Sahin-Tóth, Loss of chymotrypsin-like protease (CTRL) alters intrapancreatic protease activation but not pancreatitis severity in mice. *Sci. Rep.* **10**, 11731 (2020).
118. B. Z. Németh, A. Demcsák, A. Micsonai, B. Kiss, G. Schlosser, A. Geisz, E. Hegyi, M. Sahin-Tóth, G. Pál, Arg236 in human chymotrypsin B2 (CTRB2) is a key determinant of high enzyme activity, trypsinogen degradation capacity, and protection against pancreatitis. *Biochim. Biophys. Acta Proteins Proteom.* **1870**, 140831 (2022).
119. R. H. Pfützer, M. M. Barmada, A. P. Brunskill, R. Finch, P. S. Hart, J. Neoptolemos, W. F. Furey, D. C. Whitcomb, SPINK1/PSTI polymorphisms act as disease modifiers in familial and idiopathic chronic pancreatitis. *Gastroenterology* **119**, 615–623 (2000).
120. L.-T. Nguyen, H. A. Schmidt, A. von Haeseler, B. Q. Minh, IQ-TREE: A Fast and Effective Stochastic Algorithm for Estimating Maximum-Likelihood Phylogenies. *Mol. Biol. Evol.* **32**, 268–274 (2015).
121. H. Išerić, C. Alkan, F. Hach, I. Numanagić, Fast characterization of segmental duplication structure in multiple genome assemblies. *Algorithms Mol. Biol.* **17**, 4 (2022).
122. S. Bröer, Intestinal amino acid transport and metabolic health. *Annu. Rev. Nutr.* **43**, 73–99 (2023).
123. R. Kleta, E. Romeo, Z. Ristic, T. Ohura, C. Stuart, M. Arcos-Burgos, M. H. Dave, C. A. Wagner, S. R. M. Camargo, S. Inoue, N. Matsuura, A. Helip-Wooley, D. Bockenhauer, R. Warth, I. Bernardini, G. Visser, T. Eggermann, P. Lee, A. Chairoungdua, P. Jutabha, E. Babu, S. Nilwarangkoon, N. Anzai, Y. Kanai, F. Verrey, W. A. Gahl, A. Koizumi, Mutations in SLC6A19, encoding B0AT1, cause Hartnup disorder. *Nat. Genet.* **36**, 999–1002 (2004).
124. M. G. E. Knol, V. C. Wulfmeyer, R.-U. Müller, M. M. Rinschen, Amino acid metabolism in kidney health and disease. *Nat. Rev. Nephrol.* **20**, 771–788 (2024).
125. H. Quan, K. Athirakul, W. C. Wetsel, G. E. Torres, R. Stevens, Y. T. Chen, T. M. Coffman, M. G. Caron, Hypertension and impaired Glycine handling in mice lacking the orphan transporter XT2. *Mol. Cell. Biol.* **24**, 4166–4173 (2004).
126. N. Torres, G. López, S. De Santiago, S. M. Hutson, A. R. Tovar, Dietary protein level regulates expression of the mitochondrial branched-chain aminotransferase in rats. *J. Nutr.* **128**, 1368–1375 (1998).
127. N. Torres, S. Tobón-Cornejo, L. A. Velazquez-Villegas, L. G. Noriega, G. Alemán-Escondrillas, A. R. Tovar, Amino acid catabolism: An overlooked area of metabolism. *Nutrients* **15** (2023).
128. E. Márquez, M. Bracho, A. Archile, L. Rangel, B. Benítez, Proteins, isoleucine, lysine and methionine content of bovine, porcine and poultry blood and their fractions. *Food Chem.* **93**, 503–505 (2005).
129. A. Hallen, J. F. Jamie, A. J. L. Cooper, Lysine metabolism in mammalian brain: an update on the importance of recent discoveries. *Amino Acids* **45**, 1249–1272 (2013).
130. Y. Tan, M. Chrysopoulou, M. M. Rinschen, Integrative physiology of lysine metabolites. *Physiol. Genomics* **55**, 579–586 (2023).
131. S. M. Houten, S. Denis, H. Te Brinke, A. Jongejan, A. H. C. van Kampen, E. J. Bradley, F. Baas, R. C. M. Hennekam, D. S. Millington, S. P. Young, D. M. Frazier, M. Gucsavas-Calikoglu, R. J. A. Wanders, Mitochondrial NADP(H) deficiency due to a mutation in NADK2 causes dienoyl-CoA reductase deficiency with hyperlysinemia. *Hum. Mol. Genet.* **23**, 5009–5016 (2014).
132. M. E. Brosnan, J. T. Brosnan, Histidine metabolism and function. *J. Nutr.* **150**, 2570S–2575S (2020).

bioRxiv preprint doi: https://doi.org/10.64898/2026.07.24.740446; this version posted July 24, 2026. The copyright holder for this preprint (which was not certified by peer review) is the author/funder, who has granted bioRxiv a license to display the preprint in perpetuity. It is made available under a CC-BY-NC 4.0 International license.

133. J. E. Dominy Jr, J. Hwang, M. H. Stipanuk, Overexpression of cysteine dioxygenase reduces intracellular cysteine and glutathione pools in HepG2/C3A cells. *Am. J. Physiol. Endocrinol. Metab.* **293**, E62–9 (2007).
134. M. Chen, J.-Y. Zhu, W.-J. Mu, L. Guo, Cysteine dioxygenase type 1 (CDO1): Its functional role in physiological and pathophysiological processes. *Genes Dis.* **10**, 877–890 (2023).
135. J. B. Kohl, A.-T. Mellis, G. Schwarz, Homeostatic impact of sulfite and hydrogen sulfide on cysteine catabolism: Homeostatic impact of sulfite and H_2S on cysteine catabolism. *Br. J. Pharmacol.* **176**, 554–570 (2019).
136. M. M. Adeva, G. Souto, Diet-induced metabolic acidosis. *Clin. Nutr.* **30**, 416–421 (2011).
137. G.-J. Ko, C. M. Rhee, K. Kalantar-Zadeh, S. Joshi, The effects of high-protein diets on kidney health and longevity. *J. Am. Soc. Nephrol.* **31**, 1667–1679 (2020).
138. K. Chan, S. M. Busque, M. Sailer, C. Stoeger, S. Bröer, H. Daniel, I. Rubio-Aliaga, C. A. Wagner, Loss of function mutation of the Slc38a3 glutamine transporter reveals its critical role for amino acid metabolism in the liver, brain, and kidney. *Pflugers Arch.* **468**, 213–227 (2016).
139. Y. Zhou, T. Eid, B. Hassel, N. C. Danbolt, Novel aspects of glutamine synthetase in ammonia homeostasis. *Neurochem. Int.* **140**, 104809 (2020).
140. I. Rubio-Aliaga, C. A. Wagner, Regulation and function of the SLC38A3/SNAT3 glutamine transporter. *Channels (Austin)* **10**, 440–452 (2016).
141. Y.-H. Hung, A. L. Carreiro, K. K. Buhman, Dgat1 and Dgat2 regulate enterocyte triacylglycerol distribution and alter proteins associated with cytoplasmic lipid droplets in response to dietary fat. *Biochim. Biophys. Acta Mol. Cell Biol. Lipids* **1862**, 600–614 (2017).
142. K. Johnson, L. Ross, R. Miller, X. Xiao, M. E. Lowe, Pancreatic lipase-related protein 2 digests fats in human milk and formula in concert with gastric lipase and carboxyl ester lipase. *Pediatr. Res.* **74**, 127–132 (2013).
143. X. He, S. McClorry, O. Hernell, B. Lönnerdal, C. M. Slupsky, Digestion of human milk fat in healthy infants. *Nutr. Res.* **83**, 15–29 (2020).
144. B. B. Johansson, K. Fjeld, K. El Jellas, A. Gravdal, M. Dalva, E. Tjora, H. Ræder, R. N. Kulkarni, S. Johansson, P. R. Njølstad, A. Molven, The role of the carboxyl ester lipase (CEL) gene in pancreatic disease. *Pancreatology* **18**, 12–19 (2018).
145. G. Zhu, Q. Fang, F. Zhu, D. Huang, C. Yang, Structure and function of pancreatic lipase-related protein 2 and its relationship with pathological states. *Front. Genet.* **12**, 693538 (2021).
146. W. B. Kinlaw, J. L. Church, J. Harmon, C. N. Mariash, Direct evidence for a role of the “spot 14” protein in the regulation of lipid synthesis. *J. Biol. Chem.* **270**, 16615–16618 (1995).
147. D. L. Aipoalani, B. L. O’Callaghan, D. G. Mashek, C. N. Mariash, H. C. Towle, Overlapping roles of the glucose-responsive genes, S14 and S14R, in hepatic lipogenesis. *Endocrinology* **151**, 2071–2077 (2010).
148. G. Fernandez-Fuente, M. J. Rigby, L. Puglielli, Intracellular Citrate/acetyl-CoA flux and endoplasmic reticulum acetylation: Connectivity is the answer. *Mol. Metab.* **67**, 101653 (2023).
149. J. D. Bergstrom, The lipogenic enzyme acetoacetyl-CoA synthetase and ketone body utilization for denovo lipid synthesis, a review. *J. Lipid Res.* **64**, 100407 (2023).
150. A. J. Rauckhorst, R. D. Sheldon, D. J. Pape, A. Ahmed, K. C. Falls-Hubert, R. A. Merrill, R. F. Brown, K. Deshmukh, T. A. Vallim, S. Deja, S. C. Burgess, E. B. Taylor, A hierarchical hepatic de novo lipogenesis substrate supply network utilizing pyruvate, acetate, and ketones. *Cell Metab.* **37**, 255–273.e6 (2024).
151. E. D. Queathem, Z. Moazzami, D. B. Stagg, A. B. Nelson, K. Fulghum, A. Hayir, A. Seay, J. R. Gillingham, D. A. d’Avignon, X. Han, H.-B. Ruan, P. A. Crawford, P. Puchalska, Ketogenesis supports hepatic polyunsaturated fatty acid homeostasis via fatty acid elongation. *Sci. Adv.* **11**, eads0535 (2025).
152. W. Xiao, R.-S. Wang, D. E. Handy, J. Loscalzo, NAD(H) and NADP(H) redox couples and cellular energy metabolism. *Antioxid. Redox Signal.* **28**, 251–272 (2018).
153. S.-I. Oka, A. S. Titus, D. Zablocki, J. Sadoshima, Molecular properties and regulation of NAD+ kinase (NADK). *Redox Biol.* **59**, 102561 (2023).
154. K. Zhang, H. Kim, Z. Fu, Y. Qiu, Z. Yang, J. Wang, D. Zhang, X. Tong, L. Yin, J. Li, J. Wu, N.

bioRxiv preprint doi: https://doi.org/10.64898/2026.07.24.740446; this version posted July 24, 2026. The copyright holder for this preprint (which was not certified by peer review) is the author/funder, who has granted bioRxiv a license to display the preprint in perpetuity. It is made available under a CC-BY-NC 4.0 International license.

R. Qi, S. M. Houten, R. Zhang, Deficiency of the mitochondrial NAD kinase causes stress-induced hepatic steatosis in mice. *Gastroenterology* **154**, 224–237 (2018).

155. G. C. Murray, P. Bais, C. L. Hatton, A. L. D. Tadenev, B. R. Hoffmann, T. J. Stodola, K. H. Morelli, S. L. Pratt, D. Schroeder, R. Doty, O. Fiehn, S. W. M. John, C. J. Bult, G. A. Cox, R. W. Burgess, Mouse models of NADK2 deficiency analyzed for metabolic and gene expression changes to elucidate pathophysiology. *Hum. Mol. Genet.* **31**, 4055–4074 (2022).

156. J. P. Dewulf, S. Paquay, E. Marbaix, Y. Achouri, E. Van Schaftingen, G. T. Bommer, ECHDC1 knockout mice accumulate ethyl-branched lipids and excrete abnormal intermediates of branched-chain fatty acid metabolism. *Journal of Biological Chemistry* **297**, 101083 (2021).

157. E. H. Van Beers, H. A. Büller, R. J. Grand, A. W. Einerhand, J. Dekker, Intestinal brush border glycohydrolases: structure, function, and development. *Crit. Rev. Biochem. Mol. Biol.* **30**, 197–262 (1995).

158. W. Lissens, L. De Meirleir, S. Seneca, I. Liebaers, G. K. Brown, R. M. Brown, M. Ito, E. Naito, Y. Kuroda, D. S. Kerr, I. D. Wexler, M. S. Patel, B. H. Robinson, A. Seyda, Mutations in the X-linked pyruvate dehydrogenase (E1) alpha subunit gene (PDHA1) in patients with a pyruvate dehydrogenase complex deficiency. *Hum. Mutat.* **15**, 209–219 (2000).

159. K. P. Patel, T. W. O'Brien, S. H. Subramony, J. Shuster, P. W. Stacpoole, The spectrum of pyruvate dehydrogenase complex deficiency: clinical, biochemical and genetic features in 371 patients. *Mol. Genet. Metab.* **105**, 34–43 (2012).

160. S. Park, J. H. Jeon, B. K. Min, C. M. Ha, T. Thoudam, B. Y. Park, I. K. Lee, Role of the pyruvate dehydrogenase complex in metabolic remodeling: Differential pyruvate dehydrogenase complex functions in metabolism. *Diabetes Metab. J.* **42**, 270–281 (2018).

161. K. Sofou, M. Dahlin, T. Hallböök, M. Lindefeldt, G. Viggedal, N. Darin, Ketogenic diet in pyruvate dehydrogenase complex deficiency: short- and long-term outcomes. *J. Inherit. Metab. Dis.* **40**, 237–245 (2017).

162. P. N. Wahjudi, M. E. Patterson, S. Lim, J. K. Yee, C. S. Mao, W.-N. P. Lee, Measurement of glucose and fructose in clinical samples using gas chromatography/mass spectrometry. *Clin. Biochem.* **43**, 198–207 (2010).

163. S. Munro, H. Ceulemans, M. Bollen, J. Diplexcito, P. T. W. Cohen, A novel glycogen-targeting subunit of protein phosphatase 1 that is regulated by insulin and shows differential tissue distribution in humans and rodents: Novel glycogen-targeting subunit of PP1. *FEBS J.* **272**, 1478–1489 (2005).

164. M. C. Petersen, D. F. Vatner, G. I. Shulman, Regulation of hepatic glucose metabolism in health and disease. *Nat. Rev. Endocrinol.* **13**, 572–587 (2017).

165. M. B. Freitas, C. B. C. Passos, R. B. Vasconcelos, E. C. Pinheiro, Effects of short-term fasting on energy reserves of vampire bats (Desmodus rotundus). *Comp. Biochem. Physiol. B Biochem. Mol. Biol.* **140**, 59–62 (2005).

166. C. Machado-Santos, J. C. F. Aquino, J. S. Mikalauka, What difference exists in the pancreas of mammals with sanguivorous diet? A morphological, stereological and immunohistochemical study of the pancreatic islets of the hematophagous bat Diphylla ecaudata. *Regul. Pept.* **183**, 62–68 (2013).

167. X. Zhu, A. Zhou, A. Dey, C. Norrbom, R. Carroll, C. Zhang, V. Laurent, I. Lindberg, R. Ugleholdt, J. J. Holst, D. F. Steiner, Disruption of PC1/3 expression in mice causes dwarfism and multiple neuroendocrine peptide processing defects. *Proc. Natl. Acad. Sci. U. S. A.* **99**, 10293–10298 (2002).

168. P. Stijnen, B. Ramos-Molina, S. O'Rahilly, J. W. M. Creemers, PCSK1 mutations and human endocrinopathies: From obesity to gastrointestinal disorders. *Endocr. Rev.* **37**, 347–371 (2016).

169. V. Lang, P. E. Light, The molecular mechanisms and pharmacotherapy of ATP-sensitive potassium channel gene mutations underlying neonatal diabetes. *Pharmgenomics. Pers. Med.* **3**, 145–161 (2010).

170. J. S. McTaggart, R. H. Clark, F. M. Ashcroft, The role of the KATP channel in glucose homeostasis in health and disease: more than meets the islet. *J. Physiol.* **588**, 3201–3209 (2010).

171. F. Chimienti, S. Devergnas, A. Favier, M. Seve, Identification and cloning of a beta-cell-specific zinc transporter, ZnT-8, localized into insulin secretory granules. *Diabetes* **53**, 2330–2337 (2004).

172. T. J. Nicolson, E. A. Bellomo, N. Wijesekara, M. K. Loder, J. M. Baldwin, A. V.

bioRxiv preprint doi: https://doi.org/10.64898/2026.07.24.740446; this version posted July 24, 2026. The copyright holder for this preprint (which was not certified by peer review) is the author/funder, who has granted bioRxiv a license to display the preprint in perpetuity. It is made available under a CC-BY-NC 4.0 International license.

Gyulkhandanyan, V. Koshkin, A. I. Tarasov, R. Carzaniga, K. Kronenberger, T. K. Taneja, G. da Silva Xavier, S. Libert, P. Froguel, R. Scharfmann, V. Stetsyuk, P. Ravassard, H. Parker, F. M. Gribble, F. Reimann, R. Sladek, S. J. Hughes, P. R. V. Johnson, M. Masseboeuf, R. Burcelin, S. A. Baldwin, M. Liu, R. Lara-Lemus, P. Arvan, F. C. Schuit, M. B. Wheeler, F. Chimienti, G. A. Rutter, Insulin storage and glucose homeostasis in mice null for the granule zinc transporter ZnT8 and studies of the type 2 diabetes-associated variants. *Diabetes* **58**, 2070–2083 (2009).

173. A. D. Mancini, V. Poitout, The fatty acid receptor FFA1/GPR40 a decade later: how much do we know? *Trends Endocrinol. Metab.* **24**, 398–407 (2013).

174. S. Edfalk, P. Steneberg, H. Edlund, Gpr40 is expressed in enteroendocrine cells and mediates free fatty acid stimulation of incretin secretion. *Diabetes* **57**, 2280–2287 (2008).

175. E. L. Edghill, S. E. Flanagan, A.-M. Patch, C. Boustred, A. Parrish, B. Shields, M. H. Shepherd, K. Hussain, R. R. Kapoor, M. Malecki, M. J. MacDonald, J. Støy, D. F. Steiner, L. H. Philipson, G. I. Bell, Neonatal Diabetes International Collaborative Group, A. T. Hattersley, S. Ellard, Insulin mutation screening in 1,044 patients with diabetes: mutations in the INS gene are a common cause of neonatal diabetes but a rare cause of diabetes diagnosed in childhood or adulthood. *Diabetes* **57**, 1034–1042 (2008).

176. J. Støy, E. De Franco, H. Ye, S.-Y. Park, G. I. Bell, A. T. Hattersley, In celebration of a century with insulin - Update of insulin gene mutations in diabetes. *Mol. Metab.* **52**, 101280 (2021).

177. T. Gutmann, K. H. Kim, M. Grzybek, T. Walz, Ü. Coskun, Visualization of ligand-induced transmembrane signaling in the full-length human insulin receptor. *J. Cell Biol.* **217**, 1643–1649 (2018).

178. K. Yamada, J. L. Carpentier, B. Cheatham, E. Goncalves, S. E. Shoelson, C. R. Kahn, Role of the transmembrane domain and flanking amino acids in internalization and down-regulation of the insulin receptor. *J. Biol. Chem.* **270**, 3115–3122 (1995).

179. M. R. Riddle, A. C. Aspiras, K. Gaudenz, R. Peuß, J. Y. Sung, B. Martineau, M. Peavey, A. C. Box, J. A. Tabin, S. McGaugh, R. Borowsky, C. J. Tabin, N. Rohner, Insulin resistance in cavefish as an adaptation to a nutrient-limited environment. *Nature* **555**, 647–651 (2018).

180. S. Jiang, J. L. Young, K. Wang, Y. Qian, L. Cai, Diabetic-induced alterations in hepatic glucose and lipid metabolism: The role of type 1 and type 2 diabetes mellitus (Review). *Mol. Med. Rep.* **22**, 603–611 (2020).

181. D. Morton, W. A. Wimsatt, Distribution of iron in the gastrointestinal tract of the common vampire bat: evidence for macrophage-linked iron clearance. *Anat. Rec.* **198**, 183–192 (1980).

182. G. Unlu, B. Prizer, R. Erdal, H.-W. Yeh, E. C. Bayraktar, K. Birsoy, Metabolic-scale gene activation screens identify SLCO2B1 as a heme transporter that enhances cellular iron availability. *Mol. Cell* **82**, 3750 (2022).

183. H. Li, D. Wang, H. Wu, H. Shen, D. Lv, Y. Zhang, H. Lu, J. Yang, Y. Tang, M. Li, SLC46A1 contributes to hepatic iron metabolism by importing heme in hepatocytes. *Metabolism* **110**, 154306 (2020).

184. H.-O. Pae, H.-T. Chung, Heme oxygenase-1: its therapeutic roles in inflammatory diseases. *Immune Netw.* **9**, 12–19 (2009).

185. D. M. Ward, J. Kaplan, Ferroportin-mediated iron transport: expression and regulation. *Biochim. Biophys. Acta* **1823**, 1426–1433 (2012).

186. E. Nemeth, M. S. Tuttle, J. Powelson, M. B. Vaughn, A. Donovan, D. M. Ward, T. Ganz, J. Kaplan, Hepcidin regulates cellular iron efflux by binding to ferroportin and inducing its internalization. *Science* **306**, 2090–2093 (2004).

187. B. Jiang, G. Liu, J. Zheng, M. Chen, Z. Maimaitiming, M. Chen, S. Liu, R. Jiang, B. K. Fuqua, J. L. Dunaief, C. D. Vulpe, G. J. Anderson, H. Wang, H. Chen, Hephaestin and ceruloplasmin facilitate iron metabolism in the mouse kidney. *Sci. Rep.* **6**, 39470 (2016).

188. A. T. McKie, D. Barrow, G. O. Latunde-Dada, A. Rolfs, G. Sager, E. Mudaly, M. Mudaly, C. Richardson, D. Barlow, A. Bomford, T. J. Peters, K. B. Raja, S. Shirali, M. A. Hediger, F. Farzaneh, R. J. Simpson, An iron-regulated ferric reductase associated with the absorption of dietary iron. *Science* **291**, 1755–1759 (2001).

189. F. Meng, B. A. Fleming, X. Jia, A. A. Rousek, M. A. Mulvey, D. M. Ward, Lysosomal iron

bioRxiv preprint doi: https://doi.org/10.64898/2026.07.24.740446; this version posted July 24, 2026. The copyright holder for this preprint (which was not certified by peer review) is the author/funder, who has granted bioRxiv a license to display the preprint in perpetuity. It is made available under a CC-BY-NC 4.0 International license.

recycling in mouse macrophages is dependent upon both LcytB and Steap3 reductases. *Blood Adv.* **6**, 1692–1707 (2022).

190. R. S. Ohgami, D. R. Campagna, E. L. Greer, B. Antiochos, A. McDonald, J. Chen, J. J. Sharp, Y. Fujiwara, J. E. Barker, M. D. Fleming, Identification of a ferrireductase required for efficient transferrin-dependent iron uptake in erythroid cells. *Nat. Genet.* **37**, 1264–1269 (2005).
191. L. Blanc, J. Papoin, G. Debnath, M. Vidal, R. Amson, A. Telerman, X. An, N. Mohandas, Abnormal erythroid maturation leads to microcytic anemia in the TSAP6/Steap3 null mouse model: Dyserythropoiesis and microcytic anemia in Steap3−/− mice. *Am. J. Hematol.* **90**, 235–241 (2015).
192. M. J. Koury, P. Ponka, New insights into erythropoiesis: the roles of folate, vitamin B12, and iron. *Annu. Rev. Nutr.* **24**, 105–131 (2004).
193. J. L. Johns, M. M. Christopher, Extramedullary hematopoiesis: a new look at the underlying stem cell niche, theories of development, and occurrence in animals. *Vet. Pathol.* **49**, 508–523 (2012).
194. I. Udroiu, Storage of blood in the mammalian spleen: An evolutionary perspective. *J. Mamm. Evol.* **24**, 243–260 (2017).
195. H. J. Cha, Erythropoiesis: insights from a genomic perspective. *Exp. Mol. Med.* **56**, 2099–2104 (2024).
196. I. Andolfo, R. Russo, A. Gambale, A. Iolascon, New insights on hereditary erythrocyte membrane defects. *Haematologica* **101**, 1284–1294 (2016).
197. Y. Y. Yien, M. Perfetto, Regulation of heme synthesis by mitochondrial homeostasis proteins. *Front. Cell Dev. Biol.* **10**, 895521 (2022).
198. R. S. Ohgami, D. R. Campagna, E. L. Greer, B. Antiochos, A. McDonald, J. Chen, J. J. Sharp, Y. Fujiwara, J. E. Barker, M. D. Fleming, Identification of a ferrireductase required for efficient transferrin-dependent iron uptake in erythroid cells. *Nat. Genet.* **37**, 1264–1269 (2005).
199. M. Di Stefano, L. Galassi, G. Magni, Unique expression pattern of human nicotinamide mononucleotide adenylyltransferase isozymes in red blood cells. *Blood Cells Mol. Dis.* **45**, 33–39 (2010).
200. K. Hikosaka, M. Ikutani, M. Shito, K. Kazuma, M. Gulshan, Y. Nagai, K. Takatsu, K. Konno, K. Tobe, H. Kanno, T. Nakagawa, Deficiency of nicotinamide mononucleotide adenylyltransferase 3 (nmnat3) causes hemolytic anemia by altering the glycolytic flow in mature erythrocytes. *J. Biol. Chem.* **289**, 14796–14811 (2014).
201. J. Li, M. Sun, J. Guo, L. Xu, Case report: Diagnosis and treatment of DGAT1 deficiency-induced congenital diarrhea in two cases and literature review. *Front. Pediatr.* **11**, 1253800 (2023).
202. M. N. Rojas Velazquez, F. Blanco, A. Ayala-Lugo, Lady Franco, V. Jolly, D. Di Tore, I. Martínez de Lapiscina, M. Janner, C. E. Flück, A. V. Pandey, A novel mutation in the INSR gene causes severe insulin resistance and Rabson-Mendenhall syndrome in a Paraguayan patient. *Int. J. Mol. Sci.* **25**, 3143 (2024).
203. V. Sharma, N. Hecker, J. G. Roscito, L. Foerster, B. E. Langer, M. Hiller, A genomics approach reveals insights into the importance of gene losses for mammalian adaptations. *Nat. Commun.* **9**, 1215 (2018).
204. N. Hecker, V. Sharma, M. Hiller, Convergent gene losses illuminate metabolic and physiological changes in herbivores and carnivores. *Proc. Natl. Acad. Sci. U. S. A.* **116**, 3036–3041 (2019).
205. M. Huelsmann, N. Hecker, M. S. Springer, J. Gatesy, V. Sharma, M. Hiller, Genes lost during the transition from land to water in cetaceans highlight genomic changes associated with aquatic adaptations. *Sci Adv* **5**, eaaw6671 (2019).
206. J. Sambrook, W. D. Russell, Protocol: DNA isolation from mammalian tissue. *Molecular Cloning: A Laboratory Manual (Sambrook J* (2001).
207. A. Astashyn, E. S. Tvedte, D. Sweeney, V. Sapojnikov, N. Bouk, V. Joukov, E. Mozes, P. K. Strope, P. M. Sylla, L. Wagner, S. L. Bidwell, L. C. Brown, K. Clark, E. W. Davis, B. Smith-White, W. Hlavina, K. D. Pruitt, V. A. Schneider, T. D. Murphy, Rapid and sensitive detection of genome contamination at scale with FCS-GX. *Genome Biol.* **25**, 60 (2024).
208. H. Li, Minimap2: pairwise alignment for nucleotide sequences. *Bioinformatics* **34**, 3094–3100

bioRxiv preprint doi: https://doi.org/10.64898/2026.07.24.740446; this version posted July 24, 2026. The copyright holder for this preprint (which was not certified by peer review) is the author/funder, who has granted bioRxiv a license to display the preprint in perpetuity. It is made available under a CC-BY-NC 4.0 International license.

(2018).

209. R. Poplin, P.-C. Chang, D. Alexander, S. Schwartz, T. Colthurst, A. Ku, D. Newburger, J. Dijamco, N. Nguyen, P. T. Afshar, S. S. Gross, L. Dorfman, C. Y. McLean, M. A. DePristo, A universal SNP and small-indel variant caller using deep neural networks. *Nat. Biotechnol.* **36**, 983–987 (2018).

210. H. Li, A statistical framework for SNP calling, mutation discovery, association mapping and population genetical parameter estimation from sequencing data. *Bioinformatics* **27**, 2987–2993 (2011).

211. H. Zhang, L. Song, X. Wang, H. Cheng, C. Wang, C. A. Meyer, T. Liu, M. Tang, S. Aluru, F. Yue, X. S. Liu, H. Li, Fast alignment and preprocessing of chromatin profiles with Chromap. *Nat. Commun.* **12**, 6566 (2021).

212. K. Howe, W. Chow, J. Collins, S. Pelan, D.-L. Pointon, Y. Sims, J. Torrance, A. Tracey, J. Wood, Significantly improving the quality of genome assemblies through curation. *Gigascience* **10** (2021).

213. D. Guan, S. A. McCarthy, J. Wood, K. Howe, Y. Wang, R. Durbin, Identifying and removing haplotypic duplication in primary genome assemblies. *Bioinformatics* **36**, 2896–2898 (2020).

214. H. Li, R. Durbin, Fast and accurate long-read alignment with Burrows-Wheeler transform. *Bioinformatics* **26**, 589–595 (2010).

215. J. Ghurye, A. Rhie, B. P. Walenz, A. Schmitt, S. Selvaraj, M. Pop, A. M. Phillippy, S. Koren, Integrating Hi-C links with assembly graphs for chromosome-scale assembly. *PLoS Comput. Biol.* **15**, e1007273 (2019).

216. M. Uliano-Silva, J. G. R. N. Ferreira, K. Krasheninnikova, Darwin Tree of Life Consortium, G. Formenti, L. Abueg, J. Torrance, E. W. Myers, R. Durbin, M. Blaxter, S. A. McCarthy, MitoHiFi: a python pipeline for mitochondrial genome assembly from PacBio high fidelity reads. *BMC Bioinformatics* **24**, 288 (2023).

217. S. Nowoshilow, S. Schloissnig, J.-F. Fei, A. Dahl, A. W. C. Pang, M. Pippel, S. Winkler, A. R. Hastie, G. Young, J. G. Roscito, F. Falcon, D. Knapp, S. Powell, A. Cruz, H. Cao, B. Habermann, M. Hiller, E. M. Tanaka, E. W. Myers, The axolotl genome and the evolution of key tissue formation regulators. *Nature* **554**, 50–55 (2018).

218. J. M. Flynn, R. Hubley, C. Goubert, J. Rosen, A. G. Clark, C. Feschotte, A. F. Smit, RepeatModeler2 for automated genomic discovery of transposable element families. *Proc. Natl. Acad. Sci. U. S. A.* **117**, 9451–9457 (2020).

219. R. S. Harris, “Improved pairwise alignment of genomic DNA,” thesis, Ph.D. Thesis, The Pennsylvania State University (2007).

220. V. Sharma, M. Hiller, Increased alignment sensitivity improves the usage of genome alignments for comparative gene annotation. *Nucleic Acids Res.* **45**, 8369–8377 (2017).

221. W. J. Kent, R. Baertsch, A. Hinrichs, W. Miller, D. Haussler, Evolution’s cauldron: Duplication, deletion, and rearrangement in the mouse and human genomes. *Proceedings of the National Academy of Sciences* **100**, 11484–11489 (2003).

222. E. Osipova, N. Hecker, M. Hiller, RepeatFiller newly identifies megabases of aligning repetitive sequences and improves annotations of conserved non-exonic elements. *Gigascience* **8**, 1–10 (2019).

223. H. G. Suarez, B. E. Langer, P. Ladde, M. Hiller, chainCleaner improves genome alignment specificity and sensitivity. *Bioinformatics* **33**, 1596–1603 (2017).

224. A. Frankish, M. Diekhans, I. Jungreis, J. Lagarde, J. E. Loveland, J. M. Mudge, C. Sisu, J. C. Wright, J. Armstrong, I. Barnes, A. Berry, A. Bignell, C. Boix, S. Carbonell Sala, F. Cunningham, T. Di Domenico, S. Donaldson, I. T. Fiddes, C. García Girón, J. M. Gonzalez, T. Grego, M. Hardy, T. Hourlier, K. L. Howe, T. Hunt, O. G. Izuogu, R. Johnson, F. J. Martin, L. Martínez, S. Mohanan, P. Muir, F. C. P. Navarro, A. Parker, B. Pei, F. Pozo, F. C. Riera, M. Ruffier, B. M. Schmitt, E. Stapleton, M.-M. Suner, I. Sycheva, B. Uszczynska-Ratajczak, M. Y. Wolf, J. Xu, Y. T. Yang, A. Yates, D. Zerbino, Y. Zhang, J. S. Choudhary, M. Gerstein, R. Guigó, T. J. P. Hubbard, M. Kellis, B. Paten, M. L. Tress, P. Flicek, GENCODE 2021. *Nucleic Acids Res.* **49**, D916–D923 (2021).

225. V. Ranwez, E. J. P. Douzery, C. Cambon, N. Chantret, F. Delsuc, MACSE v2: Toolkit for the

bioRxiv preprint doi: https://doi.org/10.64898/2026.07.24.740446; this version posted July 24, 2026. The copyright holder for this preprint (which was not certified by peer review) is the author/funder, who has granted bioRxiv a license to display the preprint in perpetuity. It is made available under a CC-BY-NC 4.0 International license.

Alignment of Coding Sequences Accounting for Frameshifts and Stop Codons. *Mol. Biol. Evol.* **35**, 2582–2584 (2018).

226. A. Stamatakis, RAxML-VI-HPC: maximum likelihood-based phylogenetic analyses with thousands of taxa and mixed models. *Bioinformatics* **22**, 2688–2690 (2006).
227. M. J. Sanderson, r8s: inferring absolute rates of molecular evolution and divergence times in the absence of a molecular clock. *Bioinformatics* **19**, 301–302 (2003).
228. S. A. Smith, B. C. O'Meara, TreePL: Divergence time estimation using penalized likelihood for large phylogenies. *Bioinformatics* **28**, 2689–2690 (2012).
229. P. Ewels, M. Magnusson, S. Lundin, M. Käller, MultiQC: summarize analysis results for multiple tools and samples in a single report. *Bioinformatics* **32**, 3047–3048 (2016).
230. A. M. Bolger, M. Lohse, B. Usadel, Trimmomatic: a flexible trimmer for Illumina sequence data. *Bioinformatics* **30**, 2114–2120 (2014).
231. N. L. Bray, H. Pimentel, P. Melsted, L. Pachter, Near-optimal probabilistic RNA-seq quantification. *Nat. Biotechnol.* **34**, 525–527 (2016).
232. M. I. Love, W. Huber, S. Anders, Moderated estimation of fold change and dispersion for RNA-seq data with DESeq2. *Genome Biol.* **15**, 550 (2014).
233. Y. Zhou, B. Zhou, L. Pache, M. Chang, A. H. Khodabakhshi, O. Tanaseichuk, C. Benner, S. K. Chanda, Metascape provides a biologist-oriented resource for the analysis of systems-level datasets. *Nat. Commun.* **10**, 1523 (2019).
234. A. Löytynoja, Phylogeny-aware alignment with PRANK. *Methods Mol. Biol.* **1079**, 155–170 (2014).
235. G. M. Sastry, M. Adzhigirey, T. Day, R. Annabhimoju, W. Sherman, Protein and ligand preparation: parameters, protocols, and influence on virtual screening enrichments. *J. Comput. Aided Mol. Des.* **27**, 221–234 (2013).
236. *Schrödinger Release 2025-1: Maestro* (Schrödinger LLC, New York, 2025).
237. P. Bankhead, M. B. Loughrey, J. A. Fernández, Y. Dombrowski, D. G. McArt, P. D. Dunne, S. McQuaid, R. T. Gray, L. J. Murray, H. G. Coleman, J. A. James, M. Salto-Tellez, P. W. Hamilton, QuPath: Open source software for digital pathology image analysis. *Sci. Rep.* **7**, 16878 (2017).